Investigating the neurovascular coupling in the cerebellar granular layer

Giuseppe Gagliano

Investigating the neurovascular coupling in the cerebellar granular layer

Giuseppe Gagliano

Cover

“Ostinazione nella ricerca del sapere attraverso lo studio e la casualità”
Courtesy of Geno
instagram: @genotattoo
geno.cidio@yahoo.it
www.twilighttattoopavia@gmail.com

To me

Investigating the neurovascular coupling in the cerebellar granular layer

Università degli Studi di Pavia

PhD School in Biomedical Sciences

XXXI Cycle

Coordinator: Prof. Egidio D'Angelo

Department of Brain and Behavioral Sciences

Doctoral Dissertation by Giuseppe Gagliano

Supervisor: Prof. Egidio D'Angelo

Co-supervisor: Dr. Lisa Mapelli

Academic Year 2017-2018

Table of contents

Chapter 1

Introduction

1. Introduction

The brain consists of 10^{12} neural cells and 10^{15} synapses. In brain, the elaboration of external inputs (visual, olfactory, auditory, tactile and gustatory stimuli) generate an output response that allows the interactions of the body with the surrounding environment. The intricate network of information processes and the rules of human brain functions are not still completely unveiled. In order to facilitate the investigation of brain processes biology, animal models are required. The most studied models are rat and mice brains due to the easy availability of these animals and the high analogy between rodents and human brains. Molecular and genetic techniques of DNA manipulation permit to easily generate transgenic mice, mimicking specific pathologies phenotype in animals. Moreover, the use of rodent brain slices facilitates the investigations of neuronal mechanisms. Animal models represent an optimal strategy of investigation to gain more understanding of brain functions.

1.1 The Cerebellum

The brain weighs ~1.5kg and contains about 100 billion of neurons. Although the cerebral cortex represents the 82% of the brain mass, it contains only a minority of neuronal cells. Surprisingly, the cerebellum weighs 154g and is formed by 69 billions of neurons, most of that as granule cells (GrCs) (Herculano-Houzel, 2009). In fact, in the cerebellar cortex GrCs are extremely packed.

The cerebellum is one of the most primitive parts of the brain. The mass of the cerebellum constitutes only the tenth part of the brain but it contains most of central nervous system (CNS) neurons (Herculano-Houzel, 2010). Besides, it is well known the role of cerebellum in motor behavior, movements coordination, timing and sensory functions, its involvement in cognitive and emotional functions was widely debated.

During the last decades, the cerebellum has been deeply investigated by anatomists, physiologists and scientist interested in defining its structure, function and connections. The studies of the physiologist Flourens underlined the involvement of the cerebellum in motor control (the first pillar of the classic cerebellar doctrine), paving the way for the more recent discoveries about cerebellar functions (Galliano and De Zeeuw, 2014). Sometime later, the invention of the histological technique “black reaction” by Camillo Golgi, allowed Ramon y Cajal to identify the single neurons of the cerebellar network and to describe the connectivity of these elements in the cerebellar cortex (Galliano and De Zeeuw, 2014). The latter discovery constitutes the second pillar of the cerebellar doctrine. The third pillar was formulated more recently thanks to the studies of David Marr, James Albus and Masao Ito about the cellular mechanisms of synaptic transmission

(Marr, 1969; Albus, 1971; Ito, 2006; Galliano and De Zeeuw, 2014). In the cerebellum, synapses are able to modify their structural and/or functional properties in response to different spatial and temporal input stimuli, showing different degrees of plasticity. These brought to the assumption that the cerebellum is involved in motor learning.

1.1.2 Anatomical organization of the cerebellum

The cerebellum is located behind the brain stem and it is organized in lobes. The primary fissure separates the anterior and the posterior lobes while the posterior and flocculonodular lobes are divided by the posterolateral fissure. Three peduncles (superior, middle and inferior) connect the cerebellum to the rest of the brain. The superior peduncle consists mostly of efferent fibers connecting the cerebellum to the brain stem, thalamus and hypothalamus; the middle peduncles contain the afferents from the contralateral pontine nuclei and connects the cerebellum to the pons; in the inferior peduncles, the afferents (posterior spinocerebellar, cuneocerebellar, trigeminocerebellar tracts, olivocerebellar and vestibulocerebellar fibers) connect the cerebellum to the brain stem and the spinal cord, while the efferent fibers to the vestibular nuclei. The central region of the cerebellum, the *vermis*, separates the left from the right *hemisphere*. The gray matter of the cerebellum formed the *cerebellar cortex* which contains most of the cerebellar neurons. The inner white matter formed the so called *arbor vitae* and contain the deep cerebellar nuclei (Fig. 1.1) (Swenson et al., 1984).

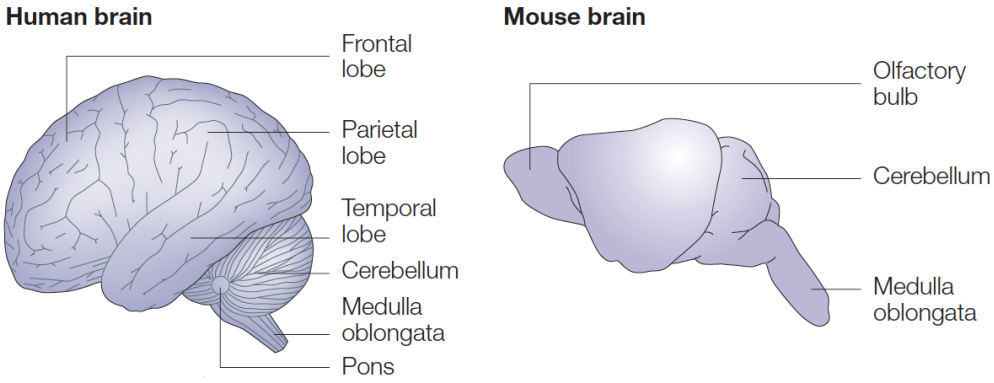

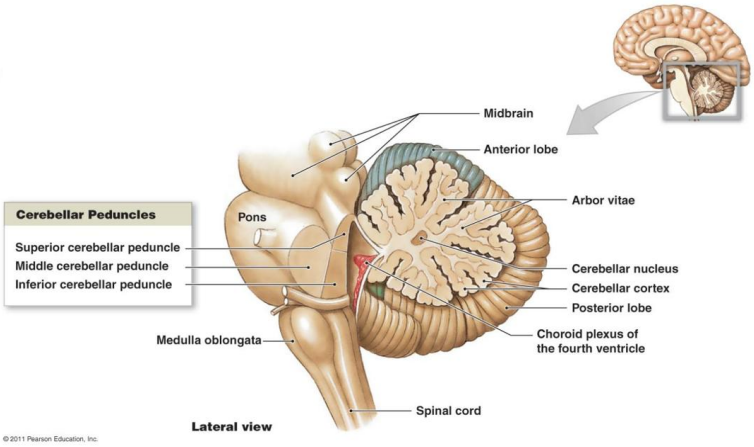

Figure 1.1 | Comparison between human and mouse brain. In human, the cerebellum is located under the temporal and parietal lobe of the brain and dorsally to the pons (*top panel*, *left*). In rodents, the cerebellum is located behind the midbrain, on the dorsal surface of the pons (*top panel*, *right*) (Cryan and Holmes, 2005). In both cases, the three peduncles connect the cerebellum to the brain. In the lower part of the figure the sagittal section of the vermis shows the anatomical organization of the cerebellum (*bottom panel*).

The cerebellar cortex is divided into three different layers: the inner granular layer (GL), the intermediate Purkinje cells (PCs) layer and the molecular layer (ML). In the GL, the excitatory granule cells (GrCs) receive glutamatergic excitatory inputs from the mossy fibers (MFs), and GABAergic inhibitory inputs from Golgi cells (GoC) (Fig 1.2). The GL is therefore the input stage of the cerebellar cortex. Excitatory and inhibitory connections among MFs, GrCs and GoCs are located in peculiar structures called *cerebellar glomeruli*, that contain GrCs dentrites, GoCs axons and MFs terminals (or *rosettes*), enwrapped by a glial sheathing.

The GrC axons arise from the GL (as ascending axons) and reach the ML where they bifurcate originating the parallel fibers (PFs), that make excitatory glutamatergic synapses with PCs, GoCs and molecular layer interneurons (MLIs) dendrites. The Purkinje cells are organized in a monolayer, situated between the GL and the ML. The PCs represent the only output of the cerebellar cortex. PCs dendrites receive excitatory inputs from PFs and climbing fibers (CFs, from the inferior olive); GABAergic inhibitory inputs from MLIs such as basket and stellate cells (BCs and SCs, respectively); while their axons penetrate into the white matter where they make inhibitory

synapses with deep cerebellar nuclei (DCN) neurons (the output stage of cerebellum) (Fig. 1.2) (Witter et al., 2016). Besides the function of the main cell types of the cerebellar cortexhas been well investigated and described, not much is known about the non-traditional large cells (NTc), such as unipolar brush cells (UBCs), Lugaro cells, synarmotic neurons, candelabrum neurons and the perivascular neurons of the GL (Ambrosi et al., 2007).

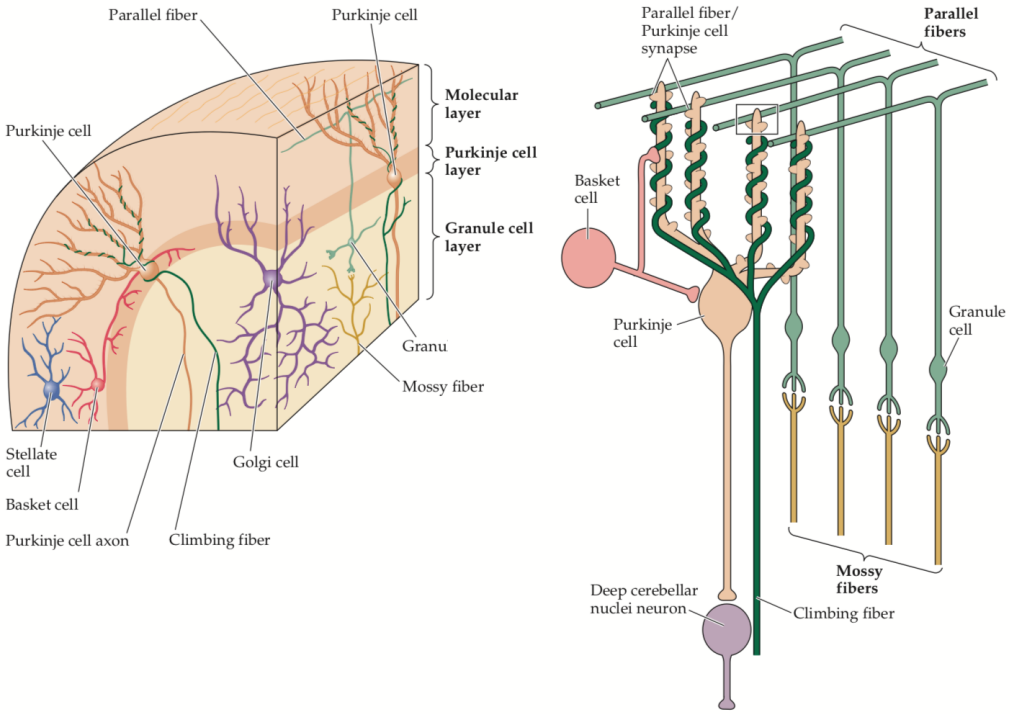

Figure 1.2 | Cerebellar cortex circuit organization. The cerebellar cortex consists of three layers in which different cell types interact among each other. The complex network of the cerebellum processes the incoming information conveyed by MFs and CFs. The DCN carry the output response (Purves et al., 2001).

1.1.3 Functions of the cerebellum

The cerebellum may be divided in three different functional divisions: vestibulocerebellum, spinocerebellum and neocerebellum. The vestibulocerebellum or *archicerebellum* is the most ancient part of the cerebellum and includes the flocculonodular lobe that is involved in the regulation of balance and eye movement; the spinocerebellum or *paleocerebellum* includes the

vermis and the intermediate part of the hemispheres that controls body and limb movements including feedback adjustments; the part of the cerebellum of most recent formation is the cerebrocerebellum or *neocerebellum*, which includes the lateral part of the hemispheres and have many functions in the planning of movements and in cognition (Rand and Swenson, 2006). The sensory inputs coming from different regions of the brain are stored and processed in the cerebellum who tunes the motor activity. This latter traditional view of motor function has been confirmed during the years. Nevertheless, in the last years the hypothesis of cerebellar cognitive functions has been increasingly debated and questioned.

Besides its role in control, coordination, adaptation and learning of motor behavior, recent evidence reports a role for the cerebellum in cognition (Glickstein and Doron, 2008; Kansal et al., 2017) and described its anatomical connections with higher cognitive areas such as the neocortex (Middleton and Strick, 2001). Moreover, in cerebellar cognitive affective syndrome (CCAS), patients with cerebellar lesions showed cognitive dysfunctions (Schmahmann and Sherman, 1998). The region of the cerebellum involved in cognitive functions was recently demonstrated to be the hemispheres (Glickstein and Doron, 2008), although cerebellar connectivity to the neocortex is revealing to be more complex than expected and this field of investigation is constantly growing. Furthermore, investigations on human fMRI showed that cerebellar vermis and hemispheres respond with different BOLD signals (respectively linear and non-linear) in relationship to the grip force application during the same motor task, suggesting that different cerebellar regions might process information in different ways (Alahmadi et al., 2017).

1.1.4 Cerebellar plasticity

Plasticity increases or reduces the strength of synaptic transmission in neurons. The activity-dependent changes in synaptic transmission, namely long-term potentiation (LTP) or depression (LTD), provide the biological basis for learning and memory in the brain. The modifications in connections structure (morphology of dendrites and boutons) and function (neural excitability and synaptic efficacy) are properties distributed throughout the whole cerebellar network, involving almost all neuronal types studied so far.

In the cerebellar cortex, PF-PC synapse LTD, under the control of CFs activation, is often considered as the basis mechanism for cerebellar learning. Nevertheless, novel hypotheses consider that not only the PF-PC synaptic depression is essential for learning process, but that all the different forms of cerebellar plasticity synergistically cooperate in the generation of the cerebellar-derived behavioral responses (Gao et al., 2012; D'Angelo et al., 2016). Several experiments

described the existence of different form of synaptic and non-synaptic cerebellar plasticity (Mapelli et al. 2015). The excitatory MF-DCN and inhibitory PC-DCN synapses may generate both forms of long-term plasticity (LTP or LTD), in slice (Morishita and Sastry, 1996; Ouardouz and Sastry, 2000). The theta-burst stimulation (TBS; consisting in 10 pulses at 100 Hz bursts, repeated at 4 Hz) of MFs and the sensory tactile stimuli organized in theta patterns (theta sensory stimulation, TSS) proved able to induce long-term synapse modifications (LTP or LTD) in cerebellar cortex respectively *ex vivo* (Armano et al., 2000; Mapelli and D'Angelo, 2007) and *in vivo* (Roggeri et al., 2008; Ramakrishnan et al., 2016). Moreover, the changes in GrCs intrinsic excitability are associated to the genesis of LTP or LTD at MF-GrC synapses (Armano et al., 2000).

At the MF-GrC relay, synaptic potentiation involves the glutamate-dependent NMDARs and mGluRs activation which lead to external Ca^{2+} entry and Ca^{2+} release from intracellular compartments (D'Angelo et al., 1999). The LTP-LTD balance can be regulated by stimulation patterns, likely depending on a threshold set by $[Ca^{2+}]_i$. MFs high frequency long stimulation induced a great increase in intracellular $[Ca^{2+}]$, leading to LTP. LTD is generated by short and less frequent bursts that determine a minor Ca^{2+} entry (Armano et al., 2000; Gall et al., 2005)LTP-LTD balance may be controlled also by neuromodulators such as acetylcholine. In fact, short MFs stimulation pattern in presence of acetylcholine or nicotine (nicotinic receptors agonist) activate the α7 isoform of the nicotinic receptor (α7-nAChRs) inducing an increase in intracellular level of Ca^{2+}that facilitate the LTP at MF-GrC synapse but not LTD (Prestori et al., 2013). Moreover, the vasoactive agent NO works as retrograde messenger that orchestrates the equilibrium between LTP or LTD at MF-GrC synapse through a NMDAR/nNOS-dependent mechanism. The retrograde signal generated by NO release, regulates the pre-synaptic release of glutamate and facilitates LTP (Maffei et al., 2003). The duality function of NO in synaptic plasticity modulation and neurovascular coupling events suggests the pivotal role of this molecule in brain.

1.2 Neurovascular coupling

In humans, the blood flowing in the ~644km of brain vessels provides nutrients to all districts of the central nervous system (Sweeney et al., 2018). The *primum movens* of the blood flow is the heart, as described in the pioneering study *De motu cordis* wrote by Harvey in 1628 (Ribatti, 2009). The main vessels which transported blood from and to the brain are veins and arteries. In 1661, the Italian anatomist Marcello Malpighi identified the microscopic blood vessels connecting small veins and arteries, called capillaries (Romero, 2011). These tiny vessels actively participate in the exchange of substances between blood and organs in human body (Krogh, 1929).

Capillaries widely contribute to the control of local blood flow through the action of pericytes, a kind of contractile cells located on microvasculature (Attwell et al., 2016).

In the brain, the *internal carotid artery* and the *vertebral artery* distribute the blood to the central nervous system. The vertebral artery anastomoses at the level of the pons into the *basilar artery* that supplies blood to the cerebellum. The basilar artery branches off in the *anterior inferior cerebellar artery*, *superior cerebellar artery* and *posterior cerebral artery*. The ramifications of these arteries give off the small capillaries that supply the cerebellum (Fig. 1.3) (Miller et al., 2005). The proximal portion of the basilar artery generates the *posterior cerebral arteries* which communicate with the internal carotid artery through the *posterior communicating arteries*. The *anterior cerebral arteries* rising from the internal carotid arteries are linked with the *anterior communicating artery*. This network of vessels originates the so-called *circle of Willis* (Fig. 1.3). Therefore, superficial biggest vessels of the brain give off arterioles and capillaries which supply with blood the brain (Lee, 1995). Immunostudies conducted on mouse cerebral cortex showed how superficial arteries and penetrating arterioles branch into pre-capillary arteriole and then capillaries giving rise to the dense network of brain microvasculature (Grant et al., 2017).

In order to ensure the proper nutrients and oxygen requirements to the brain, blood flow needs to be finely regulated. In fact, neuronal activity regulates blood vessel diameter changes and controls cerebral blood flow (CBF) adaptations. The existence of interactions between neuronal cells and blood vessels has first been described by Angelo Mosso, in 1880, and by Roy and Sherrington, in 1890 (Iadecola, 2002). This phenomenon is called neurovascular coupling (NVC) or *"functional hyperemia"*. The NVC ensures the proper supply of nutrients and metabolites to the brain during steady states and during sudden changes in neuronal activity range.

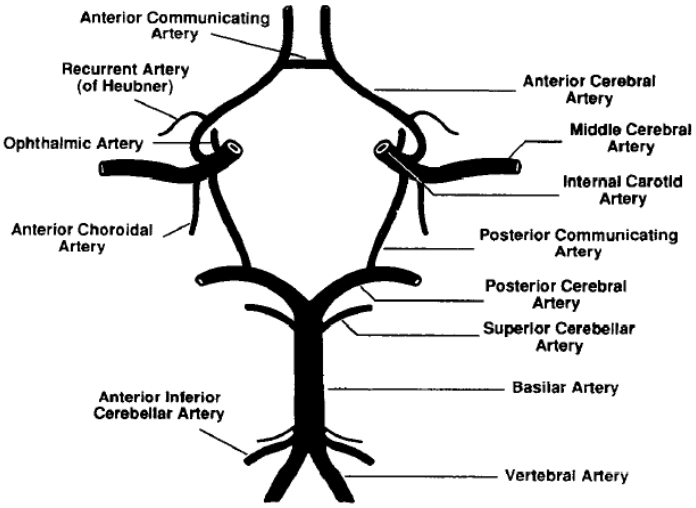

Figure 1.3 | Circle of Willis. Scheme of the principal arteries that constitute the circle of Willis in the central nervous system. In the superior part of the circle, the arteries gave off the vessels that supply the frontal region of the brain. In the bottom part of the figure, the vessels bifurcate into the small arterioles and capillaries that supply the cerebellum (Lee, 1995).

1.2.1 Neurovascular unit

The regulation of the local CBF by neural activity is mediated by the release of different substances acting on brain blood vessels. In brain, neurons and glial cells synthesize several molecules that directly or indirectly determine blood vessels dilation or constriction, called vasoactive agents. The release of neurotransmitters triggers the signaling pathways for the synthesis of these molecules (Filosa and Blanco, 2007; Filosa et al., 2016; McConnell et al., 2017).

The hemodynamic changes of CBF adjustments require tight interactions between neuronal and vascular cells. The anatomical coupling of neurons, interneurons, astrocytes, endothelial cells, vascular smooth muscle cells (VSMCs) and pericytes is called *neurovascular unit* and constitute the functional *blood-brain barrier* (*BBB*) that protect the nervous central system from toxic substances. These cells also cooperate to regulate the CBF making sure that brain tissue receive the proper supply of nutrients. The signaling among neural and vascular components of the brain generates the NVC (Fig. 1.4, left) (Sá-Pereira et al., 2012; Muoio et al., 2014).

Besides its important structural role, it is widely accepted that endothelial cells give an essential contribution to the NVC through various interactions with the rest of neurovascular unit elements (Guerra et al., 2018). Pericytes cover and enwrap the surface of blood vessels and regulate

the permeability of the BBB. There are different types of pericytes: ensheating pericytes (EP) (on pre-capillary arterioles), mesh pericytes (MP) and thin-strand pericytes (TSP) (on capillaries) (Attwell et al., 2016; Grant et al., 2017). They also play an important role in angiogenesis, inflammation and in CBF control. The presence of the contractile system similar to that in VSMCs and the susceptibility to vasoactive agents make pericytes able to participate in the changes in small brain capillaries diameter. Astrocytes partially enwrap the walls of the vessels with their cytoplasmic extroflexions called *end-feet*. Glial cells contributes both to the stability of the BBB and to vessel caliber regulation (Lok et al., 2007).

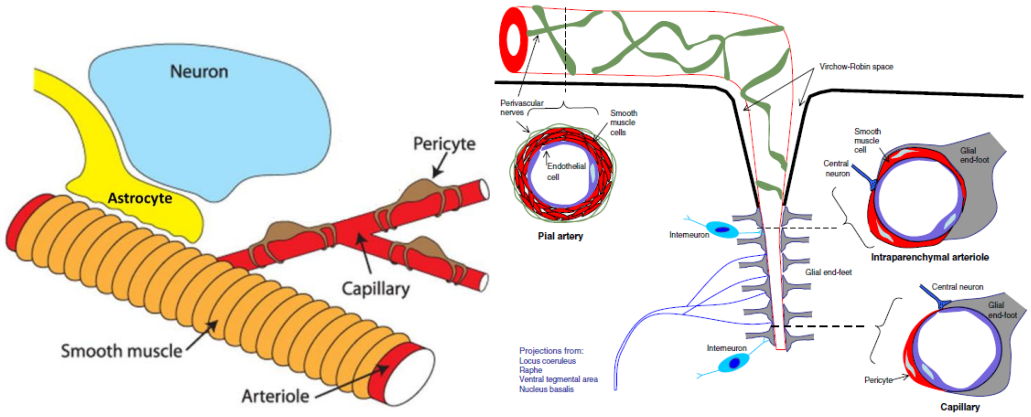

Figure 1.4 | Anatomical interactions among neurovascular unit elements. In the CNS, the anatomical and functional interactions between neurons, astrocytes, pericytes and VSMCs regulate blood flow in arterioles and capillaries (*left figure*) (Nippert et al., 2018).The diameter of the superficial pial arteries is controlled by a thick layer of VSMCs and perivascular innervations surrounding endothelial cells. The arteries penetrating in the Virchow-Robin space in the brain became arterioles. At this level, the control of local blood flow is mediated by glial end-feet and central neurons that make direct contact with VSMCs. Low depth capillaries are surrounded by glial end-feet and central neurons that regulate their inner vessel diameter through pericytes action. Capillaries does not have VSMCs around the endothelium and receive projections from local interneurons and from distant areas of the brain (*right figure*) (Drake and Iadecola, 2007).

Vasodilation or vasoconstriction can occur both at arteries, arterioles or capillaries level. In the brain, superficial pial arteries and penetrating arterioles diameters are controlled by VSMCs surrounding vessel walls, while capillaries inner diameter is regulated by pericytes contraction (Fig. 1.4, right). The status of relaxation/contraction of VSMCs and pericytes is controlled by neuronal- or astrocytic-derived vasoactive molecules (Filosa and Iddings, 2013; Nippert et al., 2018).
Recent investigation demonstrates that capillaries can dilate before the arterioles in response to neural activity and pericytes activation (Hall et al., 2014). Moreover, the vasodilation signal could propagate from capillaries to arterioles through the gap-junctions in nearby endothelial cells (Mishra, 2017). Furthermore, capillary dilations are the main responsible for blood flow increase during functional hyperemia, and pericytes control of vessel diameter is thought to be the principal regulator of CBF. The coupling between capillaries and pericytes seems to be involved in the genesis of the imaging signals detected by fMRI (Hall et al., 2014).

1.2.2 Mechanisms of NVC

The fine tuning of vessel diameters ensures the appropriate delivery of blood to the brain. The inter-synaptic neurotransmitters released activate the post-synaptic signaling pathways for vasoactive molecules synthesis. The most influencing neurotransmitter on NVC is glutamate. However, GABA-activated pathways also contribute to the net increase or decrease of the CBF (see below). Glutamate involvement in this phenomenon is well known in hippocampus, neocortex and cerebellum, where it influences blood flow with several biochemical pathways (Drake and Iadecola, 2007).

Glutamate activates post-synaptic NMDA receptors (NMDARs) that trigger the Ca^{2+}-dependent pathway that leads to activation of the neuronal isoform of nitric oxide synthase (nNOS) and thus to nitric oxide (NO) production. NO is a well-known substance able to diffuse across neuron membranes and to act as potent vasodilator (Fig. 1.5) (Attwell et al., 2010). In the cerebellum, neuronal-derived NO directly mediates the NVC (Iadecola et al., 1995; Yang and Iadecola, 1997; Yang et al., 1998; Yang et al., 1999). In *in-vivo* experiments on rats barrel cortex, the presence of NOS inhibition caused a reduction in functional hyperemia events, measured as laser doppler flowmetry percent change, suggesting that NO contribute to increase CBF (Liu et al., 2008). Besides the vasodilating action, NO is also known to inhibit 20-HETE (a well-known vasoconstrictor) synthesis by blocking the 4A isoform of the cytochrome P450 (CYP4A) enzyme (Attwell et al., 2010). In Mapelli and Gagliano (2017), we addressed the role of NO as a vasodilator. Here, experimental evidence demonstrated that, in cerebellar GL, microvessels

responded with a dilation upon MFs electrical stimulations. Importantly, we never observed vasoconstriction (in absence of selective vasoactive agents inhibitors), suggesting that NO released during neuronal activity could inhibit the vasoconstriction pathway (Mapelli et al., 2017).
Also in the cerebral cortex, the inhibition of the vasoconstriction by NO plays a permissive role for vasodilation and CBF control (Nippert et al., 2018). In conclusion, NO plays a mediating vs permissive role in NVC.

Moreover, NMDARs activation and intracellular [Ca^{2+}] increase also activate the phospholipase A_2 (PLA_2) enzyme. The arachidonic acid (AA) generated from PLA_2 can be metabolized into prostaglandins (PGs), potent vasodilators of brain vessels (Attwell et al., 2010; Muñoz et al., 2015).

Glutamate could diffuse to astrocytes where it activates metabotropic glutamate receptors (mGluRs) thus increasing the intracellular [Ca^{2+}] which is essential for the production of vasoactive agents. In astrocytes, the activation of PLA_2 and AA metabolism generate PGs and epoxyeicosatrienoic acid (EET) that dilate the neighboring vessels. Furthermore, AA could diffuse from astrocytes membranes to endothelial cells where it is converted into 20-HETE, a well-known vasoconstrictor (Petzold et al., 2011; Otsu et al., 2014). Moreover, the intracellular increase in [Ca^{2+}] activate Ca^{2+}-dependent K^+ channels. This astrocytic leakage of K^+ leads to an increase in extracellular [K^+] that facilitates the inward rectifier potassium channels (Kir) that hyperpolarize VSMCs. The relaxation of VSMCs causes vessels dilatation (Fig 1.5) (Filosa et al., 2016). The vasoactive neural-derived molecules diffuses to pericytes, which control blood vessel diameter in NVC (Sweeney et al., 2016).

Several neurons take direct contact with vessels and release neuromodulators or neuropeptides that contribute to NVC. Serotonin could induce either vasoconstriction and vasodilation depending on the target cells. Several evidences assigned constrictor power to norepinephrine and dopamine while acetylcholine generates vessel dilation and its action is associated to CBF increase through endothelial NO synthesis (Drake and Iadecola, 2007). The vasoactive intestinal peptide (VIP) is known to dilate vessels, otherwise somatostatin and neuropeptide Y which have a vasoconstrictor effect in brain (Uhlirova et al., 2016).

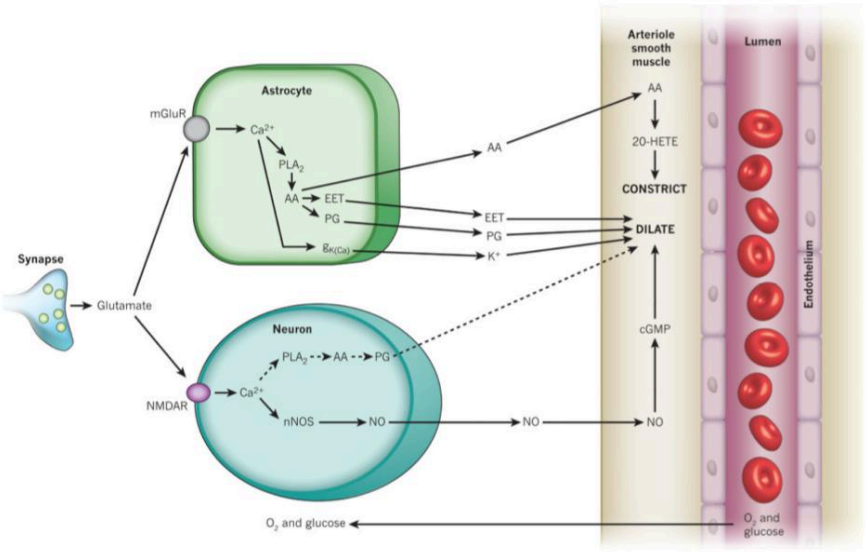

Figure 1.5 | Neural pathways for NVC. Glutamate released during synaptic transmission triggers different pathways in neurons and astrocytes in order to mediate NVC. In neurons (*blu*), NMDARs activation and intracellular [Ca^{2+}] increase lead to the production of vasodilator agents such as NO and PG. In astrocytes (*green*), the activation of mGluRs and the intracellular [Ca^{2+}] increase could activate either vasodilators (EET, PG and K^+) or vasoconstrictor (20-HETE) molecules synthesis (Attwell et al., 2010).

The neurotransmitter GABA may be involved in the control of blood flow but its direct action on vessels is uncertain (Drake and Iadecola, 2007; Attwell et al., 2010).

In the cerebral cortex, glutamate activation of GABAergic interneurons located between pyramidal cells and microvessels leads to the release of vasoactive molecules, as VIP and NO causing dilation (Cauli and Hamel, 2010). Moreover, GABAergic interneurons also produce somatostatin that induces vessel constriction (Cauli et al., 2004).

The relationship between neural cells and vessels regulates the CBF but how these elements cooperate and which mechanisms drive NVC are still poorly understood. Furthermore, the complicated double role of NO makes this phenomenon not easy to investigate. Also, the role of glial cells in NVC has been deeply investigated. The strategic position of astrocytes favors the bidirectional signaling with vessels and neurons that is fundamental for NVC regulation (Mishra, 2017). The activation of astrocytic pathways leads to capillary diameter changes via pericytes action (Mishra et al., 2016). Glial cells are also thought to be involved in the maintenance of resting vessel

tone during basal neural activity (Duchemin et al., 2012). Moreover, astrocytes may play a role in the late phase of NVC due to their slow action (Rosenegger and Gordon, 2015).

In the last few years, NVC has been considered a complex process in which all signaling pathways of the cerebrovascular network cooperate to finely tune the constriction and dilation of vessels in different brain districts and promote brain health (Iadecola, 2017). Although controversies arose about the methods (*in-vivo* or *in-vitro*) used to study the basis of neurovascular processes (Iadecola and Nedergaard, 2007), an increased scientific effort on NVC would allow to further unveil the recent discovered neurovascular pathways, to confirm the well-known mechanisms of NVC, and get new light on all processes underlying this phenomenon which are still uninvestigated or not completely understood. These improvements in our understanding of NVC would help overcoming current debates on these issues. In this work, we identified GL molecules involved in cerebellar NVC and their signaling pathways through a pharmacological approach and using a bright-field microscopy system. This strategy allowed us to monitor and describe NVC events in the GL of cerebellar rodent slices at different ranges of activity of the circuit.

1.2.3 Energy consumption and requirements of the brain

Although human brain represents only the 2% of whole body mass, it accounts for almost the 20% of the total energy consumption. The nervous central system can use two different strategies to produce energy. The first energy source used by the brain derives from the oxidative metabolism (aerobic condition), while in temporary absence of oxygen (anaerobic condition) nervous cells obtain energy from glucose metabolism or glycolysis (Drake and Iadecola, 2007).

In the cerebral cortex, pyramidal cells employ the 59% of the total energy use for synaptic transmission (postsynaptic receptors activation, neurotransmitter recycling and presynaptic Ca^{2+} entry and vesicles cycling). The rest of the energy is used to generate action potentials and to regenerate the resting potential (Na^{+}/K^{+} ATPase maintain the resting potential across the membrane in excitable cells by reversing Na^{+}/K^{+} fluxes across the membrane).

In the cerebellum, synaptic transmission accounts for the 29% of the energy use, while action potentials just for the 17%. Here, the major part of the energy (54%) is spent by GrCs to restore the potential of the membrane in their long axons. PCs consume a great percentage of energy to generate action potentials. In the cerebellar cortex, inhibitory interneurons, BCs and SCs energy use is less than that of principal spiking cells. Although ATP/cell use by GrCs is much lower than that of PCs, GL shows the most energy requirement in the cerebellar cortex taking into account the high cellular density (Howarth et al., 2012) (Fig. 1.6). GrCs are the most energy demander of

the cerebellum due to their high abundance and to their characteristic rapid activity increase when the cerebellar circuit is activated. Infact, taken together GrCs consume the 67% of cerebellar cortex energy. Therefore, in the cerebellum energy consumption of excitatory cells exceeds that of inhibitory cells (Howarth et al., 2010).

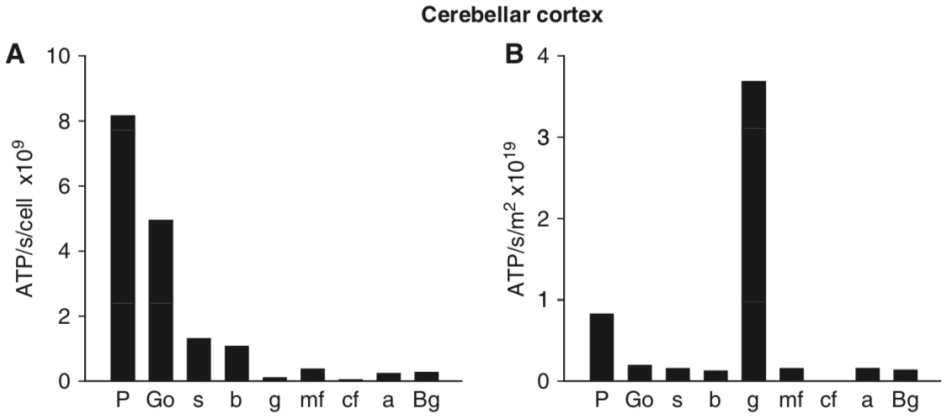

Figure 1.6 | Energy use in the cerebellar cortex. (**A**) Graph of the ATP use per cell in the cortex of the cerebellum. P = Purkinje cell; Go = Golgi cell; s = stellate cell; b = basket cell; g = granule cell; mf = mossy fiber; cf = climbing fiber; a = astrocytes; Bg = Bergmann glia. (**B**) Graph of the ATP use taking into account cellular density in the cerebellar cortex. P = Purkinje cell; Go = Golgi cell; s = stellate cell; b = basket cell; g = granule cell; mf = mossy fiber; cf = climbing fiber; a = astrocytes; Bg = Bergmann glia (Howarth et al., 2012).

The NVC processes are essential to adapt local blood flow to neural activity increase or decrease, in order to satisfy specific energy requirements for each brain region and sub-region. Therefore, CBF dysregulation may have catastrophic consequences for neurons. Indeed, NVC dysfunction is also one of the causes of cells neurodegeneration in disorders like Alzheimer's disease (Zlokovic, 2011). A few years ago, blood flow changes were thought to be controlled by the so called "metabolic signal" (decrease in blood O_2 and glucose or increase in CO_2 concentration) generated by the energy demand after ATP use. Nevertheless, blood deoxygenation was found not directly involved in CBF regulation, this latter being controlled by neural activation also in the presence of high O_2 availability (Lindauer et al., 2010). Also, increases in arterial glucose concentration and hyperoxia conditions did not affect neurovascular response in *in-vivo*

experiments in rats (Wolf et al., 1997). At last, the theory that H^+ dissociated from the excess of CO_2 in the blood can dilate brain vessels, was confuted. Indeed, during neural activity the extracellular compartment appeared alkalized due to both Ca^{2+}, H^+-ATPase activation caused by increases in $[Ca^{2+}]i$, and vessels dilation that sweep away the excess of CO_2 (Attwell et al., 2010). Today, these theories were replaced with the hypothesis of a neural-induced neurovascular mechanism that controls blood flow. In the cerebellar cortex, glutamate-mediated NMDARs signaling pathway activates the production of the vasoactive molecule NO that directly dilates capillaries (Mapelli et al., 2017). In the cortex, Ca^{2+}-mediated signaling following astrocytes activation leads to vasoactive agents synthesis that regulates capillaries motility (Mishra et al., 2016). In conclusion, it is accepted that NVC is triggered by neural activity instead, through a neurotransmitter-mediated signaling.

1.3 Neurovascular coupling application

The dynamic changes in CBF that occur in response to neuronal activity can be indirectly exploited by neuroimaging techniques like *functional magnetic resonance imaging* or fMRI. Unlike magnetic resonance imaging (MRI), that generates structural images of the brain, fMRI technique is used to map brain activity changes. NVC contributes to generate the *blood-oxygen-level-dependent* (BOLD) signals used by fMRI. The BOLD responses reflect the ratio between oxy- and deoxy-hemoglobin (HbO_2 and Hbr respectively) in brain blood vessels (Fig.1.7) (Attwell and Iadecola, 2002). Oxygen (O_2) is transported in the blood bound to the heme group iron atom of hemoglobin (Hb), contained in red blood cells. During an increase in cellular metabolism, the O_2 release by Hb changes the magnetic properties of the iron atom. In diamagnetic ferrous iron (Fe^{2+}) that is bound to the O_2, the disposition of the coupled electrons in the external electronic orbital generates a null magnetic moment. The paramagnetic ferric iron (Fe^{3+}) is not bounded to the O_2. In this condition, the uncoupled electrons in the external atomic orbital produce a not null magnetic moment. The paramagnetic iron generates a strengthening magnetic field when influenced with an external magnetic field. Therefore, the increase in cellular activity and the consequent formation of Hbr generate signals detected by imaging techniques. The variation of the fMRI signals is called BOLD effect (Garreffa et al., 2003; Logothetis and Wandell, 2004). Nevertheless, the neuronal origin of BOLD signals is still not well understood (see below, paragraph 1.3.1) and further investigations are needed to understand the mechanisms underlying this phenomenon.

NVC is also investigated in several pathologies such as stroke, hypertension and Alzheimer's disease, in which neurovascular functions were found altered. In Alzheimer, BBB breakdown (structural and functional capillary alterations, pericyte, endothelial cells and VSMCs degeneration) contributes to cerebrovascular dysregulation (inadequate brain perfusion or hypoperfusion) which anticipate the cognitive damage that characterizes the dementia (Zlokovic, 2005; Girouard and Iadecola, 2006; Zlokovic, 2011). In a recent review on Alzheimer's disease, Zlokovic and colleagues reported the "two-hit vascular hypothesis" for this pathology. According to this theory, vascular damage (hit 1), Aβ-dependent mechanism (hit 2) and the consequent neurovascular alteration lead to neuronal dysfunction and thus to dementia (Kisler et al., 2017). NVC is essential to brain health, for this reason its dysregulation causes severe pathological conditions. Therefore, investigating the mechanism that regulate CBF could be useful in the study of degenerative disorders in which the NVC is altered.

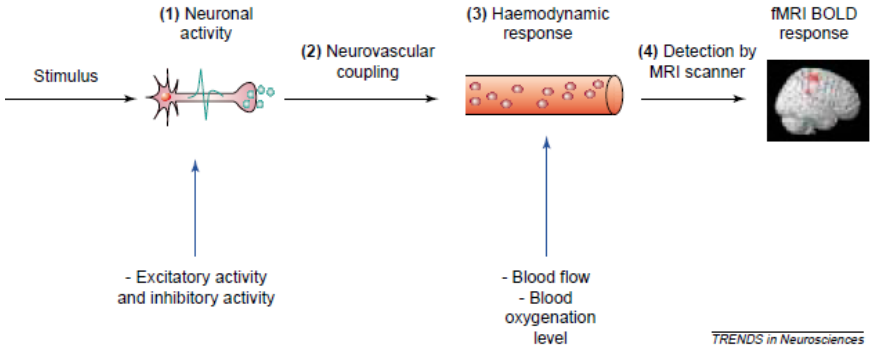

Figure 1.7 | Scheme of how BOLD signals are generated. Sequence of events that generate the images observed with fMRI. The stimulus-evoked increase in neural activity (inhibitory or excitatory) activate NVC signaling that change the hemodynamic responses (increasing or decreasing in blood flow) responsible of the imaging signals (BOLD responses) detected by fMRI (Arthurs and Boniface, 2002).

1.3.1 Neuronal activity and BOLD signal interpretation

The assumption that neuronal activity generates a visible response in fMRI can be misleading in interpreting BOLD signals origins. As a fact, these signals could reflect the activation of distant neuronal cells, therefore it could not be assumed that the regions originating the BOLD signals are the activated ones. The lack of overlap between the areas effectively generating the

signals and the ones showing the BOLD response has many explanations. One explanation of this mismatch resides in the intrinsic properties of blood vessels. In brain, neuronal-evoked stimulus of vasodilation can be propagated (back and forward) to distant vessels causing the increase in blood flow that originates a BOLD signal in regions where no neuronal activation is present (Duchemin et al., 2012). In particular, experimental evidence showed that cerebellar cortex PFs electrical stimulation induced diameter increases in arterioles located from 0.1 mm to 0.9 mm from the site of stimulation. Moreover, no field potential (neuronal activity) or laser doppler flowmetry (cerebellar blood flow) recordings were produced where arteriolar propagation of dilation was observed (Iadecola et al., 1997). It is clear, then, that further investigation on the complex properties of neuronal activity and its effect on NVC is essential to improve our understanding of BOLD representations.

In the brain, the activity state of microcircuits relies on the fine tuning of the excitation (E) - inhibition (I) balance. The hemodynamic responses can be influenced by the neurons activity states. The net excitatory activity results in fMRI responses increase, as well as during contemporary rise of both excitatory and inhibitory neuronal activity. The reduction of excitation and inhibition causes a decrease in fMRI responses (Fig. 1.8). During prevailing net inhibitory activity, the hemodynamic response might decrease leading to a negative BOLD signal, depending on the activated type of cells and their circuit (Fig. 1.8) (Logothetis, 2008).

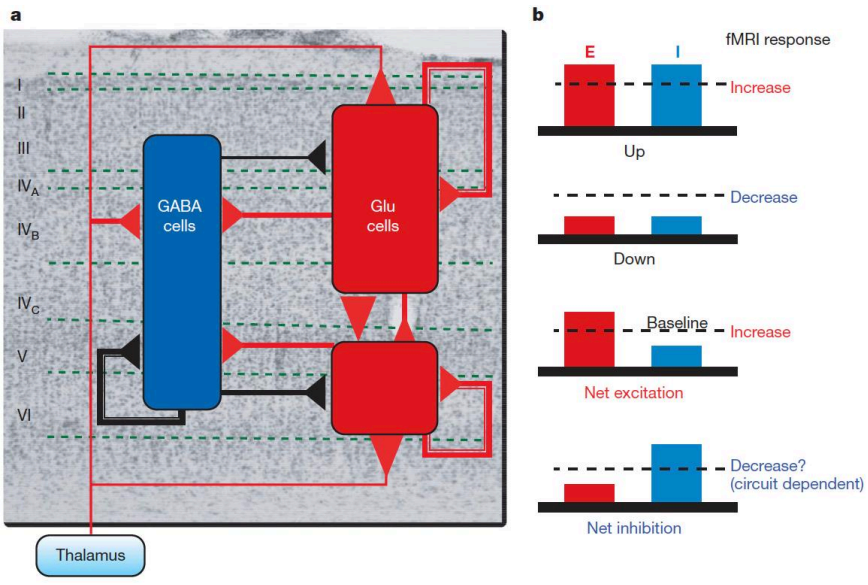

Figure 1.8 | E-I microcircuit in brain and possible fMRI responses. (**a**) Model of cerebral microcircuit in the brain. Neuronal interactions occur through excitatory (in red) and inhibitory synapses (in black). (**b**)E-I balance of neuronal activity of a typical microcircuit in brain. The increase or decrease in E-I balance in brain microcircuits generate different fMRI responses (Logothetis, 2008).

Since the neuronal origin of the signals, the interpretation of BOLD responses is not easy. In monkey brain, the investigation of the relationship between fMRI signals and neural activity showed a high correlation between local field potential (LFP) and BOLD signals than that observed between the same imaging responses and single- and multi-unit spiking activity. LFPs represent the synaptic excitation of a group of neurons and reflect the sum of the intracellular currents of each cell. The imaging signals of fMRI are determined by input activity and processing but not by output activity (Logothetis et al., 2001). In conclusion, it is difficult to correctly interpret fMRI results due to the sensibility of hemodynamic changes to the size of the neuronal population activated and to the circuit functional organization of these cells in the brain. For these reasons, the basic mechanisms underlying the BOLD signal and the nature of the neuronal activity giving rise to it are not well understood yet. That is the major limitation of fMRI (Logothetis, 2008).

In conclusion, glutamate-dependent neuronal activity mediates the changes in blood flow that generate different BOLD responses. In order to correctly decode these imaging signals and to deepen our understanding on the physiological basis of the BOLD signal (Hall et al., 2016), further investigations on neuronal signaling (on molecular, cellular and vascular levels) coupled with fMRI and BOLD analysis are needed.

1.3.2 Neurovascular coupling and the cerebellum

Given that different NVC mechanisms has been described, each brain region is likely to have a specific strategy to ensure proper oxygen supply. The cerebellar cortex is very suitable for the study of this phenomenon due to its functional and structural properties. The lack of excitatory collateral from PCs axons and the massive inhibitory synaptic activity of interneurons make impossible the genesis of epileptic events in cerebellar cortex (Lauritzen, 2001). Furthermore, the lack of Na^+ -channels in PCs dendrites and the presence of inhibitory collaterals from PCs axons to the nearby PCs disadvantage the onset of cortical propagated depression events, unlike in the cerebral cortex (Lauritzen et al., 2012). The organization of cerebellar cortex components remind

the Cartesian coordinate system and facilitate the investigations of neuronal activity-dependent CBF variation and *cerebral metabolic rate of oxygen* ($CMRO_2$) consumption (Lauritzen et al., 2012). Finally, the electrophysiological properties of the cerebellar circuit have been well described (D'Angelo et al., 1995; D'Angelo and De Zeeuw, 2009; Mapelli et al., 2014).

The investigations about cerebellar NVC by Martin Lauritzen and Costantino Iadecola identified respectively LFP as the neural activity correlate of hemodynamic changes and NO as the main vasoactive agents involved in this process. One of the first studies on NVC in the cerebellum hypothesized that the main contribution to the flow response came from PCs rather than from MLIs action (Yang et al., 1998). Electrophysiological experiments demonstrated that CFs and PFs stimulation increased PCs activity and thus CBF via glutamatergic AMPA receptors activation. Nevertheless, PFs stimulation also activates GABAergic MLIs that inhibit PCs. Indeed, it has been shown that an increase in CBF and $CMRO_2$ following cerebellar cortical activation might not be correlated with PCs firing, that can remain silent (Mathiesen et al., 1998; Caesar et al., 2003; Thomsen et al., 2009). Therefore, blood flow adaptations are dissociated from PCs spiking activity but may be originated from MLIs excitation (Thomsen et al., 2004). In the cerebellar cortex, GABAergic interneurons activation and GABA release does not contribute to blood flow changes (Mathiesen et al., 1998).

The main issue about the correlation between excitatory postsynaptic LFP and CBF resides in the lack of temporal coupling from synaptic input to hemodynamic response. The rapid LFPs were observed a few milliseconds after neural activation but CBF changes occurs after one second. In order to correlate electrophysiological and hemodynamic signals, it resulted appropriate to sum neural activities (∑LFP). In the cerebellum, the existence of temporal coupling (linear correlation) between ∑LFP and CFs system and non-linear correlation for the PFs system has been shown. In fact, PFs stimulation lead to spiking output decrease of PCs via MLIs activation but resulted in increased CBF. In this case, the ∑LFP-blood flow relationship is non-linear. The non-linearity could make the interpretation of BOLD signals difficult (Lauritzen et al. 2012, Mathiesen, Caesar and Lauritzen 2000, Lauritzen 2005).

Therefore, the differences in fMRI responses depend on the type of neurons activated, on the microcircuit, and on the balance between vasodilators and vasoconstrictors release. Moreover, the same cell could release distinct vasoactive agents depending on the region where it is activated (Akgoren et al., 1997). According to this view, brain cells exploit different molecular strategies for NVC. Concerning the molecular mechanisms involved, it has been shown that PFs stimulation induces CBF increase through glutamate and NO release. NO activates the soluble guanylyl cyclase (sGC) which elevates the cyclic guanosine monophosphate intracellular concentration $[cGMP]_I$ thus

inducing vasodilation (Iadecola et al., 1995; Iadecola et al., 1996; Yang and Iadecola, 1996, 1998; Yang et al., 1999). Moreover, the functional isoform of NOS is expressed in MLIs but not in PCs (Rodrigo et al., 1994; Rancillac et al., 2006). According to this model, the knock-out mice for cyclin D2 (regulatory protein of cycle cell) with a down-regulation in the number of SCs showed a reduced CBF (Yang et al., 2000). These evidences suggest that in the ML, NVC is drove by NO signaling. It is also important to stress that D2-null mice showed a reduction in GrCs number.

It should be noted that all the studies cited so far were conducted on the cerebellar molecular layer and focused on PCs and MLIs activity, taking into account PFs and CFs inputs. In order to understand the generation of the hemodynamic response in the cerebellum, it should be also taken into account that: i) GrCs are the most abundant brain neurons (3-7 $10^6/mm^3$) and the most energy consuming elements in the cerebellum (Howarth et al., 2010); ii) the GL shows high expression of NMDARs (Monaghan and Anderson, 1991) and of the neuronal isoform of NOS (nNOS) (Southam et al., 1992); iii) and GrCs produce and release NO following high frequency MFs stimulation (Maffei et al., 2003). It is therefore compelling to investigate the role of the GL in cerebellar NVC and its contribution in originating BOLD signals.

Chapter 2

Scope of the thesis

In this thesis, the attention was focused on the study of the NVC in the GL of the cerebellum (a detailed description of this phenomenon and the structures studied in this work can be found in **chapter 1**) with particular attention to the responses of the vascular system during the activation of the MF input.

The second part of this work (**chapter 4, 5** and **6**) is related to the investigations of the biochemical and molecular pathways of NVC in the cerebellum GL. The biochemical strategies driving this phenomenon were defined through a pharmacological approach coupled to the electrical stimulation of the tissue. Albeit the neurovascular mechanisms as well as the direct involvement of neurons and pericytes in vessel diameter modification have been largely investigated in the ML, there was no data in literature about the role of the GL in this phenomenon so far. Herein, we showed the anatomical interaction between the neurovascular unit components (neurons, brain vessels and pericytes) of the cerebellar cortex and the basic mechanisms of the NVC in the cerebellar GL. After unveiling the signaling pathways of NVC we moved to the next step of the investigation.

The aim of the third part of this work was to investigate the NVC in two different cerebellar regions, the vermis and the hemisphere (**chapter 7** and **8**). Recent fMRI studies on human subjects revealed that cerebellar vermis and hemisphere showed different BOLD responses to the same motor task (Alahmadi et al., 2017). These results suggest that the cerebellum might operate a complex region-specific information processing. Nevertheless, it has to be considered that this difference might arise from diverse cortico-cerebellar inputs. Here, in order to describe the neurophysiological basis of the different BOLD signals, we studied capillary responses to different patterns of neuronal activation in the cerebellar GL of both vermis and hemisphere. Our results strongly stand for a region-dependent NVC in the cerebellum, with different neurovascular responses, allowing to infer that a cerebral cortex-independent information processing in the cerebellum is responsible for the different BOLD signals observed in vermis and hemisphere.

In conclusion, **chapter 9** contains a general discussion about the data showed in our work in order to summarize the findings reported in the previous chapters.

Chapter 4, **5** and **6** consist respectively of one already published letter, abstract and paper about the investigation of the biochemical and molecular pathways of NVC in the GL of cerebellum. **Chapter 7** and **8** consist of one *in press* abstract and one *in preparation* paper about the investigation of NVC in cerebellar vermis and hemisphere.

Candidate contribution to the thesis

This thesis was realized autonomously by the candidate Giuseppe Gagliano as doctoral dissertation of the work performed during his three years of PhD. The introduction (**chapter 1**) was obtained from scientific literature research of papers related to the field of interest and their interpretation. **Chapter 3** included the proceedings of samples preparation for experiments and the electrophysiological techniques used by the candidate during the three years of PhD. In this thesis, results were divided into two studies. The first part of results (**chapter 4, 5** and **6**) is related to the investigations of biochemical pathways involved in cerebellar NVC. Here, the candidate collected and analyzed data reported in the published letter, abstract and paper, wrote the abstract (**chapter 5**) and partly contribute to the drafting of the manuscript (**chapter 6**) (already published in *Journal of Neuroscience*) in which he was co-author because of his equal contribution together with the first author to this paper. The second part of results (**chapter 7** and **8**) contained recent studies about the investigations of NVC in two different regions of the cerebellum. All data collection, analysis, interpretation, abstract (**chapter 7**) and paper (**chapter 8**) writing were realized by the candidate during the last part of the PhD program. In conclusion, Giuseppe Gagliano highly contributed to this work reaching more results than expected during the three years of the project.

Chapter 3

Methods

3. Materials and methods

Experiments were performed on 17-23 days old Wistar rats or C57BL/6 mice of both sexes, depending on the working project. The animals were located in cages in which water and food were available *ad libitum*. The day-night cycle was 12 hours (12 hours light from 06.00 am - 06.00 pm, 12 hours dark from 06.00 pm - 06.00 am). All experimental protocols were conducted according to the international guidelines of the European Directive 2010/63/EU on the ethical use of animals and were approved by the local ethical committee of the University of Pavia and by the Italian Ministry of Health (authorization n. 645/2017-PR).

3.1 Cerebellar slices preparation

Parasagittal slices were obtained from the cerebellum of rats or mice and were used in two independent sets of experiments. Animals were anesthetized with halothane (Sigma Aldrich) and killed by decapitation. Then, acute slice of 220μm thickness were cut in cold Krebs solution with a vibroslicer (LEICA VT1200S) and were maintained for 1h in the same solution in order to recovery from the slicing procedure. Krebs solution used for cutting and experimental procedures had the following composition (mM): 120 NaCl, 2 KCl, 1.2 $MgSO_4$, 26 $NaHCO_3$, 1.2 KH_2PO_4, 2 $CaCl_2$, and 11 glucose, and was equilibrated with 95% O_2/5% CO_2 (pH 7.4). For the sets of experiments on rats, cerebellar slices were preincubated for 1 hour in 75 nM U46619 (Tromboxane A_2 mimetic) or 200 μM L-NAME (N-ω-nitro-$_L$-arginine methyl ester hydrochloride), when specified, or 100 μM D-APV (D-(-)-2-Amino-5-phosphonopentanoic acid)+ 50 μM 7ClKyn (7-chlorokynurenate), or 10 μM ODQ (1H-[1,2,4]Oxadiazolo[4,3-a]quinoxalin-1-one), or 500 μM MCPG ((R,S)-α-Methyl-4-carboxyphenylglycine) + 300 μM CPPG ((RS)-α-Cyclopropyl-4-phosphonophenylglycine), were added to the extracellular solution. These substances were obtained from Sigma Aldrich except U46619, L-NAME, D-APV, 7-Cl-Kyn, MCPG, CPPG, and ODQ (Abcam).

Finally, slices were transferred to a recording chamber (2ml) mounted on the stage of an upright microscope (Slicescope; Scientifica) (Fig. 1.8) where Krebs solution was perfused (2ml/min) with an external peristaltic pump (ISMATEC) and maintained at 32°C or 37° (according with the different sets of experiments) with a Peltier feedback temperature controller (TC-324B; Warner Instrument Corporation). At the end of this process, slices were ready for experimental protocols.

3.2 Capillary diameter changes observation in the GL of the cerebellum

Cerebellar slices of both rats and mice obtained as described above were transferred to a recovery chamber with Krebs solution in which 75nM U46619 (thromboxane agonist) was added in order to restore the original vascular tone, loss during the slicing procedure. Slices incubation with U46619 for 1 h is essential in *ex vivo* experiments where vessels lack their intraluminal flow and pressure.

We exploited a sophisticate bright-field imaging system, consisting of an upright SLICESCOPE microscopy (Scientifica Ltd) with a 60X objective (LumPlanFl 60X/0.90 W; Olympus) (Fig. 1.9) mounted on an anti-vibration table, to identify microvessels and pericytes in the GL.

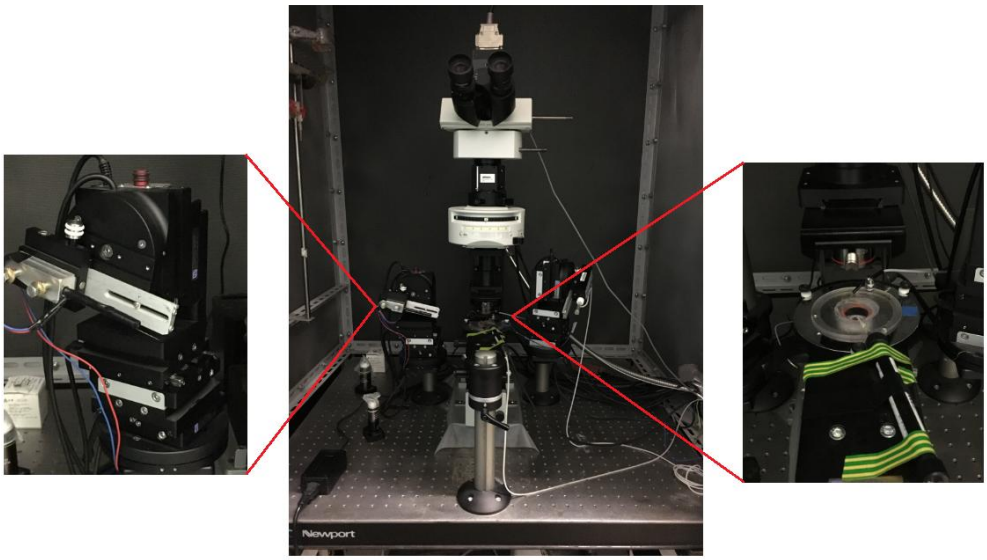

Figure 1.9 | Imaging system. The microscope was mounted on an antivibration table. The slices were mantained at 32° or 37° C in the recovery chamber of the microscope, depending on the experimental procedure (*right*). The electrode of stimulation was mounted near the microscopy (*left*) and moved by an external manipulator.

In order to investigate capillary responses to neural activity in cerebellar GL, we stimulate MFs with 12-15V intensity, at 50 Hz frequency for 35s, using a bipolar tungsten electrode (Warner Instruments), in rat/mice cerebellar slices. In the case of mice, the experimental protocols consisted in the stimulation of MFs with 12-15V of intensity using different frequencies (6, 20, 50, 100 and 300 Hz) for 35s at physiological temperature (37°C) (Fig. 1.10).

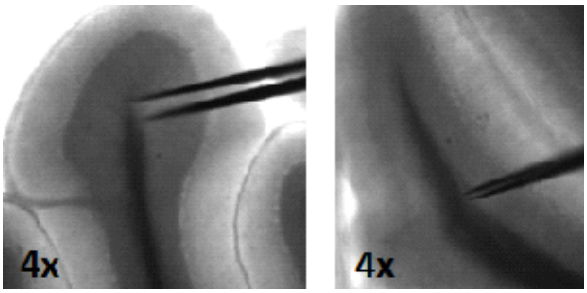

Figure 1.10 | Cerebellar slices of mice. MFs stimulation using a bipolar tungsten electrode in vermis lobule V (*left*) and hemisphere lobule VI (*right*) of cerebellar slices of mice.

Time-lapse image acquisitions of capillary diameter changes were obtained through a CCD camera (DMK41BU; Imaging Source) and the IC-capture 2.1 software (Imaging Source). Although MFs were stimulated for 35s, the duration of the acquisition was set at 130s in order to observe vessels behavior before and after electrical stimulation. The acquisition rate was set at 30s per image or 1s per image, depending on the experimental protocol, and the exposure time was set at 5ms.

The experiments were performed only in microvessels with an internal diameter <10μm and only one capillary per slice was used.

3.2.1 Images acquisition and analysis

In order to estimate the distance between the stimulating electrode and the capillary chosen for the experiment, we used a calibration slide before applying the experimental protocol. The slide consists of a 1mm ruler observable under the microscope system (Fig. 1.11). The distance between each bar allows to calibrate the distances showed by the computer monitor and to convert these measures with the real distance in μm between the stimulating electrode and the vessel.

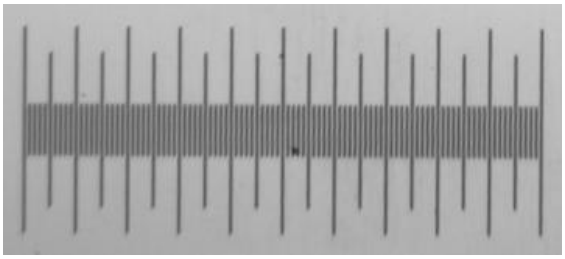

Figure 1.11| Calibration slide. The slide used before the experiments allowed to measure the real distance between the electrode of stimulation and capillaries. The total length of the slide was of 1mm.

Data were analyzed manually using ImageJ. The offline measuring tool of this software permits to place a line perpendicular to the capillary walls in the acquired sequence of images and to measure the inner caliber length in all images of the acquisition file (Fig. 1.12). Moreover, the adjust tool allows to modify the brightness and the contrast of the acquired images to better identify the walls of the capillary for a more accurate analysis (Fig. 1.13). Statistical comparisons were carried out using paired or unpaired Student's *t*-test and ANOVA test. Statistical significance was assessed when $p<0.05$. Data in the text are reported as mean ± SEM.

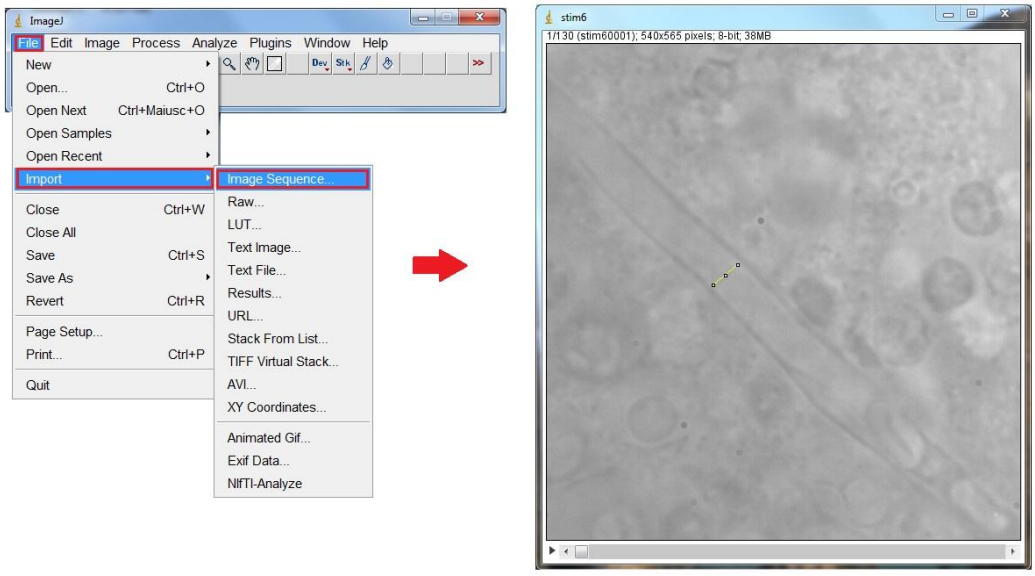

Figure 1.12 | ImageJ tool for image analysis. The software permit to open the acquisition file as images sequence and to analyze the inner diameter of the vessel through the yellow bar showed in the figure.

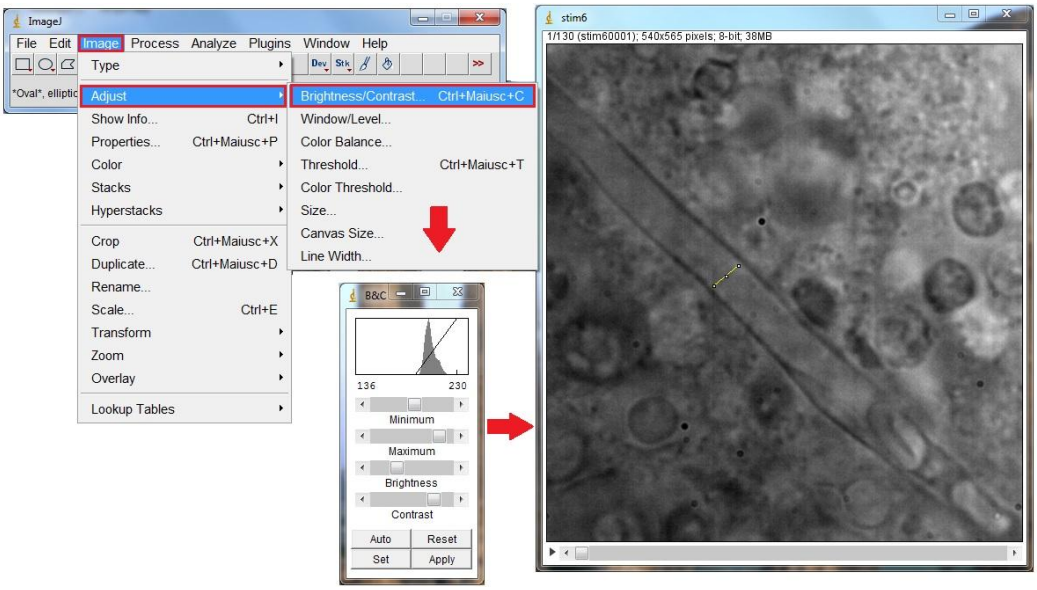

Figure 1.13 | ImageJ tool for images modification. The tool permit to change the brightness and the contrast of the images sequence before to measure the diameter modification of the capillary.

3.3 DAF-FM signals in the cerebellar GL

After the slicing procedure, cerebellar slices from rats where recovered for 1h with oxygenated Krebs solution added with 75 nM U46619 and 12 µM DAF-FM (Invitrogen, Thermo Fisher), for 40 minutes, for the staining procedure. At the end of the staining the slices were transferred to a recovery chamber with Krebs and U46619 for at least 20 minutes. The fluorescence signal of DAF-FM reaction with nitrogen derivatives, such as N_2O_3, NO_2 or ONOO, reflects NO released upon MF stimulation in the cerebellar GL. The excitation light (495/20 nm) of a MHAB-150W source (Moritex) was delivered to the tissue and then collected to the camera through a system of filters (excitation, dichroic and emission filters). The wavelengths of dichroic and emission filter were respectively 515 nm LP and 530/30 nm. The fluorescence was detected using a MICAM01 CCD camera (Brainvision), controlled by the Brainvision software for remote acquisition and shuttering. The acquisition rate was set at 15ms (339 frames for about 5s recording).

In the case of slices incubated with 200 µM L-NAME or 100 µM D-APV + 50 µM 7ClKyn in Krebs solution, recordings were acquired after 1h or 20 min of drug exposure, respectively. The

fluorescence traces were analyzed with Clampfit (pClamp10, Molecular Devices) and using *ad-hoc* Matlab routines (Mathworks).

3.4 Recordings of GL activity in the cerebellum

Parasagittal mouse cerebellar slices were also used to investigated the activity of GL during MFs stimulation in both vermis lobule V and hemisphere lobule VI. After the slicing procedure and 1-hour recovery and incubation with U46619 (75 nm), the slices were ready for experimental manipulation. Cerebellar neuronal activity in the GL was recorded as local LFP during single impulse stimulation of vermis and hemisphere MFs.

In order to investigated neuronal activity, we exploited a cutting-edge electrophysiology system called BioCAM X (3Brain AG, Wädenswil, Switzerland) (Fig. 1.14). This system is an HD-MEA (high-density multi-electrode array) and consist of a MEA platform, a CMOS microchip (Arena probe) and a workstation computer with the BrainWave X running software. The platform presents a bay in which the microchip for electrical recordings was inserted and locked (Fig. 1.14). The microchip consists of a glass chamber (diameter 25mm; height 7mm) containing the probe (4096 recording microelectrodes arranged in a 64 x 64 matrix in an area of 2.67mm x 2.67mm). The electrode size is 21μm x 21 μm with a pitch of 42 μm. This system was completed with a perfusion system consisting of an external peristaltic pump (ISMATEC) where Krebs solution was perfused (2ml/min) and maintained at 37° with a Peltier feedback temperature controller (TC-324B; Warner Instrument Corporation). Moreover, the stimulation system consisted of the integrated stimulator unit in the BioCAM X, connected to a bipolar tungsten electrode (Warner Instruments) mounted over an external micromanipulator (PatchStar, Scientifica Ltd) (Fig 1.15, left).

Firstly, cerebellar vermis or hemisphere slice was carefully positioned over the probe and stabilized with a platinum anchor to improve tissue coupling with the electrode array. Secondly, the electrode was positioned on the MFs of vermis lobule V or hemisphere lobule VI. Finally, we applied the stimulation protocol (delivery current pulses of 50 μA for 200 μs) and acquired LFP responses with BrainWave X software (Fig. 1.15, right). All signals were sampled at 17840.7 Hz/electrode. Data export and analysis were conducted with *ad-hoc* Matlab routines (Mathworks).

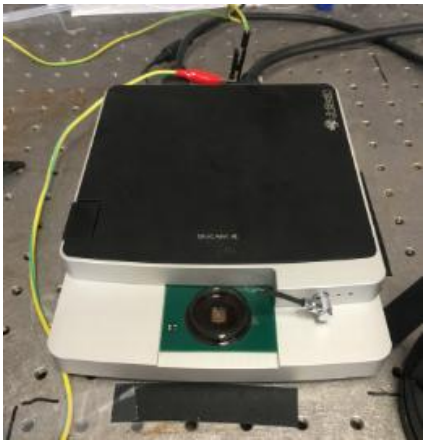

Figure 1.14 | Multielectrode array system. High density MEA (BioCAM X) used for LFP recordings in the GL of mouse cerebellar slices. In green, the CMOS chip with the recording chamber and the microelectrodes.

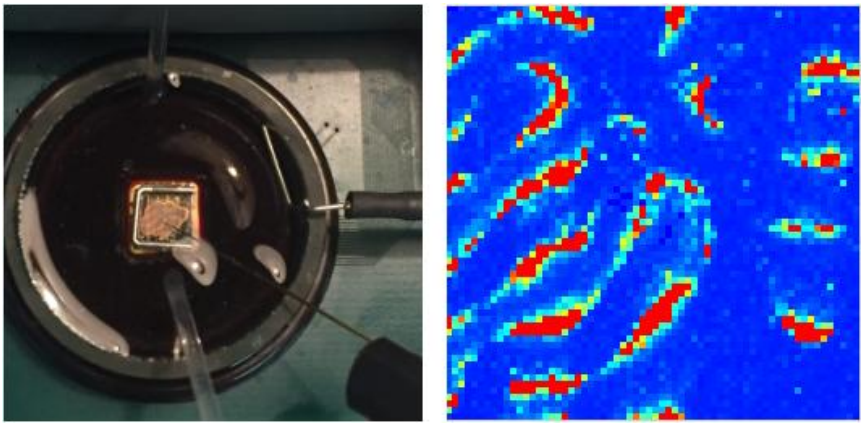

Figure 1.15 | Recording chamber of HD-MEA and data acquistion. Microchip probe and cerebellar slice (in this case vermis) with metallic anchor and stimulating electrode positioned on lobule V. Adapted glass capillaries were used to perfuse Krebs solution during the experiments (left). Brainwave software rendering of the cerebellar slice on the left, during spontaneous activity. In red, autorhythmic spiking activity of PCs (right).

Chapter 4

Neurovascular coupling at the cerebellar granular layer

4. Neurovascular coupling at the cerebellar granular layer

Lisa Mapelli [1,2], Teresa Soda [1], Giuseppe Gagliano [1], Francesco Moccia [3], Egidio D'Angelo [1,4]

[1]Dept of Brain and Behavioral Sciences, University of Pavia, Pavia, Italy

[2]Museo Storico della Fisica e Centro Studi e Ricerche Enrico Fermi, Rome, Italy

[3]Laboratory of General Physiology, Dept of Biology and Biotechnology "Lazzaro Spallanzani", University of Pavia, Italy

[4]Brain Connectivity Center, C. Mondino National Neurological Institute, IRCCS Pavia, Italy

Authors contribution: F.M. and E.D. designed research; L.M., T.S. and G.G. performed research; L.M., T.S. and G.G. analyzed data; L.M, F.M. and E.D. wrote the letter.

The authors declare no competing financial interests.

Vasc. *Pharmacol*. 2015; 75:64.

DOI:10.1016/j.vph.2015.11.057.

4.1 Objectives

The tight coupling between local neuronal activity and local cerebral blood flow, or neurovascular coupling (NVC), originates the blood-oxygen-level-dependent (BOLD) signals used by neuroimaging techniques to map changes in brain activity. In the cerebellum, the NVC has been investigated in the molecular layer, showing poor association with Purkinje cells firing, which represent the sole output of the cerebellar cortex. At the present no information is available about the control of microvascular tone in the granular layer, at the cerebellar input stage. This is surprising since granule cells (GrCs) are the most abundant brain neurons and produce nitric oxide (NO) in response to mossy fibers (MF)stimulation.

4.2 Materials and methods

Herein we exploited time-lapse bright-field microscopy, using a 60x magnification, on juvenile rat cerebellar slices in order to assess whether and how the MF- mediated activation of the granular layer modulates arteriole diameter changes. In particular, MFs were electrically stimulated with 30s 50Hz train pulses using a bipolar tungsten electrode. The slices were pre-incubated with

the vasoconstrictor U46619, since the vascular tone is usually disrupted due to the slicing procedure.

4.3 Results

MF stimulation determined a 20% increase in the arteriolar diameter in the granular layer. This vasodilation was abolished both by perfusion of NMDA receptor blockers (APV and 7-clorokynurenic acid), and in the presence of a NO synthase (NOS) blocker (L-NAME).

Interestingly, in both cases the vasodilation was turned into vasoconstriction. This switch proved to be mostly dependent on the vasoconstrictor 20-hydroxyeicosatetraenoic acid (20-HETE), whose synthesis is known to be blocked in the presence of NO.

4.4 Conclusions

These data strongly suggest that synaptic activation of GrCs causes arteriolar vasodilation in a NMDA and NO dependent manner. Notably, GrCs are known to produce NO through an activity-dependent and NMDA-dependent pathway, and this mechanism proved to be critical for MF-GrC synaptic plasticity. It would be therefore intriguing to correlate arteriolar diameter changes in relation to different patterns of granular layer activation. These data provide new insights into the NVC at the granular layer, that is likely to majorly contribute to the cerebellar BOLD signals.

Chapter 5

Neurovascular coupling in the cerebellar granular layer

5. Neurovascular coupling in the cerebellar granular layer

Giuseppe Gagliano[1], Lisa Mapelli[1,2], Teresa Soda[1,2], Umberto Laforenza[3], Francesco Moccia[4], Egidio D'Angelo[1,5]

[1]Dept of Brain and Behavioral Sciences, University of Pavia, Pavia, Italy

[2] Museo Storico della Fisica e Centro Studi e Ricerche Enrico Fermi, Rome, Italy

[3]Dept of Molecular Medicine, University of Pavia, Pavia, Italy

[4]Dept of Biology and Biotechnology "L. Spallanzani", University of Pavia, Pavia, Italy

[5] Brain Connectivity Center, C. Mondino National Neurological Institute, Pavia, Italy

Authors contribution: F.M. and E.G. designed research; G.G., L.M. and U.L. performed research; G.G., L.M. and T.S. analyzed data; G.G., L.M. and E.D. wrote the abstract.

The authors declare no competing financial interests.

Acknowledgments. This work was supported by: European Union grant Human Brain Project (HBP-604102) to ED and Fermi grant [13(14)] to ED and LM.

Front. Cell. Neurosci. Conference Abstract: The Cerebellum inside out: cells, circuits and functions.

DOI:10.3389/conf. fncel.2017.37.000025.

5.1 Introduction and methods

The tight coupling between neuronal activity and cerebral blood flow (CBF) is called neurovascular coupling (NVC). This phenomenon controls blood vessel diameter to ensure the proper supply of oxygen and nutrients to the brain and contributes to generate the BOLD (blood-oxygenation-level-dependent) signals in functional magnetic resonance imaging (fMRI). The NVC has been investigated in several brain regions, but its neuronal drive and biochemical pathways in the cerebellum are still unclear. In particular, attention has been mostly given to the cerebellar molecular layer components, as parallel fibers (Bouvier et al., 2016a), local interneurons (Akgören

et al., 1994), and Purkinje cells (where NVC was found dissociated from spiking activity, (Thomsen et al., 2004). This may be due to the inability of these cells to release nitric oxide (NO), a well known vasoactive agent. Surprisingly enough, there is no information about the role of the granular layer in this phenomenon, even though granule cells (GrCs): i) are the most abundant brain neurons and the most energy consuming elements in the cerebellum (Howarth et al., 2010), ii) show a high expression of NMDA receptors (NMDARs) (Monaghan and Anderson, 1991) and of the neural isoform of nitric oxide synthase (nNOS) (Southam et al., 1992), and iii) produce and release NO following high frequency mossy fibers (MFs) stimulation (Maffei et al., 2003). NO is also implicated in long-term synaptic plasticity at the MF-GrC connection in the cerebellar granular layer (D'Angelo, 2014).

Therefore, the granular layer is particularly suitable for the study of NVC mechanisms and it was then compelling to investigate its role in cerebellar NVC. At first, we described the vascular organization of the rat cerebellar cortex in immunostained slices. Secondly, we investigated whether and how synaptic activity was coupled to vascular motility in the granular layer, by combining bright-field microscopy an NO-related imaging techniques. We focused our attention on MF-GrC synapses (the cerebellar input stage) and on capillaries, since these vessels are able to change their lumen diameter earlier than upstream arterioles, in response to neuronal activity and following pericytes activation (Hall et al., 2014).

5.2 Results

In immunostained cerebellar slices, the molecular layer showed a more regular vascular architecture compared to the granular layer, with arterioles originating from the surface of the lamella, penetrating deep into the layer and giving off capillaries (Fig.1A). In the granular layer, these capillaries (inner diameter 4.23±0.29 μm, n=26) are surrounded by GrCs and are in close contact with pericytes (Fig. 1B, arrow).

In slices treated with the thromboxane A2 agonist (U46619; 75nM) to restore the vascular tone, MFs stimulation (35s at 50Hz, 15V) induced a rapid initial vasodilation followed by a slower increase in lumen diameter at pericytes location (10.89±2.35%, n=13; p=0.00006) (Fig. 2).The vasodilation was converted into vasoconstriction in the presence of NMDARs and NOS inhibitors (respectively 100μM D-APV+50μM 7-ClKyn; -5.9±1.8%, n=7; p=0.02 and 200μM L-NAME; -9.0±1.4%, n=9; p=0.000004) (Fig. 3A-B) and partially turned into vasoconstriction in presence of guanylyl cyclase (sGC) inhibitor (10μM ODQ; -3.6±0.9%; n=10; p=0.005) (Fig. 3C). Moreover, L-NAME perfusion alone reduced capillary diameter (-55.7±2.8%; n=8; p=0.004) (Fig. 3b inset), reflecting a tonic NO release by vascular endothelial cells. In the presence of TTX (4μM), the

stimulation failed to cause changes in capillary diameter confirming the synaptic drive of this process (Fig. 2). Therefore, MF-GrC synapses activation, and NMDARs, NOS and sGC recruitments are necessary to increase the local CBF. To further investigate this pathways, slices were pre-incubated with 12 μM of the NO production-related fluorescent dye DAF-FM. The granular layer responded to MFs stimulation with a fluorescence peak ($0.029\pm0.003\Delta F/F_0$) (Fig. 4A) which was absent in the presence of NMDARs and NOS inhibitors (respectively 100μM D-APV+50μM 7-ClKyn; -0.007±0.006ΔF/F0*ms; n=6 and 200μM L-NAME; 0.001±0.003 ΔF/F0*ms; n=7) (Fig. 4B, top). Moreover, in control condition the integral of the fluorescence signal showed a trend to increase, suggesting a residual NO production in the granular layer, (Fig. 4A, red trace) that was no longer observed in the presence of NMDARs and NOS blockers (Fig 4B, bottom). Moreover, the distance from the stimulating electrode where fluorescence peaks were observed was comparable to the distance where vessels showed the vasoactive response (158±10μm vs 191±10μm; n=20 and n=50, respectively).Interestingly, the fluorescence signal kinetics and the linear fitting of the vessel dilation rate showed a similar trend (p=0.37), allowing to speculate that the kinetics of vessel dilation might be dictated by the rate of NO production.

Besides promoting vasodilation, NO released by granular layer neurons could block the synthesis of the vasoconstrictor 20-HETE (Attwell, 2010). MFs stimulation during the perfusion of 20-HETE synthesis inhibitor (1μM HET-0016) and of metabotropic glutamate receptors (mGluRs) inhibitors (500μM MCPG+300 μM CPPG) respectively reduced (-4.2±1.9%; n=9; p<0.007) (Fig. 5A) and abolished (1.1 ± 1.5%; n=15; p=0.9) (Fig. 5B) the vasoconstriction shown in the presence of L-NAME. These data support the conclusion that mGluRs drove the synthesis of 20-HETE during synaptic transmission at the MF-GrC relay.

5.3 Discussion and conclusion

Herein, we demonstrated that synaptic activation of the cerebellar granular layer caused a NMDARs/NOS-dependent capillary vasodilation that required cGMP synthesis by sGC, presumably in pericytes. Our results are also compatible with a role of glial cells in mediating the vasoconstriction through a mGluRs-dependent mechanism leading to20-HETE synthesis. Actually, in pericytes 20-HETE is synthesized from the arachidonic acid released after mGluRs activation on astrocytes (Sweeney et al., 2016). Therefore, synaptic activity and glutamate release could activate two different competing signaling pathways (promoting either vasorelaxation or vasoconstriction), both involved in the CBF control. In conclusion, GrCs are likely to play a pivotal role in the NVC in the cerebellar circuit. These cells are also known to elaborate and store complex spatio-temporal patterns at the cerebellar input stage (D'Angelo and De Zeeuw, 2009). Taken together, these

evidences strongly stand for a huge role of GrCs in the coordination of computational and metabolic functions in the cerebellar network. Notably, since the granular layer regulation of local microvessels caliber might contribute to change the cerebellar BOLD signals (Diedrichsen et al., 2010), our results may help cerebellar fMRI data analysis, besides shedding new light on the mechanisms of NVC in this brain structure.

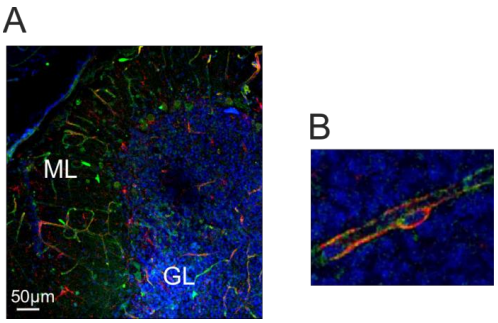

FIGURE 1 | Identification of capillary microvessels in the cerebellar granular layer. A) ML= molecular layer; GL= granular layer. B) granule cells nuclei (blue), vessel walls (green), pericytes (red).

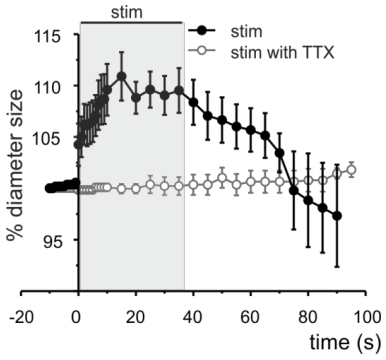

FIGURE 2 | MFs stimulation determines capillary vasodilation. MFs stimulation caused an increase in vessel diameter that is abolished by TTX perfusion.

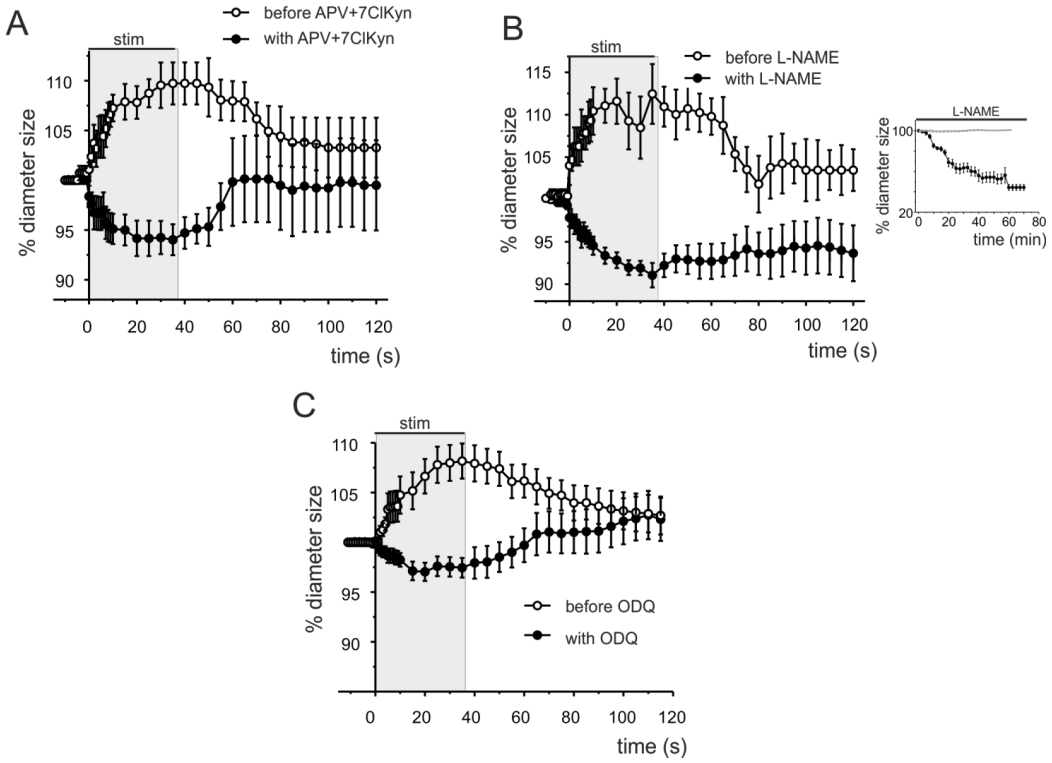

FIGURE 3 | NMDARs, NO and cGMP mediate the vasodilation. A) MFs stimulation turned vasodilation into vasoconstriction, in the presence of NMDARs blockers. B) The vasodilation war turned into vasoconstriction, in presence of NOS inhibitor during MFs stimulation. C) The perfusion of sGC blocker caused a vasoconstriction, during MFs stimulation.

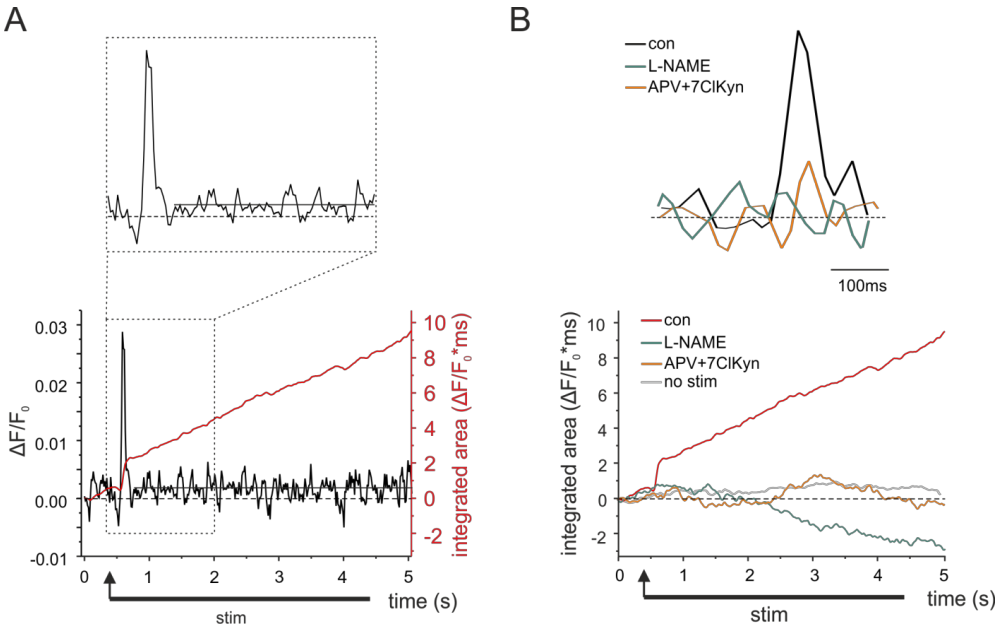

FIGURE 4 | Related NO production in the granular layer. A) DAF-FM fluorescence signal during MFs stimulation (black trace); integral of the fluorescence signal (red trace) during MFs stimulation. B) Top: DAF-FM fluorescence signal in control condition (black) and in presence of L-NAME (green) and of APV+7ClKyn (orange) during MFs stimulation; Bottom: Integral of the fluorescence signal in control condition (red), in presence of L-NAME (green) and of APV+7ClKyn (orange) and without MFs stimulation (grey).

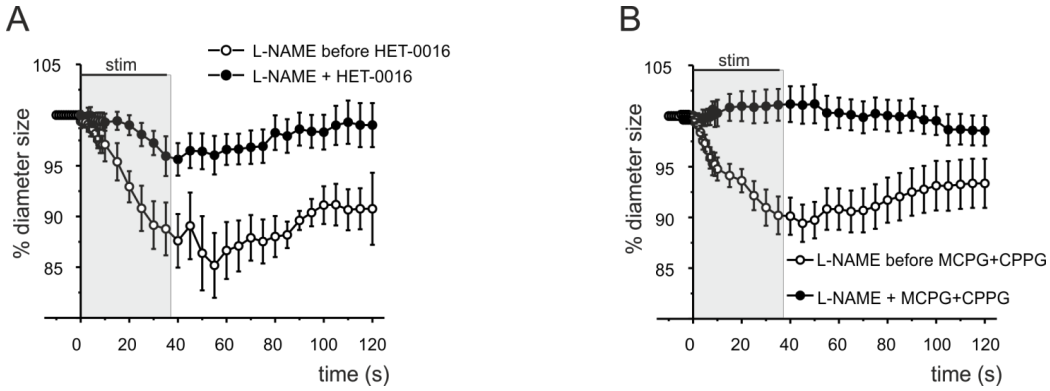

FIGURE 5 | 20-HETE and mGluRs mediate vasoconstriction. A) MFs stimulation in the presence of 20-HETE synthesis inhibitor significantly reduced vasoconstriction. B) MFs stimulation in the presence of mGluRs inhibitors abolished the vasoconstriction.

Chapter 6

Granular layer neurons control cerebellar neurovascular coupling through an NMDA receptor / NO – dependent system

6. Granular layer neurons control cerebellar neurovascular coupling through an NMDA receptor / NO – dependent system

Lisa Mapelli[1,2,], Giuseppe Gagliano[1,*], Teresa Soda[1,2], Umberto Laforenza[3], Francesco Moccia[4,§], Egidio U. D'Angelo[1,5,§]*

[1]Dept of Brain and BehavioralSciences, University of Pavia, 27100 Pavia, Italy
[2] Museo Storico della Fisica e Centro Studi e Ricerche Enrico Fermi, 00184 Rome, Italy
[3] Dept of Molecular Medicine, University of Pavia, 27100 Pavia, Italy
[4] Dept of Biology and Biotechnology "L. Spallanzani", University of Pavia, 27100 Pavia, Italy
[5] Brain Connectivity Center, C. Mondino National Neurological Institute, 27100 Pavia, Italy
***** co-first authors
§ co-last authors

Author contributions: F.M. and E.U.D. designed research; L.M., G.G. and U.L. performed research; L.M., G.G. and T.S. analyzed data; L.M., F.M. and E.U.D. wrote de paper.
***** Lisa Mapelli and Giuseppe Gagliano equally contributed to this work
***** Francesco Moccia and Egidio Ugo D'Angelo are co-senior authors

The authors declare no competing financial interests.

Acknowledgments. This work was supported by: European Union grant Human Brain Project (HBP-604102) to ED and Fermi grant [13(14)] to ED and LM.

The Journal of Neuroscience. 2017 Feb 1; 37(5):1340-1351

doi: 10.1523/JNEUROSCI.2025-16.

6.1 ABSTRACT

Neurovascular coupling (NVC) is the process whereby neuronal activity controls blood vessel diameter. In the cerebellum, the molecular layer is regarded as the main NVC determinant. However, the granular layer is a region with variable metabolic demand caused by large activity fluctuations, that shows a prominent expression of NMDA receptors (NMDARs) and nitric oxide synthase (NOS) and is therefore much more suitable for effective NVC. Here we show that, in the granular layer of acute rat cerebellar slices, capillary diameter rapidly changes following mossy fiber stimulation. Vasodilation required neuronal NMDARs and NOS stimulation and subsequent guanylyl cyclase activation that probably occurred in pericytes. Vasoconstriction required metabotropic glutamate receptors and CYP ω-hydroxylase, the enzyme regulating 20-HETE production. Therefore, granular layer capillaries are controlled by the balance between vasodilating and vasoconstriction systems, that could finely tune local blood flow depending on neuronal activity changes at the cerebellar input stage.

6.2 Significance statement

The neuronal circuitry and the biochemical pathways that control local blood flow supply in cerebellum are unclear. This is surprising given the emerging role played by this brain structure not only in motor behavior, but also in cognitive functions. While previous studies focused on the molecular layer, here we shift attention onto the mossy fiber-granule cell (GrC) relay. We demonstrate that GrC activity causes a robust vasodilation in nearby capillaries via the *N*-methyl-D-aspartate receptors-neuronal nitric oxide (NO) synthase signaling pathway. At the same time, metabotropic glutamate receptors mediate 20-HETE-dependent vasoconstriction. These results reveal a complex signaling network which hints for the first time at the granular layer as a major determinant of cerebellar blood-oxygen-level-dependent (BOLD) signals.

6.3 INTRODUCTION

Neurovascular coupling (NVC) is the mechanism whereby changes in regional cerebral blood flow (CBF) ensure the proper supply of oxygen and glucose in response to local neuronal activity. This coupling between neuronal activity and the hemodynamic response generates the blood-oxygen-level-dependent (BOLD) signals used in functional magnetic resonance imaging (fMRI) (Iadecola, 2004). Therefore, determining the cellular and molecular underpinnings of NVC is essential not just to understand local blood-flow regulation but also to interpret BOLD signals as a function of brain activity (Logothetis, 2008; Hillman, 2014).

The vascular tone is determined by the balance between competing vasoconstrictor and vasodilator factors. The nonconventional gaseous neurotransmitter, nitric oxide (NO), contributes to vasodilation in several brain regions (Iadecola, 2004). NO production is triggered by *N*-methyl-D-aspartate (NMDA) receptors (NMDARs)-mediated Ca^{2+} inflow, which activates the Ca^{2+}-dependent neuronal isoform of NO synthase (nNOS) (Attwell et al., 2010). In the cerebellum, the mossy fiber (MF)-granule cell (GrC) relay receives and processes the incoming afferent signals before relaying them to Purkinje cells - which constitute the sole output of the cerebellar cortex – through GrC parallel fibers (Mapelli et al., 2015). So far, attention has been mostly given to the role of nNOS revealed in parallel fibers (Bouvier et al., 2016b) and molecular layer interneurons, such as stellate cells and basket cells. Since nNOS is absent in Purkinje cells, parallel fibers and molecular layer interneurons have long been regarded as the main sources of NO for cerebellar NVC (Akgoren et al., 1994; Yang et al., 1999). Conversely, the role played by GrCs in the regulation of local microvessels has been neglected. This is surprising for several reasons. First, the cerebellum granular layer has the highest expression of NMDARs (Monaghan and Anderson, 1991) and nNOS (Snyder, 1992; Southam et al., 1992) in the whole brain (*de facto* also the nNOS present in parallel fibers belongs to GrCs). What is the reason for this high expression is only party understood, although GrCs-derived NO has been implicated in long-term synaptic plasticity (Maffei et al., 2003; D'Angelo, 2014). Secondly, GrCs are the most abundant brain neurons (3-7 $10^6/mm^3$) and recent calculations suggested that they are the most energy consuming elements in the cerebellum (Howarth et al., 2010). Thirdly, once stimulated, MFs release glutamate that excites postsynaptic GrCs by activating NMDA and non-NMDARs (D'Angelo et al., 1999). NMDARs-mediated Ca^{2+} entry activates nNOS and leads to NO production (Maffei et al., 2003). Interestingly, the first demonstration at all that NO could act as a vasodilator in the brain was provided in seminal papers showing that cerebellar GrCs suspensions released NO upon NMDA report stimulation thereby causing smooth muscle relaxation through a guanylil cyclase-dependent mechanism (Garthwaite and Garthwaite, 1987; Garthwaite et al., 1989). Reasonably, GrCs-released NO could induce vasodilation in adjacent microvessels, thereby increasing local CBF. Fourthly, granule cells are almost silent at rest and respond to incoming MF bursts (Chadderton et al., 2004; Rancz et al., 2007b; Powell et al., 2015) generating dense activity clusters (Diwakar et al., 2011), thereby implying a local neuron-gated mechanisms for blood-flow regulation. Finally, whereas NO only plays a permissive role in the neocortex, NO is the primary mediator of the increase in CBF occurring in response to cerebellar activation (Akgoren et al., 1994; Yang and Iadecola, 1997). This would, however, be hard to explain by considering the molecular layer only, where NVC is dissociated from the spiking activity of Purkinje cells, which cannot produce NO (Mathiesen et al.,

1998; Caesar et al., 2003; Thomsen et al., 2004). Despite this body of evidence, the relationship between GrCs and CBF has hitherto remained undetermined.

Therefore, we investigated whether and how synaptic activity was coupled to vascular motility in the granular layer by combining bright-field microscopy and fast NO imaging in acute cerebellar slices in rats. We focused on capillaries, since stringent evidence has been provided demonstrating that they aid arterioles in initiating functional imaging signals in the cerebellum (Hall et al., 2014)

6.4 METHODS

6.4.1 Preparation of acute cerebellar slices

Acute rat cerebellar slices were obtained as reported previously (D'Angelo et al., 1995; Armano et al., 2000; Mapelli et al., 2009). Briefly, 17- to 23-days-old Wistar rats of both sexes were anesthetized with halothane (Aldrich, Milwaukee, WI) and killed by decapitation. Parasagittal 220 μm-thick acute slices were cut from the cerebellar vermis in cold Krebs solution and recovered for at least 1 hour before being transferred to a 2-ml recording chamber mounted on the stage of an upright microscope (Slicescope, Scientifica Ltd, UK). The preparations were perfused with Krebs solution (2 ml/min) and maintained at 32°C with a Peltier feedback device (TC-324B, Warner Instruments, Hamden, CT). Krebs solution for slice cutting and recovery contained (in mM): 120 NaCl, 2 KCl, 1.2 $MgSO_4$, 26 $NaHCO_3$, 1.2 KH_2PO_4, 2 $CaCl_2$, and 11 glucose, and was equilibrated with 95% O_2-5% CO_2 (pH 7.4). When specified, slices were preincubated for 1 hour in 75 nM U46619 or 200 μM L-NAME. When specified, 100 μM D-APV + 50 μM 7ClKyn, or 10 μM ODQ, or 500 μM MCPG + 300 μM CPPG, were added to the extracellular solution.

All drugs were obtained from Sigma-Aldrich, except U46619, L-NAME, D-APV, 7-Cl-Kyn, MCPG, CPPG, and ODQ (Abcam).

All experimental protocols were conducted in accordance with international guidelines from the European Union Directive 2010/63/EU on the ethical use of animals, and approved by the local ethical committee of the University of Pavia, Italy.

6.4.2 Immunofluorescence

Immunofluorescence of pericytes and capillaries in cerebellar slices was performed as described previously (Mishra et al., 2014). In brief, 220 μm slices were fixed with freshly prepared 4% paraformaldehyde in PBS for 25 min in a Petri dish. Slices were washed three times and then permeabilized and blocked with a solution containing 5% Triton X-100, 10% BSA in PBS overnight at 4°C. Slices were incubated for one day at room temperature on a rotary shaker with

primary antibodies diluted in PBS. Rabbit anti-NG2 chondroitin sulfate proteoglycan (Millipore, cat no. AB5320, 1:200 dilution) was used to stain pericytes and FITC-isolectin B4 (Sigma-Aldrich, cat. no. L2895; a stock solution of 2 mg/ml FITC-IB4 in H_2O was diluted 1:200 in PBS) was used to stain blood vessels. To prevent photobleaching Petri dishes were covered with aluminium foil. After three 15 min washes with PBS, slices were incubated for 4h at room temperature with fluorescent secondary antibody, 1:500 dilution (Jackson ImmunoResearch Inc. cat. no.111-295-045 Rhodamine Red-X-AffiniPure Goat Anti-Rabbit IgG). Slices were then washed three times for 15 min with PBS, mounted on microscope slides, ProLong® Gold antifade reagent with DAPI (Molecular Probes) and coverslips affixed. Slides were examined with a TCS SP5 II LEICA confocal microscopy system (Leica Microsystems, Italy) equipped with a LEICA DM IRBE inverted microscope. Images were acquired with 20X, 40X or 63X objectives and visualized by LAS AF Lite software (Leica Application Suite Advanced Fluorescence Lite version 2.6.0). Negative controls were performed by incubating slices with non-immune serum.

6.4.3 Time-lapse bright-field imaging of granular layer capillaries dynamics

Acute parasagittal cerebellar slices were prepared as previously described. Microvessels in the granular layer were identified using a 60X objective (LumPlanFl 60X/0.90 W, Olympus, Japan) during bright field visual inspection of the granular layer. Only vessels with internal diameter <10 μm were accepted for the experiments. In all cases slices were pre-incubated in 75 nM of the thromboxane agonist U46619, to avoid vessel relaxation due to the slicing procedure and typical of *ex-vivo* conditions, where vessels lack intraluminal flow and pressure. Only one capillary per slice was used for experiments. We focused on capillary sections covered by at least 1-2 pericytes sitting on the abluminal wall. Pericytes were identified by their large soma usually emitting two primary projections along the vessel (Hamilton et al., 2010) (see Fig. 2Bc). In each slice, a suitable capillary was identified and the objective focus was finely adjusted in order to determine the capillary diameter near pericytes, where vasoconstriction was most evident featuring a sphincter-like structure (Peppiatt et al., 2006; Fernandez-Klett et al., 2010). The focal plane on which the capillary diameter was measured, did not necessarily coincide with that of the pericytes, which therefore appear blurred in some images.

Brain slices have long been employed to unveil the molecular pathways and the local microcircuitry involved in NVC (Peppiatt et al., 2006; Rancillac et al., 2006; Hall et al., 2014), but we reasoned that it was physiologically more relevant to assess the effect of synaptic stimulation rather than directly administrating a neurotransmitter (e.g. glutamate), which could cause the unspecific activation of the whole neuronal circuit. MFs stimulation was obtained using a bipolar

tungsten electrode (Warner Instruments, UK) and consisted in 12-15 V stimuli delivered at 50 Hz for 35s. This stimulation protocol allowed vessel tone (either vasodilation or vasoconstriction) to attain near-maximal changes (e.g. observed between 2s and 30s in the case of vasodilation, Fig.2B). The stimulation frequency of 50Hz was chosen in order to efficiently activate NMDARs and calcium entry (D'Angelo et al., 1995; D'Errico et al., 2009). The consequent granular layer responses are likely to span over distances longer than about 200 μm from the stimulating electrode, where vessel responses were detected, as suggested by previous observations using voltage-sensitive dye imaging (Prestori et al., 2013). Time-lapse bright-field acquisitions of capillaries dynamics were obtained through a CCD camera (DMK41BU, Imaging Source, Germany) using the IC-capture 2.1 software (Imaging Source, Germany), acquiring images either every 30s (for >1h acquisition of basal U46619 or L-NAME effects on vessel tone) or every 1s (for acquisitions during and after MFs stimulation) with an exposure time of 5ms. The analysis of capillary inner diameter changes was made offline using the Image J measure tool, by manually placing the measurement line perpendicular to the vessel, at the location where maximal effect was visually detected, as elsewhere described (Hall et al., 2014). The average distance from the stimulating electrode of the vessels used in the analysis was 191±10 μm (n=50). The percentage change in capillary resistance and in blood flow caused by capillary dilation has been calculated according to (Peppiatt et al., 2006; Hall et al., 2014). Statistical comparisons were carried out using the Student's t test (paired or unpaired depending on the applicability). Statistical significance was assessed when $p<0.05$. Data in the text are reported as mean ± SEM.

6.4.4 Contribution of capillary vasodilation to the increase in cerebellar blood flow

Recent work has clearly shown that capillary vasorelaxation initiates before arteriole dilation in the molecular layer of the cerebellum (Peppiatt et al., 2006; Hall et al., 2014; Mishra et al., 2014). The percentage increase in granular layer blood flow produced by capillary vasodilation was evaluated by following the procedure described in (Peppiatt et al., 2006) and (Hall et al., 2014). Peppiatt and coworkers based their calculations on a mathematical model which attributes to the whole capillary bed a resistance that is 45% of the resistance in pre-capillary arterioles and arteries (Lu et al., 2004; Peppiatt et al., 2006). For instance, in slices superfused with U46619, MFs stimulation causes an initial increase in capillary diameter by 5%. According to the Poiseuille's Law ($R=8\eta l/\pi r^4$), this reduces capillary resistance by 17% and, therefore, decreases the total flow resistance by 5.5% (if we assume that the resistance ratio for capillaries is equal to 45:100). It turns out that the blood flow will increase by 5.8% [(100/(100-5.5))*100; see (Peppiatt et al., 2006) for details].

6.4.5 DAF-FM imaging in cerebellar slices

Cerebellar slices were obtained as described above. After 1h recovery from the slicing procedure, the slices were transferred to a continuously oxygenating recovery with Krebs solution added with 75 nM U46619 and 12 μM DAF-FM (Invitrogen, Thermo Fisher), for 40 minutes. After the staining, the slices were transferred to a recovery chamber with Krebs and U46619 for at least 20 minutes, before starting the experiment. DAF-FM fluorescence was detected using a MICAM01 CCD camera (Brainvision), controlled by the Brainvision software for remote acquisition and shuttering. With the 20X objective magnification (Olympus XLUMPlanFl 20X/0.95 W), with a detection matrix of 88x60 pixels, each pixel corresponded to 4.5x4.5μm which resulted in a field of view of about 400x270μm. It should be noted that this fluorescence camera is pixelated and allows to detect fluorescence responses with high spatial resolution. The fluorescence light (source MHAB-150W, Moritex) was delivered to the tissue through an excitation filter (495/20 nm), and collected by the camera through a dichroic filter (515 nm LP) and an emission filter (540/30 nm). The acquisition rate was set at 15ms (339 frames for about 5s recording). In order to obtain a better signal-to-noise ratio, up to 4 acquisitions were averaged in presence and absence of 50 Hz 4s stimulation on MFs. The average fluorescence signal in absence of MFs stimulation was subtracted to the average fluorescence signal during MFs stimulation (see Fig. 4A). The offline analysis was conducted using *ad-hoc* Matlab routines (Mathworks), to extrapolate single and averaged traces to be analyzed in Clampfit (pClamp10, Molecular Devices). When specified, 200 μM L-NAME or a cocktail of 100 μM D-APV and 50 μM 7ClKyn were added to the extracellular solution. In these cases, DAF-FM fluorescence recordings were acquired after 1h or 20 min of drug exposure, respectively. The average distance from the stimulating electrode of the regions where the DAF-FM signal was detected and analyzed was 158±10 μm (n=20), which is in the same range as the distance of the vessels used to analyze microvascular reactivity, as described above (see Fig.4C).

A caveat about the interpretation of DAF-FM measurements is that this dye does not directly react with NO, but rather with a number of nitrogen derivatives, such as N_2O_3, NO_2 or ONOO. Nevertheless, a number of observations converge to indicate that the fluorescence signal recorded in our experiments actually reflects NO released upon MF stimulation. First, the DAF-FM fluorescence signal was fully blocked by L-NAME, that inhibits the NO synthesizing enzyme, NOS, and by APV+7ClKyn, that block NMDA receptors and therefore the calcium influx needed to activate NOS. Secondly, NO release upon high frequency MF stimulation was measured directly using electrochemical probes and, similar to the DAF-FM fluorescence signal, was prevented by L-NAME and APV application (Maffei et al., 2003). Finally, since capillary vasodilation depends on NO, its block by L-NAME confirms that NO was produced during synaptic stimulation.

6.5 RESULTS

6.5.1 Identification of capillary microvessels in the granular layer of the cerebellum

Recent studies have convincingly shown that capillaries can respond to neuronal activity by changing their luminal diameter earlier than upstream arterioles, thereby contributing to initiate cerebellar BOLD signals (Hall et al., 2014; Attwell et al., 2016). This is due to the presence of contractile pericytes, which ensheath the capillary wall from the outside and make direct contact with endothelial cells (Dalkara and Alarcon-Martinez, 2015a; Attwell et al., 2016) controlling microcirculation by sensing the vasoactive messengers released by either neurons or astrocytes located within the neurovascular unit (Peppiatt et al., 2006; Hall et al., 2014). Although this observation has been challenged (Fernandez-Klett et al., 2010; Hill et al., 2015), a subsequent reinterpretation supported again the critical role of pericytes (Attwell et al., 2016). A recent investigation elegantly described the overall architecture of cerebellar microvessels (Kolinko et al., 2016). Here, we focused our attention on intra-parenchymal capillaries (Fig. 1A) that reside in close contact with GrCs (see asterisks in Fig. 1A) and are, therefore, strategically located to rapidly sense any changes in local neuronal activity. Bright-field microscopy revealed that these microvessels have a mean inner diameter of 4.23±0.29 μm (n=26; Fig. 1A), which is well within the range expected for brain capillaries (Attwell et al., 2016), and lack a continuous layer of smooth muscle cells. Visual inspection further identified them as capillaries by the characteristic bump-on-log location of pericytes on the abluminal wall (see arrows in Fig. 1A). Accordingly, cerebellar granular layer capillaries were positive to the labeling with isolectin B4 and the proteoglycan NG2 antibody, which bind to the basal membrane and pericytes (Mishra et al., 2014), respectively (Fig. 1Ba). Capillaries were not enwrapped by a continuous layer of pericytes (Fig. 1Ba and co-localization of isolectin B4 and NG2 antibody staining in Fig. 1Bb), which is fully consistent with their original definition by Zimmermann (Zimmermann, 1923; Krueger and Bechmann, 2010); see (Attwell et al., 2016). Finally, immunostaining with NG2 antibody clearly revealed the conspicuous somata with a bump-on-log morphology from which two thinner processes depart that features capillary pericytes (Fig. 1Bc) (Peppiatt et al., 2006; Attwell et al., 2016). Our subsequent analysis of the cellular and molecular underpinnings of NVC in the cerebellar granular layer was therefore carried out by evaluating the vascular reactivity of these structures.

We also examined cerebellar slices at a lower magnification (20x and 40x) to gain more insights into the differences in the organization of the vascular network between molecular and granular layers. As depicted in Fig. 1Ca, the molecular layer displayed a more regular vascular architecture which consisted of an array of parallel arterioles that originated from the surface of the lamella, penetrated deep into the layer, were interconnected through lateral branches, and gave off

capillaries. Fig. 1Cb shows that the granular layer is fed by the arterioles incoming from the molecular layer that give raise to a diffused network of capillary vessels enmeshed within the highly compacted GrCs.

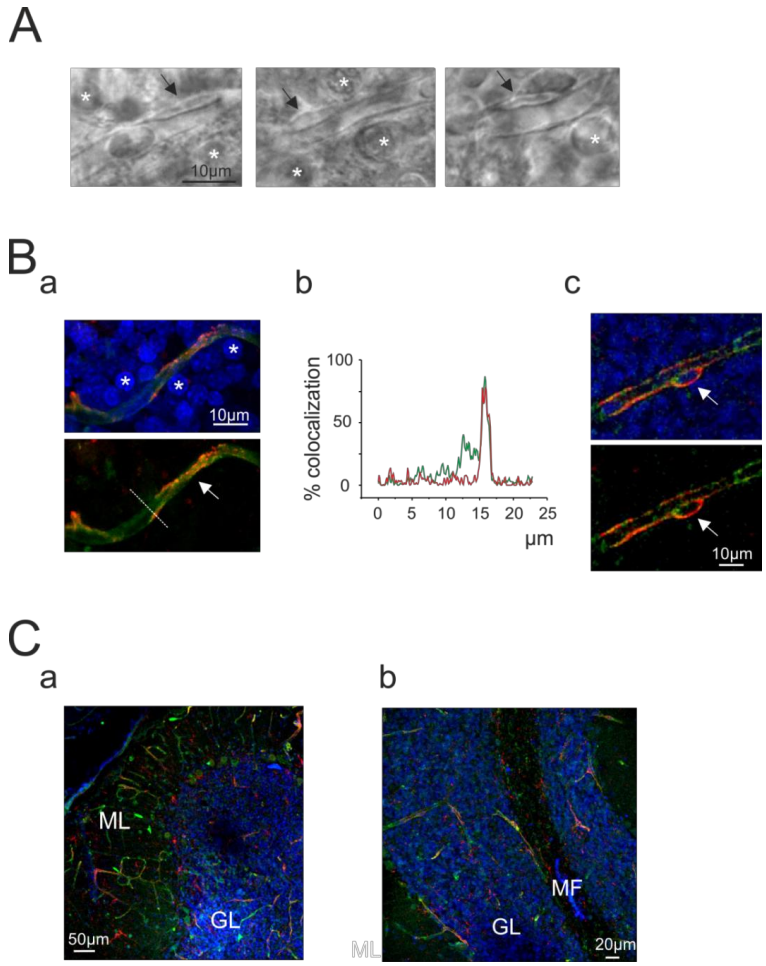

FIGURE 1 | Identification of capillary microvessels in the cerebellar granular layer. (A) Examples of bright-field images of three capillaries in the cerebellar granular layer. Note that GrCs (*asterisks*) are in close contact with nearby capillaries. The *arrows* indicate putative pericytes in close contact with the vessels wall. **(B)** Confocal fluorescent images of cerebellar slices stained for IB4 (*green*), NG2 (*red*) and DAPI (*blue*) to reveal capillaries, pericytes and cell nuclei, respectively. **(Ba)** *Top*: the image shows a capillary surrounded by GrCs (*asterisks*). *Bottom*: the same capillary (excluding DAPI) reveals the colocalization of IB4 and NG2 staining. The dashed line indicates the section analyzed for IB4 - NG2 colocalization in Bb. **(Bb)** Colocalization graph showing the overlap of the fluorescence signals originated by capillaries (*green*)

and pericytes (*red*) staining. **(Bc)** A granular layer capillary from another staining than in Ba, where the pericyte soma (*arrow*) and its bump-on-log morphology are visible in close contact with the capillary wall. **(C)** Confocal acquisitions from a cerebellar slice stained for IB4 (*green*), NG2 (*red*) and DAPI (*blue*), as in Ba,c. (**Ca**) The image shows the more regular microvessels organization in the molecular layer (ML) compared to the granular layer (GL) (20x objective). **(Cb)** The image shows the granular layer (GL) and the MF bundle (MF) of another lamella at a higher magnification (40x objective).

6.5.2 MFs stimulation causes vasodilation in the microcirculation of the cerebellar granular layer

In order to investigate the vasomotor response to MFs stimulation, cerebellar brain slices were pre-incubated with the thromboxane A2 agonist, U446619 (75 nM), as described elsewhere (Rancillac et al., 2006). This is an established approach to reproduce the vascular tone in unperfused and unpressurized brain microvessels (Fernandez-Klett et al., 2010; Mishra et al., 2014). We did not pre-constrict the capillaries with noradrenaline, as suggested elsewhere (Hall et al., 2014), since earlier work showed that this neurotransmitter may also activate rat cerebellar GrCs (Xu and Chuang, 1987; Dillon-Carter and Chuang, 1989). As depicted in Fig. 2Aa and 2Ab, U46619 caused a slowly developing vasoconstriction in the granular layer, since capillary diameter decreased to approximately 60% of its initial value at 45 min after drug perfusion (-39.9±12.1%; n=7; p=0.02). The vasomotor response to U46619 was usually spatially restricted at pericyte locations (see arrow in Fig. 2Ab), which therefore serve as sphincter-like structures that control microvascular blood flow, as also reported in the molecular layer (Rancillac et al., 2006; Hall et al., 2014). Control experiments confirmed that capillary diameter did not undergo any significant change in the absence of U46619 (Fig. 2Aa, *grey trace*). Under these conditions, high-frequency MFs stimulation caused a significant capillary vasodilation at spatially restricted locations near pericytes (Fig. 2Bc). The kinetics and magnitude of the hemodynamic signal evoked by neuronal activity are shown in Fig. 2Ba. The changes in vascular tone started immediately after the stimulus and consisted in a rapid initial vasodilation followed by a slower increase in lumen diameter (10.9±2.4%, n=13; p=0.00006) that peaked within 20s (16.5±2.6s; n=13) from the onset of the response and returned to the baseline within 20s (16.4±8.6s; n= 13) after interruption of the train. Fig. 2Bb displays an enlargement of the early phase of activity-induced vasodilation: it clearly shows that capillary diameter increased by 5±2% (n=13) already at 1s after MFs stimulation. This issue is particularly relevant when considering that the Poiseuille's law predicts that blood flow is directly proportional to the fourth power of the vessel radius; therefore, the activation of the MF-GrC synapse could

rapidly boost local blood flow by as much as 13% (see Discussion). In order to confirm the synaptic dependence of this process, cerebellar slices were pre-incubated in the presence of tetrodotoxin (TTX; 4 μM), a selective inhibitor of voltage-dependent Na^+ channels. As shown in Fig. 2Ba, MFs stimulation failed to cause any evident change in capillary diameter under these conditions, thereby providing evidence that synaptic activity controls the microvascular tone also in the granular layer (0.19±0.87%, n=5; p=0.8).

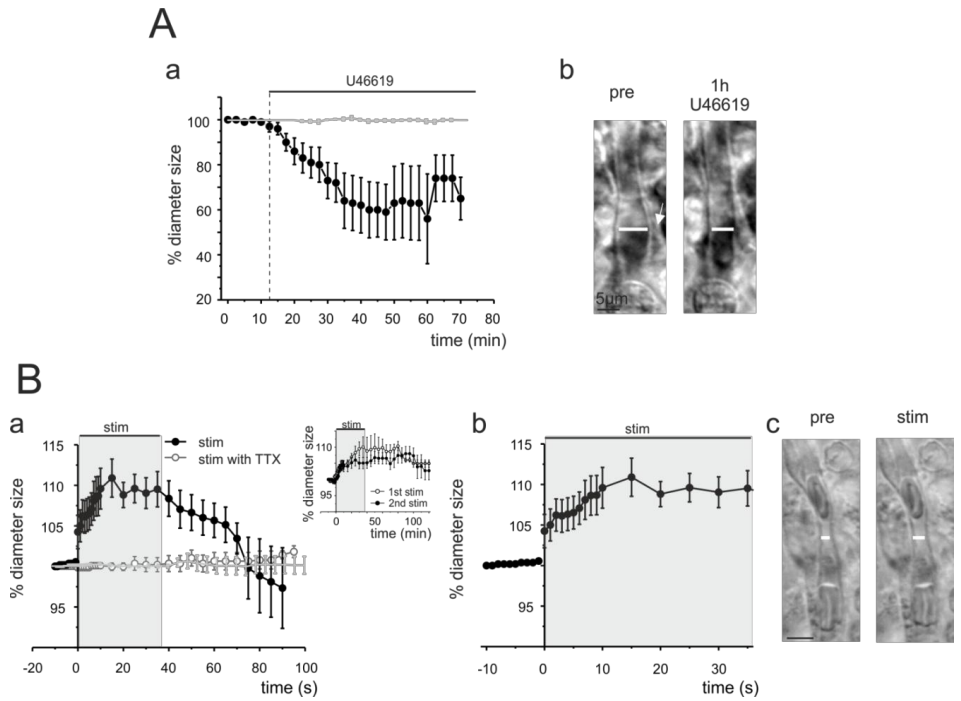

FIGURE 2 | MFs stimulation determines capillary vasodilation. (A) U46619 perfusion restores the vascular tone in the granular layer capillaries. **(Aa)** Average time course of the normalized capillary lumen diameter size in slices incubated for 1h with U46619 (thromboxane A2 agonist; 75 nM; n=7). The *grey line* shows that capillary diameter did not change in the absence of U46619 perfusion. **(Ab)** The pictures show a capillary before (*left*) and after U46619 perfusion (*right*). White bars indicate the location of lumen diameter measurements, near the pericyte indicated by the arrow. **(B)** MFs stimulation causes vasodilation of pre-constricted capillaries. **(Ba)** Average time course of capillary diameter size (n=13) before, during (*grey filled rectangle*) and after MFs stimulation (t=0s; 50Hz) (*black circles*); the *grey trace* shows the average time course of capillary diameter size in the absence of stimulation (n=10), while the *grey empty circles* show the average time course of capillary diameter size in the presence of 4μM TTX (n=5) As a control, in 5 slices a second stimulation (after 15 minutes) shows an average vasodilation not statistically different from the first

one (inset). **(Bb)** The same time course in Ba is shown on an expanded time scale, in order to appreciate the initial dynamics of vessels dilation during MFs stimulation. Note that vasodilation is evident as soon as 1s after MFs stimulation is started. **(Bc)** The pictures show capillary diameters before (*left*) and during (*right*) MFs stimulation. White bars mark the lumen diameter. In these and all subsequent experiments, capillaries are pre-constricted using U46619.

6.5.3 NMDARs and NO mediate vasodilation upon MFs stimulation

We have previously shown that high-frequency MFs stimulation causes a robust NMDARs- and NOS-dependent NO release in the granular layer of rat cerebellar slices (Maffei et al., 2003). Therefore, we first assessed whether NMDAR blockage affects the vasomotor response to synaptic activity. The co-application of D-APV (100 μM) and 7ClKyn (50 μM), which specifically target NMDARs, transformed the vasodilation evoked by MFs stimulation into a significant vasoconstriction (Fig. 3A). The decrease in capillary diameter started immediately (i.e. 1s) after the delivery of the stimulus, achieved a steady-state level (-5.9±1.8%, n=7; p=0.02) within 20s (19.5±3.9s; n=7) and returned to the baseline within approximately 21s (21.3±27.7s; n= 7) after interruption of the high-frequency train. Therefore, the kinetics of the vasoconstricting response to synaptic activity mirrors the vasodilation occurring when NMDARs are functional. Control experiments confirmed that two consecutive stimuli, delivered at 15 min intervals from each other, elicited the same hemodynamic signal in the absence of any pharmacological treatment (first: 10.0±3.1%, n=5; p=0.01; second: 6.0±1.8%, n=5; p=0.0004; first vs. second dilation not statistically different, p=0.2; Fig 2B inset).

The role played by NO in NVC at the MF-GrC relay was investigated by using the selective NOS inhibitor, L-N^G-Nitroarginine methyl ester (L-NAME), that is widely employed to prevent NO release (Mehta et al., 2008). Our preliminary experiments revealed that the addition of L-NAME (200 μM) to U46619-preconstricted cerebellar slices caused a further 40% reduction in microvessel diameter (-55.7±2.8%; n=8; p=0.004; inset in Fig. 3B), which is consistent with the tonic NO release by vascular endothelial cells (Hopper and Garthwaite, 2006). Control experiments showed that capillary diameter did not undergo any significant change in the absence of L-NAME perfusion (*grey trace* in Fig.3B inset). As observed upon inhibition of NMDARs, stimulation-evoked vasodilation reversed to vasoconstriction in the presence of L-NAME (Fig. 3B). The vasoconstrictor response initiated at 1s, reached a plateau (-9.0±1.4%, n=9 of 9; p=0.000004) at 35±3s (n=9), and did not fully return to resting levels upon interruption of the stimulus. Similar results were obtained when the slices were pre-incubated with 1H-[1,2,4]oxadiazolo[4,3-a]quinoxalin-1-one (ODQ; 10

μM; mean, -3.6±0.9%; n=10; p=0.005; Fig. 3C), an inhibitor of soluble NO-dependent guanylyl cyclase (sGC) activity (Sakagami et al., 2001). As expected by the block of sGC activation by NO, ODQ prevented pericyte-dependent vasodilation, while it did not affect pericyte-dependent vasoconstriction in the presence of L-NAME (-8.2±1.7%, n=8; p=0.001; vs. L-NAME alone -12.8±1.9%, n=8; p=0.00005; the two vasoconstrictions are not statistically different, p=0.1; Fig.3Ba)

Taken together, these data demonstrate that activation of the MF-GrCs relay decreases the microvascular tone and increases local CBF by recruiting NMDARs and NOS. GrCs express both NMDARs and nNOS (Southam et al., 1992; D'Angelo et al., 1995; Maffei et al., 2003), while cerebellar glial cells and brain endothelial cells lack functional NMDARs (Busija et al., 2007; Dzamba et al., 2013). Therefore, GrCs are the most likely candidates to trigger the vasoactive response to MFs stimulation. To further support these conclusions, we exploited a high-resolution imaging system to directly measure NO production in the granular layer of cerebellar slices loaded with the NO-sensitive dye DAF-FM, as reported below.

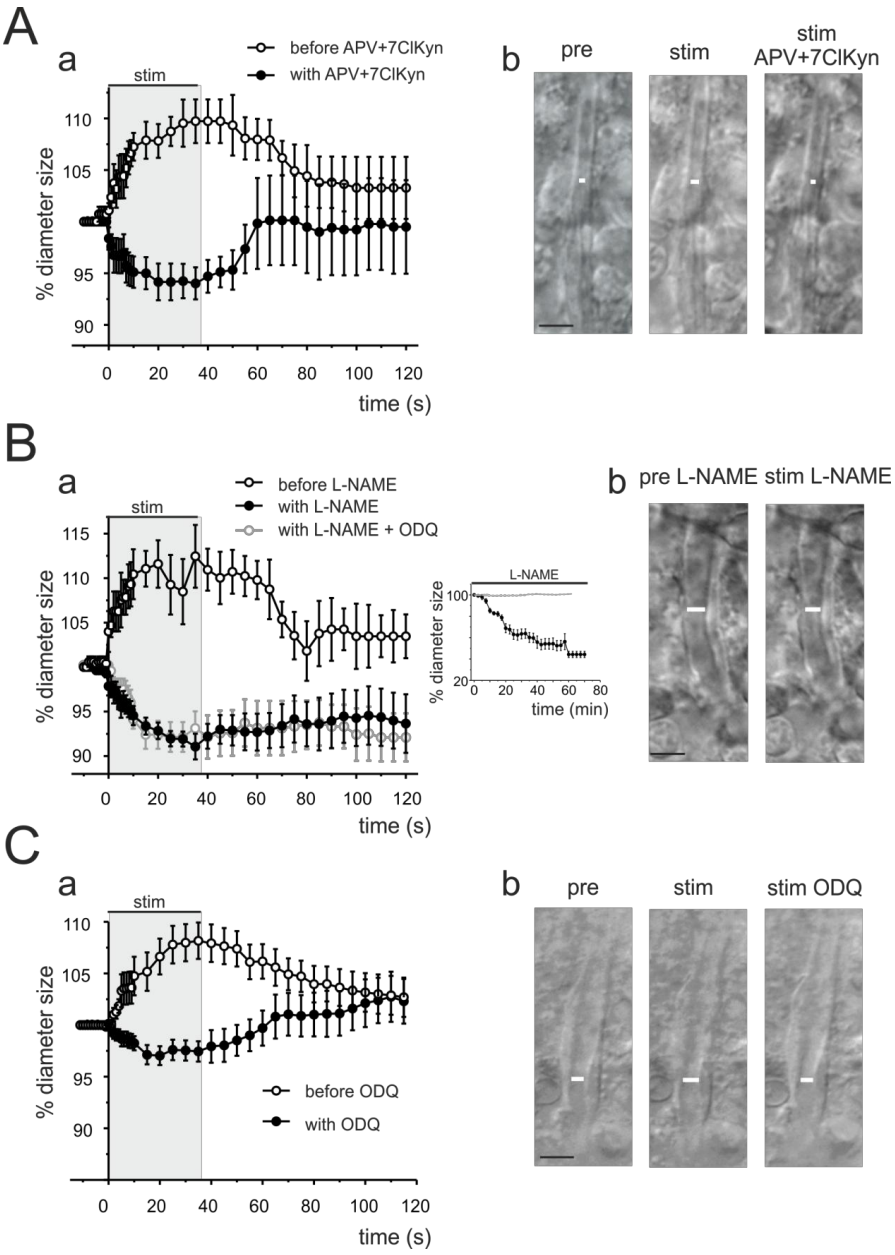

FIGURE 3 | NMDARs, NO and cGMP mediate the vasodilation. (A) Capillary vasodilation depends on NMDARs activation. **(Aa)** Average time course of capillaries diameter changes during the same MFs stimulation protocol in Fig. 2B, in control (*empty circles*) and during (*full circles*) APV+7ClKyn perfusion (NMDARs inhibitors; 100μM and 50μM, respectively; n=7; the vessels diameter at the end of the control stimulation is re-normalized to show the relative size changes after the stimulation in APV+7ClKyn).

NMDARs blockage turns the vasodilation into a vasoconstriction. **(Ab)** The pictures show capillary diameters before (*left*), during MFs stimulation in control (*center*) and during MFs stimulation in the presence of APV+7ClKyn (*right*). White bars marks lumen diameter. **(B)** NO production is necessary for vasodilation. **(Ba)** Average time course of the capillary diameters changes during the MFs stimulation protocol before (*black empty circles*), after (*filled circles*) L-NAME perfusion (NOS inhibitor; 200μM, n=9), and after L-NAME and 10μM ODQ perfusion (*grey empty circles*). The stimulus-evoked vasodilation is turned into vasoconstriction in both cases. Note that during the hour of L-NAME perfusion the vessels diameter decreases (*black* circles, n=8; compared to controls without L-NAME perfusion, *grey line*, n=5) as shown in the inset. The vessels diameter relative size reported in the graph is therefore re-normalized to the pre-stimulus condition in L-NAME. **(Bb)** The pictures show capillary diameter before (*left*) and after (*right*) MFs stimulation in slices treated with L-NAME (1h). White bars mark lumen diameter. **(C)** sGC activation by NO is involved in vasodilation. **(Ca)** Average time course of capillaries diameter size during the stimulation protocol before (*empty circles*) and after (*filled circles*) ODQ perfusion (sGC inhibitor; 10μM; n=10). The blockage of sGC activity abolishes vasodilation that is partially reversed toward vasoconstriction. **(Cb)** The pictures show the same capillary before (*left*) and during MFs stimulation in control (*center*) and in the presence of ODQ (*right*). White bars mark lumen diameter.

6.5.4 Evidence for NO production in the granular layer

Previous results indirectly stand for NO production by GrCs in the granular layer in response to MFs stimulation. In order to obtain evidence of NO production in the granular layer, we loaded the slices with the DAF-FM dye. DAF-FM fluorescence is related to NO production (as well as NO production derivates) inside cells with fast reaction kinetics (Balcerczyk et al., 2005; Namin et al., 2013). Therefore, the DAF-FM signal is thought to reflect intracellular NOS activity, rather than extracellular NO accumulation. In order to investigate neuronal activity-dependent NO production in the granular layer following MFs stimulation, we detected DAF-FM fluorescence changes during a 5s trial, with 4s 50Hz MFs stimulation. In order to enhance the signal-to-noise ratio, pure noise was averaged out by subtracting the average of 4 trials without MFs stimulation to that of 4 trials with MFs stimulation 4, allowing to subtract the stimulus-independent component of the fluorescence signal (acquisition rate was set at 15ms, see Methods for detailed description of the procedure). Interestingly, the granular layer responded to MFs stimulation with a fluorescence signal peak at 212.8±20.5ms delay, with an average fluorescence at peak of 0.029±0.003$\Delta F/F_0$ (n=20; Fig. 4A). The analysis of the average trace in Fig. 4A resulted in a rise-time (10-90%) of 25.6ms, a decay-time (90-10%) of 95.5ms, and a half-width of 55.0ms. Notably, these values are in good agreement with the nNOS kinetics described in literature (Salerno, 2008; Salerno and Ghosh,

2009; Garthwaite, 2016), supporting the nNOS role as a primer of activity, more than a "classic" enzyme with a Michaelis-Menten steady-state kinetics (Salerno, 2008).

Since the DAF-FM signal could be influenced by other NO-related chemical species, we repeated the same recordings after NOS blockage using 200μM L-NAME perfusion for at least 1h. In the presence of L-NAME, the fluorescence peak was no longer observed (0.001±0.003 $\Delta F/F_0$*ms at the time of peak in control, n=7; Fig. 4B). Moreover, we tested the neuronal origin of the signal by blocking NMDARs using 100μM D-APV and 50μM 7ClKyn, and repeated the same experiment after at least 20 minutes of blockers perfusion. Again, the fluorescence peak triggered by MFs stimulation was no longer observed (-0.007±0.006 $\Delta F/F_0$*ms at the time of peak in control, n=6; Fig. 4B). Moreover, the distance from the stimulating electrode of the fluorescence signals (158±10 μm, n=20) was comparable to the distance of the vessels used for the analysis (191±10 μm, n=50, N.S.), as evident in the scatter plot in Fig. 4C. Therefore, we provide evidence that the MFs stimulation used could indeed determine neuronal NO production at the distances used for the analysis of stimulus-induced vessel diameter changes.

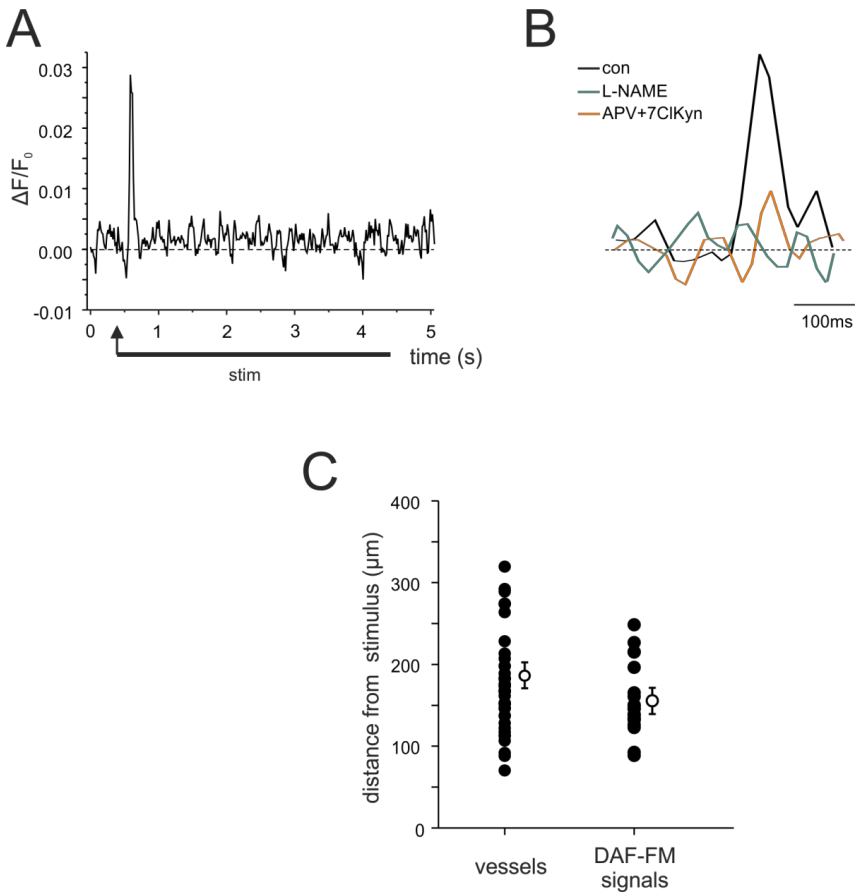

FIGURE 4 | DAF-FM fluorescence induced by synaptic activity in the granular layer. (A) Average trace showing the peak in DAF-FM fluorescence in response to 4s MFs stimulation (n=20 slices). **(B)** Average traces of DAF-FM fluorescence signals evoked as in A in cerebellar granular layers before (*black*), after 1h L-NAME perfusion (*green*; 200µM; n=7), and after APV+7ClKyn perfusion (orange; 100µM and 50µM, respectively; n=6). The superimposed traces are on the same amplitude scale as in A, while the time scale is dilated to appreciate the fluorescence peaks. **(C)** Scatter plot showing the distances from the stimulating electrode of each vessel and DAF-FM fluorescence signal analyzed (*full circles*). The *empty circles* show the average values of the single points.

6.5.5 mGluRs and 20-HETE mediate vasoconstriction in the absence of NO release

The question then arose as to the molecular nature of the vasoactive agent inducing vasoconstriction in the absence of GrCs-derived NO. NO may inhibit the enzyme CYP ω-hydroxylase, thereby suppressing the synthesis of 20-HETE (Attwell et al., 2010), which has

recently been shown to increase the contractile tone in cerebellar pericytes(Hall et al., 2014). Therefore, 20-HETE is a suitable candidate to mediate the reduction in the microvascular tone of granular layer unveiled by NOS inhibition. To address this issue, cerebellar slices were pre-treated with L-NAME (200 μM, 1h) to prevent NO production. Subsequently, they were perfused with HET-0016 (1 μM) to block 20-HETE synthesis by CYP ω-hydroxylase (Metea and Newman, 2006). Control experiments revealed that this treatment did not alter the hemodynamic signal recorded in the absence of L-NAME (4.1±1.2%, n=4; p=0.04; vs. 6.3±2.2%, n=4; p=0.0005; respectively; not statistically different dilations, p=0.4; Fig.5A). However, as displayed in Fig.5B, HET-0016 significantly reduced neuronal activity-dependent vasoconstriction (mean -4.2±1.9%; n=9; p=0.007) in the presence of L-NAME. Moreover, HET-0016 (1 μM) significantly reduced the vasoconstriction response to MFs stimulation upon NMDARs inhibition with D-APV (100 μM) and 7ClKyn (50 μM) (-2.1±0.7%, n=5; p=0.02; vs. -5.2±2.5%, n=5; p=0.005; statistically different constrictions, p=0.02; Fig.5C). These findings lend support to the hypothesis that 20-HETE plays a key role in NVC in the granular layer of the cerebellum when NO release is hampered. According to the most popular model (Attwell et al., 2010; Duchemin et al., 2012), 20-HETE is synthesized from arachidonic acid (AA) liberated by astrocytes upon synaptic stimulation. Accordingly, synaptically-released glutamate could activate mGluRs expressed on the perisynaptic end-feet of nearby astrocytes, thereby leading to Ca^{2+}-dependent activation of phospholipase A2 (Mulligan and MacVicar, 2004; Attwell et al., 2010). If this was true also in the granular layer of the cerebellum, then inhibiting mGluRs should attenuate neuronal activity-evoked vasoconstriction occurring in the presence of L-NAME. Consistent with this hypothesis, the broad spectrum mGluRs antagonists, alpha-methyl-4-carboxyphenylglycine (MCPG; 500 μM) and (RS)-alpha-cyclopropyl-4-phosphonophenylglycine (CPPG; 300 μM), abolished the vasoconstrictor response to MFs stimulation in L-NAME-pretreated slices (mean 1.1±1.5%; n=15; p=0.9 Fig. 5D). These data support the conclusion that mGluRs drive the synthesis of 20-HETE during synaptic transmission at the MF-GrC relay. The interaction between these two diverging vasoactive pathways, i.e. NO and 20-HETE, could have profound implications for the mechanism of NVC at the input stage of the cerebellum.

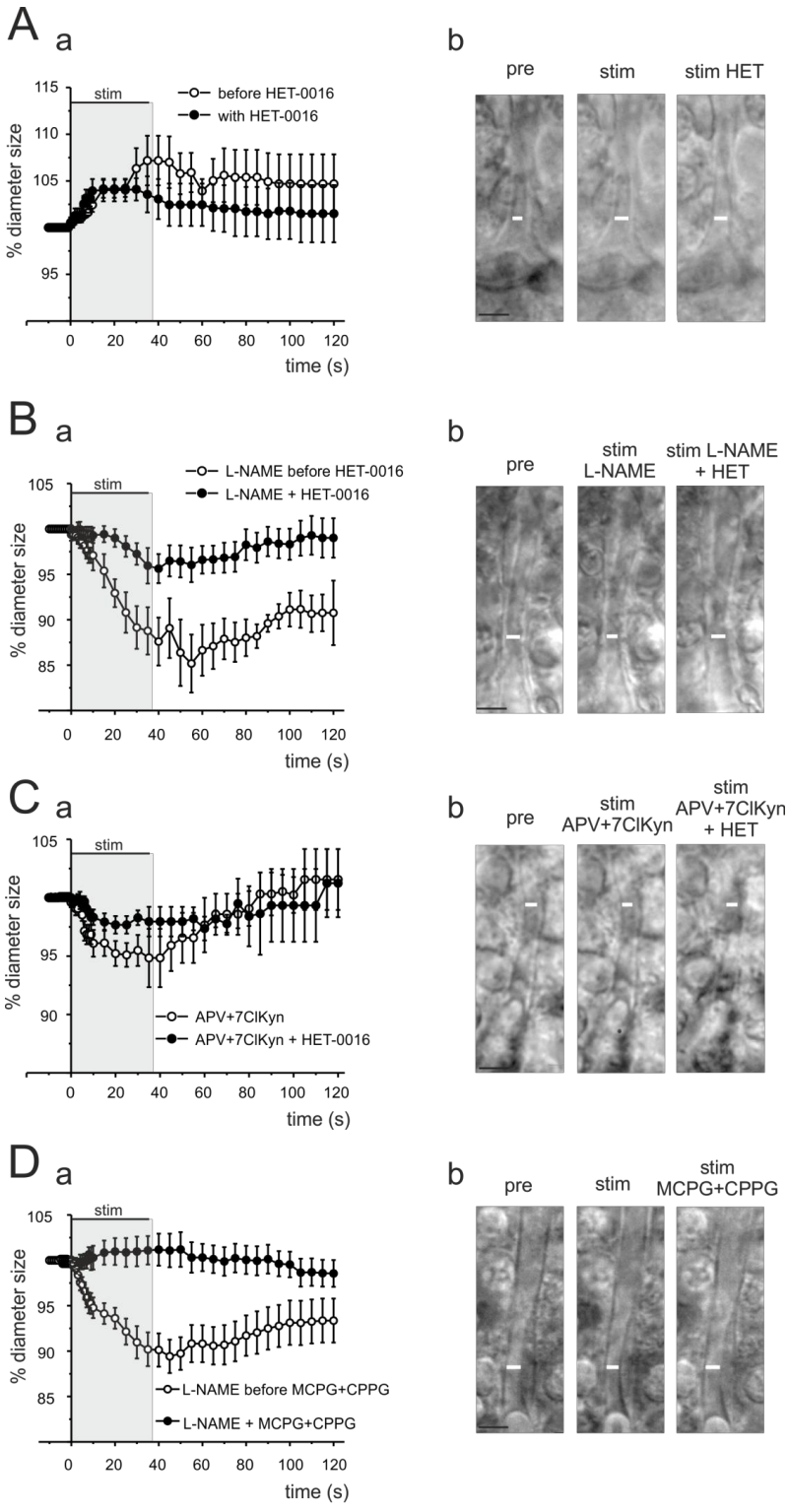
A
a
b
stim
before HET-0016
with HET-0016
% diameter size
time (s)
pre
stim
stim HET
B
a
b
L-NAME before HET-0016
L-NAME + HET-0016
pre
stim
L-NAME
stim L-NAME
+ HET
C
a
b
APV+7ClKyn
APV+7ClKyn + HET-0016
pre
stim
APV+7ClKyn
stim
APV+7ClKyn
+ HET
D
a
b
L-NAME before MCPG+CPPG
L-NAME + MCPG+CPPG
pre
stim
stim
MCPG+CPPG

FIGURE 5 | 20-HETE and mGluRs mediate vasoconstriction. (A) 20-HETE does not influence vasodilation. **(Aa)** Average time course of capillary diameter size in cerebellar slices, during the same MFs stimulation protocol as in Fig. 2B and Fig. 3, before (*empty circles*) and after 1h of HET-0016 perfusion (CYP ω-hydroxylase inhibitor; 1μM; n=4). The presence of HET-0016 does not significantly change vasodilation. **(Ab)** The pictures show the diameter variation of a capillary before (*left*) and during MFs stimulation in the absence (*center*) or presence (*right*) of HET-0016. White bars show lumen diameter. **(B-C)** 20-HETE is the main vasoconstriction agent. **(Ba)** Average time course of capillaries diameter size in slices exposed to 1h L-NAME, during the same MFs stimulation protocol as in (A), before (*empty circles*) and during (*filled circles*) HET-0016 perfusion (CYP ω-hydroxylase inhibitor; 1μM; n=9). Note that the blockage of 20-HETE synthesis reduced vasoconstriction. **(Bb)** The pictures show the diameter variations of the same capillary following 1h L-NAME perfusion, before (*left*) and during MFs stimulation in absence (*center*) and in presence (*right*) of HET-0016. White bars show lumen diameter. **(Ca)** Average time course of capillary diameter size in slices perfused with APV+7ClKyn (as in Fig.3A), during MFs stimulation before (*empty circles*) and during (*filled circles*) HET-0016 perfusion. **(Cb)** The pictures show the changes in capillary diameter following perfusion with APV+7ClKyn before (*left*) and during MFs stimulation in the absence (*center*) or presence (*right*) of HET-0016. White bars show lumen diameter. **(D)** Capillary vasoconstriction depends on mGluRs activation. **(Da)** Average time course of capillary responses in cerebellar slices exposed to 1h L-NAME, after MFs stimulation protocol in the absence (*empty circles*) or presence (*filled circles*) of MCPG+CPPG (mGluRs blockers; 500μM and 300μM, respectively; n=15). The perfusion of mGluRs antagonists abolishes stimulus-evoked vasoconstriction. **(Db)** The pictures show the changes in capillary diameter before (*left*) and during MFs stimulation in the absence (*center*) or presence (*right*) of MCPG+CPPG. White bars show lumen diameter.

6.6 DISCUSSION

In this paper, we demonstrate that synaptic activation of the cerebellar granular layer causes capillary vasodilation through an NMDAR/NOS-dependent mechanism. It is probable that the main neurons involved are GrCs, which represent the largest neuronal population and express NMDARs and nNOS at the highest levels in the brain (Monaghan and Anderson, 1991; Snyder, 1992; Southam et al., 1992). GrCs actually produce NO under NMDARs activation causing smooth muscle relaxation in *in vitro* systems (Garthwaite and Garthwaite, 1987; Garthwaite et al., 1989). The present result thus focuses the NVC mechanism onto these small neurons forming the NOergic backbone of the cerebellum and releasing NO also in the molecular layer through parallel fibers (see (D'Angelo, 2014)), while the most renowned Purkinje cells do not express nNOS nor produce NO (Rancillac et al., 2006). Interestingly, GrCs display strong burst-related activity fluctuations *in vivo* (Chadderton et al., 2004; Rancz et al., 2007b; Powell et al., 2015) and are therefore especially

suited to coordinate NVC, while Purkinje cells usually show frequency-modulated activity changes (Bosman et al., 2010; Herzfeld et al., 2015; Cheron et al., 2016; Ramakrishnan et al., 2016). The Golgi cells, which also express NMDARs and nNOS (Southam et al., 1992; Christie and Jahr, 2008; Robberechts et al., 2010), could contribute to the response. The present results also suggest the involvement of cellular elements other than neurons, including pericytes and glial cells, in the local control of microcirculation. Therefore, the granular layer emerges as an integrated cellular system capable of controlling NVC in the cerebellar circuit.

6.6.1 Neuronal activity controls NVC in the cerebellar granular layer

Capillaries in the cerebellar molecular layer may dilate in response to sensory stimulation earlier than upstream arterioles and substantially contribute to increase CBF *in vivo* (Hall et al., 2014). Consistently, in the granular layer, the application of a high-frequency train to MFs caused a robust capillary vasodilation that occurred at pericyte locations. This feature supports the role played by these contractile cells in the regional control of CBF (Attwell et al., 2016).

Following MFs stimulation, vasorelaxation showed biphasic kinetics. According to Poiseuille's Law, the initial (~5%) and late (~10%) diameter changes are predicted to reduce capillary resistance by 17% and 32%, respectively (Peppiatt et al., 2006; Hall et al., 2014). Thus, with a 45:100 capillary:arteri(ole)s ratio (venule resistance is considered negligible), the total flow resistance would decrease by 5.5% and 10.3% (Peppiatt et al., 2006; Hall et al., 2014) and the blood flow would increase by 5.8% and 11.5%, respectively (see Methods for calculations).

As capillaries are significantly closer to neurons than upstream arterioles (8-23 μm vs. 70-160 μm according to (Attwell et al., 2010)), the robust increase in local CBF evoked by MFs activation would seemingly satisfy the high metabolic demand of granular layer neurons, which consume as much as 67% of cerebellar energy (Howarth et al., 2010).

Moreover, the BOLD effect is contributed both by an increase in CBF (which tends to increase the signal by washing out deoxyhemoglobin) and by the cerebral metabolic rate of O_2 ($CMRO_2$, which tends to decrease the signal by generating more deoxyhemoglobin). Thus, the rapid (1s) step-like increase in capillary diameter (see Fig. 2B) will boost the $CBF/CMRO_2$ ratio and the BOLD signal more efficiently than a gradual relaxation. As further illustrated below, this hemodynamic response faithfully reflects GrCs activity. Intriguingly, recent 7-Tesla fMRI studies showed that the BOLD signal onset in the gray matter is associated to the capillary bed (Siero et al., 2011; Siero et al., 2013). In this view, the control of microvascular tone at capillary level is the most efficient means to redistribute CBF to the highly restricted (<3mm diameter) activation patches that

7T fMRI analysis revealed in the cerebellum in response to single finger stimulation or movement (Wiestler et al., 2011).

6.6.2 Granular layer neuronal activity determines NMDAR / NO–dependent vasodilation

Four lines of evidence indicate that synaptically-released glutamate recruits NMDARs located on postsynaptic granular layer neurons to trigger NO-dependent vasodilation.

First, the hemodynamic signal was turned into vasoconstriction by the pharmacological inhibition of either NMDARs or NOS. NMDARs determine the extent of GrCs activation by MFs (D'Angelo et al., 1995; D'Angelo et al., 1999). Conversely, rat cerebellar Bergman glial cells and brain endothelial cells lack functional NMDARs (Usowicz et al., 1989; Domoki et al., 2002; Dzamba et al., 2013).

Secondly, imaging of DAF-FM fluorescence supported the notion that NMDARs control NO production in granular layer neurons upon MFs stimulation. Although DAF-FM measurements do not directly reveal NO but other cross-reactive species (Balcerczyk et al., 2005), the increase in fluorescence immediately followed MFs stimulation, was inhibited by either L-NAME or APV+7ClKyn and strongly resembled the kinetics of neuronal NO production revealed with different techniques (Salerno, 2008; Salerno and Ghosh, 2009; Garthwaite, 2016).

Thirdly, NO activates sGC to elevate $[cGMP]_i$ and induces vasodilation in the cerebellum (Yang and Iadecola, 1997, 1998). Accordingly, ODQ mimicked the effects of L-NAME by turning vasodilation into vasoconstriction. Given the kinetics of sGC activation and its exquisite sensitivity to NO (Batchelor et al., 2010; Garthwaite, 2016), cGMP production can outlast the NO pulse, which is likely to account for the slower kinetics of the ensuing vasorelaxation.

Fourthly, NADPH-diaphorase staining revealed that nNOS, the NOS isoform which converts NMDARs-mediated Ca^{2+} inflow into NO release (Garthwaite, 2016), is abundantly expressed in GrCs but not in cerebellar astrocytes or endothelial cells (Southam et al., 1992).

The combination of the present DAF-FM measurements with NADPH-diaphorase staining (Southam et al., 1992), NOS immunohistochemistry (Snyder, 1992) and electrochemical NO determination (Maffei et al., 2003) provides solid evidence that NO was generated by granular layer neurons. The GrCs, which outnumber Golgi cells by about 2000 times in rats (Korbo et al., 1993) and show prominent NMDARs-dependent responses (D'Angelo et al., 1995), are likely to play the major role, although the contribution of Golgi cells (which also express NMDARs and nNOS) (Southam et al., 1992; Cesana et al., 2013; D'Angelo et al., 2013) cannot be ruled out.

6.6.3 Non-neuronal antagonistic systems balance the capillary diameter

Besides promoting vasodilation, NO released by granular layer neurons could inhibit the synthesis of the potent vasoconstrictor, 20-HETE (Attwell et al., 2010). Accordingly, when NO production was suppressed by blocking NMDARs or NOS, MFs stimulation resulted in a marked vasoconstriction that was antagonized by HET-0016. 20-HETE could be generated by pericytes metabolizing AA released upon activation of mGluRs located on perisynaptic astrocytes (Attwell et al., 2010; Sweeney et al., 2016). In support to this model, a mixture of selective mGluRs inhibitors abolished synaptic activity-dependent vasoconstriction. Combined application of inhibitors of NOS, NMDAR, sGC and CYP showed that NO does not need to prevent 20-HETE formation to induce capillary vasorelaxation in the granular layer as it acts through cGMP (Hall et al., 2014). This sets a difference with the molecular layer, in which vasodilation is triggered by prostaglandin E2, but NO plays a permissive role by suppressing 20-HETE synthesis (Hall et al., 2014). This model would also explain why vasoconstriction observed in the presence of ODQ was smaller than with L-NAME, NO being still released and partially inhibiting the vasoconstriction branch depending on 20-HETE synthesis. The difference between molecular and granular layers mechanisms may (at least in part) be related with the different architecture of their microvascular networks (Kolinko et al., 2016). Taken together, these observations suggest that glutamate couples synaptic activity to microvascular tone in the cerebellum granular layer engaging two competing signaling pathways promoting either vasorelaxation (i.e. through NMDARs) or vasoconstriction (i.e. through mGluRs).

6.7 Summary and Conclusions

While most studies have hitherto examined NVC in the molecular layer (Peppiatt et al., 2006; Rancillac et al., 2006; Lauritzen et al., 2012; Hall et al., 2014), herein we provide evidence that synaptic activation of NMDARs stimulates granular layer neurons to release NO, which in turn vasodilates adjacent capillaries and has the potential to cause a remarkable (up to 23%) increase in local CBF. The NO-dependent vasorelaxation overcomes a contrasting vasoconstrictor response mediated by 20-HETE induced by mGluRs probably located in non-neuronal cells. Converging evidence suggests that GrCs play a pivotal role in granular layer NVC and this opens an intriguing scenario since these cells are also pivotal to elaborate and store complex spatio-temporal patterns at the MF input (D'Angelo and De Zeeuw, 2009). This may explain the fact that GrCs are NOergic neurons that release NO both in the granular and molecular layer (D'Angelo, 2014; Bouvier et al., 2016b) thus coordinating computational and metabolic functions in the whole cerebellar network. This conclusion remains to be validated *in vivo*, but it sheds novel light on the hemodynamic response to NA in the cerebellum.

As originally proposed by (Diedrichsen et al., 2010) and (Howarth et al., 2010), the granular layer regulation of local microvessels could remarkably contribute to shaping cerebellar BOLD signals, which, conversely, proved largely independent from Purkinje cell activity (Thomsen et al., 2004). This observation may provide useful cues for further NVC investigations and cerebellar fMRI analysis.

Chapter 7

Neurovascular responses of the granular layer of cerebellar vermis and hemispheres to different input patterns

7. Neurovascular responses of the granular layer of cerebellar vermis and hemispheres to different input patterns

G. Gagliano[1], L. Mapelli[1], T. Soda[1,2], U. Laforenza[3], F. Moccia[4], E. D'Angelo[1,5]

[1]*Dept of Brain and Behavioral Sciences, University of Pavia, Pavia, Italy*
[2] *Museo Storico della Fisica e Centro Studi e Ricerche Enrico Fermi, Rome, Italy*
[3]*Dept of Molecular Medicine, University of Pavia, Pavia, Italy*
[4]*Dept of Biology and Biotechnology "L. Spallanzani", University of Pavia, Pavia, Italy*
[5] *Brain Connectivity Center, C. Mondino National Neurological Institute, Pavia, Italy*

Authors contribution: F.M. and E.G. designed research; G.G., L.M. and U.L. performed research; G.G., L.M. and T.S. analyzed data; G.G., L.M. and E.D. write the abstract.

The authors declare no competing financial interests.

Acknowledgments. This work was supported by: European Union grant Human Brain Project (HBP-604102) to ED and Fermi grant [13(14)] to ED and LM.

Front. Cell. Neurosci. Conference Abstract: From cell physiology to integrated signals and emerging brain functions

In press

7.1 Introduction and methods

Neurovascular coupling (NVC) is the process whereby neural activity controls blood vessel diameter. NVC regulates the cerebral blood flow (CBF) ensuring oxygen and metabolic supply to the brain. A precise characterization of NVC mechanisms has recently been reported for the cerebellum granular layer. There, granule cells control NVC through an NMDARs/NO-dependent system (Mapelli et al., 2017), acting on pericytes surrounding the capillaries.

NVC contributes to generate the blood-oxygen-level-dependent (BOLD) signal used in functional magnetic resonance imaging (fMRI) to map changes in brain activity (Iadecola, 2004). Interestingly, recent fMRI recordings revealed that BOLD signals in the cerebellar vermis lobule V and hemisphere lobule VI are different in their relationship to grip force, being respectively linear

or non-linear (Alahmadi et al., 2017).In order to understand the neurophysiological basis of this difference, we investigated the vascular organization of the cerebellar cortex in mouse cerebellar slices and measured capillary diameter changes in response to mossy fibers stimulation (50Hz, 100Hz and 300Hz; 37°C) in the corresponding cerebellar regions.

7.2 Results

In this abstract we report preliminary data on the response of the cerebellar granular layer of lobules V (vermis) and VI (hemisphere) to input spike trains at different frequencies. The capillary diameter at rest was in line with the size of brain capillaries (inner diameter 2.39±0.16µm n= 38) and changed after stimulation. Immunostained cerebellar slices showed no difference in the vascular architecture of vermis (fig.1A) and hemisphere (fig.1B). Moreover, in the granular layer of both vermis lobule V and hemisphere lobule VI capillaries were surrounded by pericytes(fig.2A and 2B).In physiological experiments in acute cerebellar slices, the distance of microvessels from the stimulating electrode was similar for vermis lobule V (141±9µm, n=20)and for hemisphere lobule VI (136±12µm, n=7)(p=0.73).

In the vermis, neural activity caused a significant vasodilation that reached the maximum after 35s of electrical stimulation (fig.3, left). Capillary responses to mossy fibers stimulation at 50Hz were smaller than responses to 100Hz and 300Hz, suggesting the existence of a input frequency dependence of the capillary responses (fig.3, right).

In the hemisphere, mossy fibers stimulation induced a significant increase in capillary diameters both at 50Hz, 100Hz and 300Hz (fig.4, left). The capillary responses at 100Hz and 300Hz were statistically different (fig.4, right).

Figure 5 summarizes the different trends in the time course of capillary dilation during the application of the stimulus at different frequencies in the two lobules of the cerebellum.

7.3 Discussion and conclusion

The cerebellar granular layer shows a similar structural vascular organization (fig.1A and 1B), with capillaries surrounded by pericytes (fig.2A and 2B), both in vermis lobule V and hemisphere lobule VI. Mossy fibers stimulation (50Hz, 100Hz and 300Hz) caused a significant capillary vasodilation in the granular layer of both vermis (fig.3) and hemisphere (fig.4). Our preliminary data suggest that capillary responses in vermis and hemisphere might be different, suggesting that NVC in the cerebellum might be region-dependent. Further experiments are needed to determine whether a difference is confirmed and to what extent this could explain BOLD

differences reported by Alahmadi and colleagues. The results of this investigation will provide new clues for understanding cerebellum-cerebral connections activity.

These results will add to a growing scientific background on NVC in the cerebellum. Recent investigations showed that capillaries change their lumen diameter earlier than upstream arterioles in response to neural activity and following pericytes activation(Hall et al., 2014), and that capillaries mobility seems to generate the blood flow increase that initiate the imaging signals (Mishra et al., 2016). Moreover, it has to be considered that the complexity of granular layer information processing (D'Angelo and De Zeeuw, 2009)must be accompanied and determine NVC rules in this area.

Finally, since fMRI limitations have neural origins (Logothetis, 2008), these results and future investigations (combined with bottom-up models of NVC) will improve our understanding on how NVC and neural activity generate the BOLD signal.

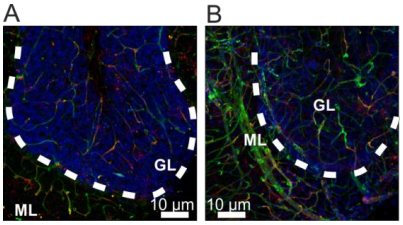

Figure 1 | Vascular organization of the cerebellar cortex.A) Vermis lobule V; ML= molecular layer; GL= granular layer. **B)** Hemisphere lobule VI; ML= molecular layer; GL= granular layer. Nuclei (blue), vessel walls (green), pericytes (red).

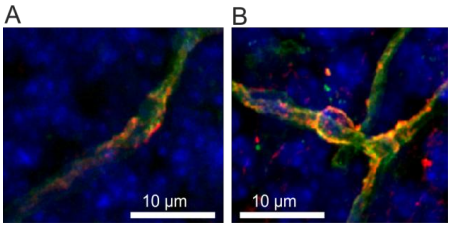

Figure 2 | Identification of capillary microvessels in the cerebellar granular layer. A) Vermis lobule V. **B)** Hemisphere lobule VI. Nuclei (blue), vessel walls (green), pericytes (red).

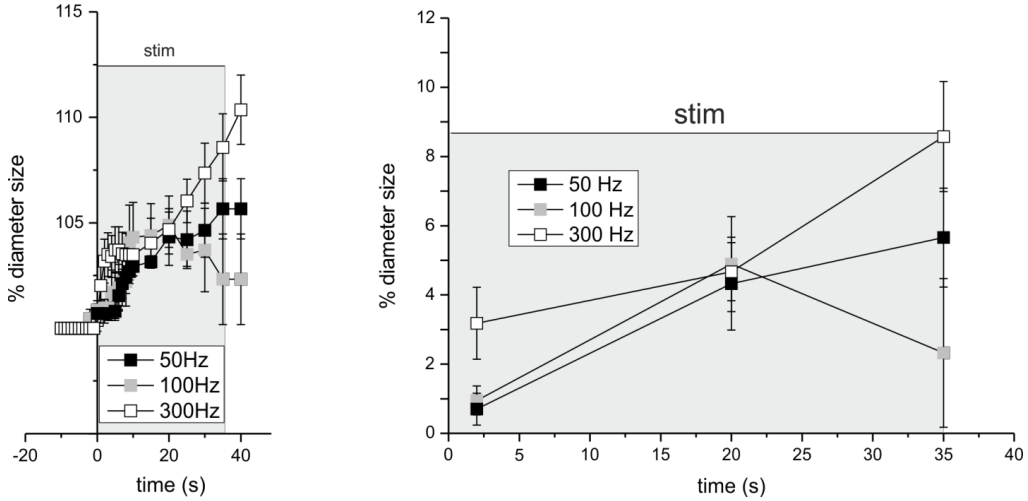

Figure 3 | Mossy fibers stimulation in the granular layer of cerebellar vermis lobule V. Average time course of percent change of capillary diameter size during mossy fiber stimulation at 50Hz (n= 6; p= 0,001), 100Hz (n= 7; p= 0,0004) and 300Hz (n= 7; p=0,001) (*left*) and average time course at 2s, 20s and 35s (*right*).

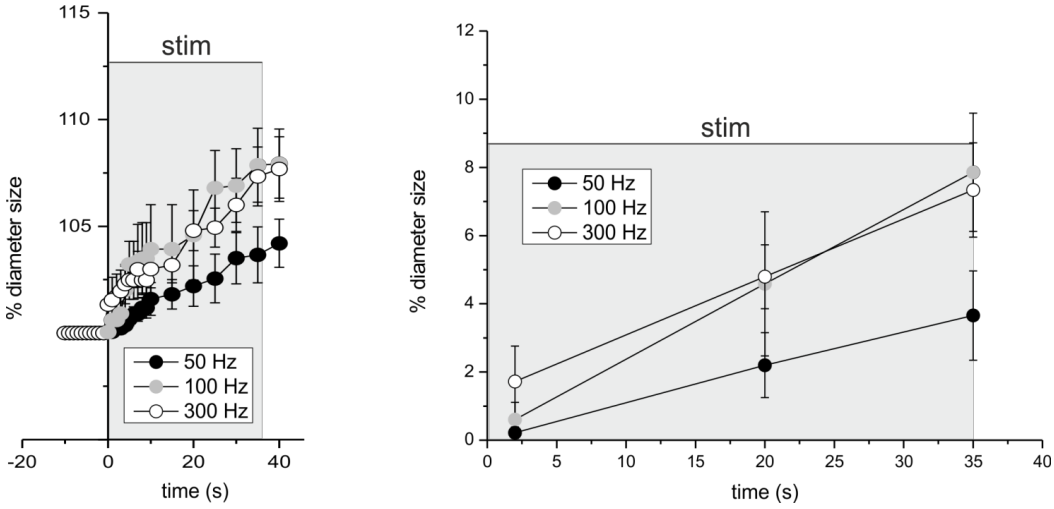

Figure 4 | Mossy fibers stimulation in the granular layer of cerebellar hemisphere lobule VI. Average time course of percent change of capillary diameter size during mossy fiber stimulation at 50Hz (n= 5; p= 0,001), 100Hz (n= 6; p= 0,0009) and 300Hz (n= 7; p=0,002) (*left*) and average time course at 2s, 20s and 35s (*right*).

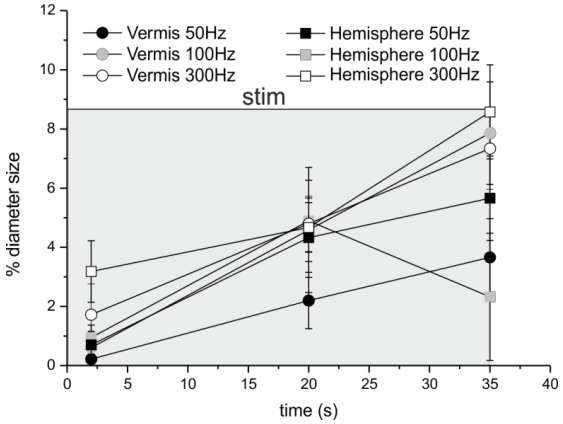

Figure 5 | Capillary responses in cerebellar granular layer. Average time course of vessel vasodilation in vermis lobule V and hemisphere lobule VI during mossy fiber stimulation at 50Hz, 100Hz and 300Hz.

Chapter 8

Different neurovascular responses in the granular layer of the cerebellar vermis and hemisphere

8. Different neurovascular responses in the granular layer of the cerebellar vermis and hemisphere

Giuseppe Gagliano[1], Anita Monteverdi[1], Teresa Soda[1,2], Umberto Laforenza[3], Francesco Moccia[4], Lisa Mapelli[1,§], Egidio U. D'Angelo[1,§]

[1] Dept of Brain and Behavioral Sciences, University of Pavia, 27100 Pavia, Italy
[2] Museo Storico della Fisica e Centro Studi e Ricerche Enrico Fermi, 00184 Rome, Italy
[3] Dept of Molecular Medicine, University of Pavia, 27100 Pavia, Italy
[4] Dept of Biology and Biotechnology "L. Spallanzani", University of Pavia, 27100 Pavia, Italy
§ co-last authors

Author contributions: F.M., L.M. and E.U.D. designed research; G.G., A.M. and U.L. performed research; G.G., A.M. and T.S. analyzed data; G.G., L.M. and E.U.D. wrote the paper.
§ Lisa Mapelli and Egidio Ugo D'Angelo are co-senior authors

The authors declare no competing financial interests.

Acknowledgments. This project/research received funding from the European Union's Horizon 2020 Framework Program for Research and Innovation under the Framework Partnership Agreement No. 650003 (HBP FPA); the European Union's Horizon 2020 Framework Program for Research and Innovation under the Specific Grant Agreement No. 720270 (Human Brain Project SGA1), and under the Specific Grant Agreement No. 785907 (Human Brain Project SGA2). This work was supported by grant [7(17)] of Centro Fermi to ED.

In preparation

8.1 ABSTRACT

The neurovascular coupling (NVC) is the phenomenon that allows to regulate local blood flow in response to neuronal activity, thus originating the blood-oxygen-level-dependent (BOLD) signals used by imaging techniques to investigated brain functions. The cerebellar cortex is particularly suitable for investigating NVC (Mapelli et al., 2017). Recent studies on human fMRI (functional magnetic resonance imaging) showed different motor-dependent activity in cerebral cortex and cerebellum. In particular, cerebellar vermis and hemisphere showed respectively linear and non-linear BOLD responses to the same motor task performance (Alahmadi et al., 2017). Knowing that vermis and hemisphere are connected to different brain regions and are involved in different functions, we wondered whether the above mentioned differences in BOLD signals in these two areas are due to different NVC events. To this aim, we tested vascular reactivity to several input fibers stimulation frequencies mimicking brain activation patterns, in the granular layer of cerebellar vermis and hemisphere. Vermis and hemisphere neurovascular responses proved to be frequency-dependent in a non-linear way, but showing clear differences in the two regions, suggesting that NVC, and thus BOLD signal genesis, in the cerebellum might be region-dependent.

8.2 INTRODUCTION

The existence of tight relationships between neuronal and blood vessels activity was described for the first time by Roy and Sherrington in the past 1890. This process, called neurovascular coupling (NVC), allows the brain to regulate local cerebral blood flow (CBF) in order to satisfy cellular metabolic requirements for neurons health (Iadecola, 2017). The NVC provides the physiological basis for the blood-oxygen-level-dependent (BOLD) signals exploited by functional magnetic resonance imaging (fMRI) to map changes in brain activity. Although cellular and molecular mechanisms underlying vaso-dilation and -constriction are often known, the interpretation of BOLD signals is much debated and still under investigation (Logothetis, 2008; Hillman, 2014; Hall et al., 2016).

The cerebellum is very suitable for the study of NVC. Mossy fiber - granule cell synapses store and process incoming signals in the granular layer. This information is conveyed to the inhibitory auto-rhythmic Purkinje cells (the sole output stage of the cerebellar cortex) by granule cells axons (parallel fibers) spanning the molecular layer. The spatial distribution of cerebellar cortex fibers and cells is similar to that of Cartesian coordinate, thus facilitate the signal processing function of cerebellum (O'Hearn and Molliver, 2009). This peculiar structural organization, together with the impossibility to generate epileptic and propagated depression events in the cerebellar

circuit, facilitate the study of CBF changes in response to neuronal activity (Lauritzen, 2001; Lauritzen et al., 2012).

In the cerebellum, NVC was long been investigated in the molecular layer where it was found to be dissociated from Purkinje cells spiking activity but drove by molecular layer interneurons excitation (Mathiesen et al., 1998; Caesar et al., 2003; Thomsen et al., 2004; Rancillac et al., 2006). In the granular layer, mossy fibers activation induced capillary vasodilation through an NMDA receptor/NO-dependent system acting on pericytes (Mapelli et al., 2017). This is in agreement with recent investigations showing the direct involvement of capillaries in NVC during neural-evoked pericytes activation, hypothesizing a contribution of these microvessels in the initiation of BOLD signals (Hamilton et al., 2010; Hall et al., 2014). Granule cells are the most abundant brain neurons, the most energy consuming cells in the cerebellum (Howarth et al., 2010; Howarth et al., 2012), and their activation after mossy fiber stimulation leads to NO production and vasodilation (Maffei et al., 2003; Mapelli et al., 2017). Therefore, NVC in the granular layer might be the main responsible for the CBF changes that translate into BOLD signals in the cerebellum.

In humans, fMRI investigations showed different BOLD responses in cerebral cortex and cerebellum, during the same motor task performance (Alahmadi et al., 2015; Alahmadi et al., 2016). Moreover, cerebellar vermis lobule V and hemisphere lobule VI showed respectively linear and non-linear BOLD signals in fMRI analysis of force-related brain activation. In particular, the BOLD signal in vermis lobule V increased linearly with increasing grip force (1^{st} order), while it increased non-linearly in hemisphere lobule VI (4^{th} order). This might reflect different functional roles of distinct areas in human cerebellum (Alahmadi et al., 2017). In the same investigation, linear and non-linear BOLD signals were detected during the execution of the same tasks also in different areas of the cerebral cortex. It was impossible for the authors to discern whether the linearity (or absence of it) in the cerebellar responses originated locally or depended on the properties of a cortical input. Herein, we investigated whether these two different cerebellar regions are able to differentiate the neurovascular response in a input frequency-dependent manner. This is of particular interest, since cerebellar vermis and hemisphere are differently connected to other brain areas, with lateral cerebellar hemispheres involved in non-motor functions such as language generation (Petersen et al., 1988; Leiner et al., 1993; Raichle et al., 1994; De Smet et al., 2013), cognition and emotion (Leiner et al., 1989; Schmahmann, 1991, 2010; Timmann et al., 2010), and more recently in memory (Kuper et al., 2016). Assuming this, it was compelling to target if vermis and hemisphere would equally contribute to NVC during the different states of brain and cerebellar activity. Since the main frequency bands observed during brain activity can be related to local computation (slower bands) or long range connectivity (faster bands) (Buzsaki, 2006), we asked

whether the different cerebellar vermis and hemisphere connections to other brain regions might be reflected in their neurovascular responses to input bearing different frequencies.

8.3 METHODS

8.3.1 Proceedings for cerebellar slices preparation.

C57BL/6 mice of both sexes aged between 17 and 23 days, were used in order to obtain cerebellar slices as reported previously (D'Angelo et al., 1995; Armano et al., 2000; Mapelli et al., 2009; Mapelli et al., 2017). Mice were anesthetized with halothane (Aldrich, Milwaukee, WI) and killed by decapitation. Acute parasagittal slices of 220μm thickness were cut from the cerebellar vermis and hemisphere with a vibroslicer (LEICA VT1200S). During the cutting procedure, slices were maintained in cold Krebs solution. Then, slices were recovered for at least 1h in the same solution before to be incubated for 1 h with 75 nM U46619 (Abcam), a thromboxane agonist. This drug was added to Krebs solution in order to restore the original vascular tone in slices. Finally, biological samples were transferred to a 2-ml recording chamber mounted on the stage of an upright microscope (Slicescope, Scientifica Ltd, UK). Here, preparations were perfused with Krebs solution (2 ml/min) and maintained at 37°C with a Peltier feedback device (TC-324B, Warner Instruments, Hamden, CT). Krebs solution for slice cutting and recovery contained (in mM): 120 NaCl, 2 KCl, 1.2 $MgSO_4$, 26 $NaHCO_3$, 1.2 KH_2PO_4, 2 $CaCl_2$, and 11 glucose, and was equilibrated with 95% O_2-5% CO_2 (pH 7.4). Substances for solution were obtained from Sigma Aldrich.

Animal maintenance and experimental protocols were performed according to the international guidelines from the European Union Directive 2010/63/EU on the ethical use of animals and approved by the national committee of animal health. All experimental procedures were performed in order to prevent animal suffering, and were approved by the local ethical committee of the University of Pavia (Italy) and by the Italian Ministry of Health (authorization n. 645/2017-PR).

8.3.2 Immunofluorescence staining in cerebellar slices

Pericytes and capillaries were stained in the granular layer of both cerebellar vermis and hemisphere slices as previously described (Hall et al., 2014; Mapelli et al., 2017).We focused on the vermis lobule V and hemisphere lobule VI. First, slices (220 μm-thick) were fixed with 4% paraformaldehyde in PBS for 25 min in a Petri dish. Secondly, slices were washed three times before being permeabilized and blocked with 5% Triton X-100, 10% BSA added to PBS, overnight at 4°C. Thus, slices were ready for the incubation with the primary and secondary antibodies. Thirdly, preparations were incubated for 24 h at 25°C on a rotary shaker with rabbit anti-NG2

chondroitin sulfate proteoglycan (Millipore, cat no. AB5320, 1:200 dilution) and FITC-isolectin B4 (Sigma-Aldrich, cat. no. L2895; 1:200 dilution of a stock solution of 2 mg/ml FITC-IB4 in PBS) primary antibodies to stain respectively pericytes and blood vessels. Before the incubation with secondary antibodies, slices were washed three times (each of 15 min) with PBS. Fourthly, samples were incubated for 4 h at 25°C with fluorescent secondary antibody Rhodamine Red-X-AffiniPure Goat Anti-Rabbit IgG (Jackson ImmunoResearch Inc. cat. no.111-295-045; 1:500 dilution). Finally, slices were washed in the same way as for primary antibodies incubation. In order to analyze the results in our biological treated samples, we filled microscope slides,ProLong® Gold antifade reagent with DAPI (Molecular Probes) and coverslips were positioned. Fluorescence of cerebellar samples was observed with a TCS SP5 II LEICA confocal microscopy system (Leica Microsystems, Italy) furnished with a LEICA DM IRBE inverted microscope. The confocal system exploited a 20X, 40X and 63X objectives to acquire images. All acquisition files were visualized by LAS AF Lite software (Leica Application Suite Advanced Fluorescence Lite version 2.6.0) installed on a desktop PC. We also carried out negative controls by treating slices with non-immune serum during the incubation procedures.

8.3.3 Analysis of capillaries activity in the granular layer of the cerebellum.

Bright-field microscopy was exploited in order to identify granular layer vessels in parasagittal slices of cerebellar vermis and hemisphere. Lobule V of vermis and lobule VI of hemisphere were first identified using a 4X objective (XL Fluor 4X/340, N.A.: 0.28, Olympus, Japan). Secondly, GL of both lobules was inspected using a 60X objective (LumPlanFl 60X/0.90 W, Olympus, Japan) which allowed to recognize capillaries and neighboring pericytes. Vessels must have an inner diameter <10μm to be considered and they had to be surrounded by at least 1 pericyte (arrowheads in Fig. 1a). The inner diameter of capillaries and the nearby pericytes were identified by bright-field microscopy. Only one capillary per slice was used for experiments. In *ex-vivo* conditions, capillaries lose intraluminal flow and pressure due to the mechanical stress of the slicing procedure. Before proceeding with the experimental protocol, slices were treated with 75nMU46619, a thromboxane agonist that re-establish the vascular diameter mimicking physiological conditions. Once the focus of the objective was adjusted on the capillary, it might happen that capillary walls and pericyte soma were not visible together on the same plan. With their long projections, pericytes regulate the caliber of distant portions of the vessels (Hamilton et al., 2010). Therefore, pericytes membrane adjacent vessel walls may appear blurry when the focal plane was chosen.

Since mossy fibers electrical stimulation was shown to determine synaptic-dependent vasodilation in the granular layer of the cerebellum (Mapelli et al., 2017), here we stimulated mossy

fibers with 15 V stimuli at 6Hz, 20Hz, 50Hz, 100Hz, and 300Hz for 35s, using a bipolar tungsten electrode (Warner Instruments, UK) in both cerebellar lobule V and lobule VI of respectively vermis and hemisphere slices.

First, our attention was focused on vascular responses during 6Hz stimulation. This frequency is associated to sensorimotor activation of the granule cells in cerebellum and to cognitive states (De Zeeuw et al., 2008). Secondly, we stimulated mossy fibers with the same experimental protocol set at 20Hz. Several experimental evidence showed local field potential (LFP) oscillations of 18-25Hz in motor and cerebellar cortex (primarily in granular layer) of primates during voluntary movements and active and passive expectancy (Pellerin and Lamarre, 1997; Donoghue et al., 1998; Courtemanche et al., 2002; Courtemanche and Lamarre, 2005). Since cerebellum exert motor response through sensory and motor cortex connections via pontine nuclei (Bjaalie and Leergaard, 2000; Nagao, 2004), we stimulated mossy fibers in the cerebellar granular layer of vermis lobule V and hemisphere lobule VI at 50Hz and 100Hz. These frequencies of stimulation are known to induce synaptic facilitation in rat pontine nuclei neurons in *in vitro* experiments (Mock et al., 1997; Schwarz et al., 1997). Finally, we tested 300Hz mossy fibers stimulation effect on vascular activity. Mossy fiber – granules cell synapses show strong fidelity of high-frequency transmission during stimulation (Rancz et al., 2007a; van Beugen et al., 2013; Delvendahl and Hallermann, 2016).

In the text, we reported the values of the diameter changes observed in vermis and hemisphere during the application of different frequencies stimulation protocols. In any case, mossy fibers stimulation induced a significant vasodilation, as showed in Fig. 1b and 1c (example of capillary before and during the stimulus). Capillary responses in the granular layer were detected about 200µm distant from the stimulating electrode (average distance in vermis slices: 131.93±5.60µm; n=50 and hemisphere slices: 135.45±5.28µm; n=49; vermis vs hemisphere p=0.648). The distance between stimulus and vascular response is similar to that observed by Prestori and colleagues about stimulation spreading in cerebellar cortex using voltage-sensitive dye imaging (Prestori et al., 2013). On the top of the microscopy system a CCD camera was mounted (DMK41BU, Imaging Source, Germany), used to obtain the time-lapse bright-field images of capillaries caliber modification. The camera is governed by the IC-capture 2.1 software (Imaging Source, Germany) to acquire 1 image every second (before, during and after mossy fibers stimulation) with an exposure time of 5ms. Image sequences were analyzed offline with ImageJ software. The measure tool of ImageJ allowed to measure the inner diameter of capillaries, as performed in recent investigation (Mapelli et al., 2017). Only the region of the vessel where the maximal effect was observed was considered for the analysis. Data were compared using statistical

paired and unpaired Student's *t* test and with ANOVA test. First, we applied the normality test in order to check the normal distribution of data. After this, we used the parametric one-way ANOVA and finally the Fisher post-hoc test to validate the statistical significance. Data were considered statistically significant when $p<0.05$ and are reported as mean ± SEM (standard error of the mean).

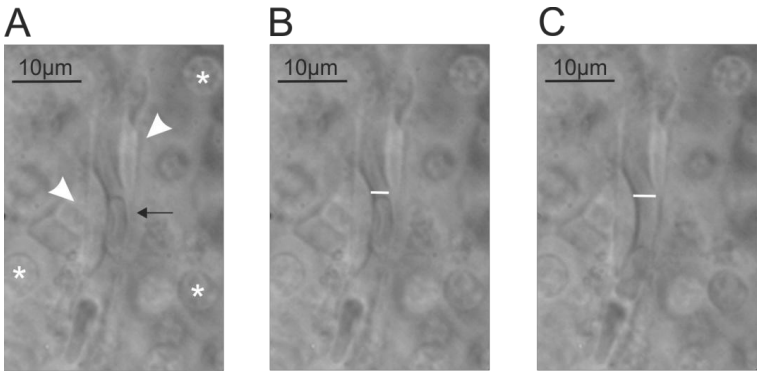

Figure 1 | Identification of capillaries in mouse cerebellar slices. ***A***, In the granular layer, capillary walls were in contact with pericytes (arrowheads) and were surrounded by granule cells (asterisks). A red blood cell (black arrow) is also visible inside the capillary. ***B***, The white bar shows the inner diameter of the capillary in the granular layer before the application of the stimulation protocol. ***C***, The diameter of the same capillary as in A,B increases (white bar) during mossy fiber stimulation.

8.3.4 Recordings of activity in the cerebellar granular layer

After slicing, recovery and incubation with U46619 (75 nm) procedures, slices were ready for experimental manipulation. Neuronal activity was recorded as local field potential (LFP) in the granular layer of vermis lobule V and hemisphere lobule VI during single pulse mossy fibers stimulation at 37° C, through a high-density multi-electrode array (HD-MEA) system (BioCAM X, 3Brain AG, Wädenswil, Switzerland). This system was equipped with a CMOS microchip consisting of 4096 recording microelectrodes (Arena probe), an external peristaltic pump (ISMATEC) for Krebs solution perfusion (2ml/min), a Peltier feedback temperature controller (TC-324B; Warner Instrument Corporation) and a bipolar tungsten electrode (Warner Instruments) for electrical stimulation (delivery currrent pulse of 50 µA for 200 µs). The microchip consists of a glass chamber (diameter 25mm; height 7mm) containing the probe (4096 recording microelectrodes arranged in a 64 x 64 matrix, covering an area of 2.67mm x 2.67mm). The electrode size is 21µm x 21 µm with a pitch of 42 µm. Neuronal activity was sampled at 17840.7 Hz/electrode and acquired

with BrainWave X software. In the granular layer, neuronal response to mossy fiber stimulation originated LFPs. In both vermis and hemisphere, the LFP shows a typical N_1–N_{2a}- N_{2b}–P_2 complex: N_1 corresponds to presynaptic volley activation, N_{2a}- N_{2b} are informative of granular cells synaptic activation and P_2 is likely to represent currents returning from the molecular layer (Mapelli and D'Angelo, 2007). In order to characterize granule cells responses to stimulation, the analysis was focused on N_{2a} and N_{2b} peaks amplitude and time to peak. Recordings were exported and analyzed with Matlab (Mathworks). In the text, data significance was assessed using paired and unpaired Student's *t* test.

8.4 RESULTS

Capillary inner diameter modifications in response to neuronal activity directly contributes to CBF changes that generate the cerebellar BOLD signals. Control of capillaries activity is mediated by the release of vasoactive molecules acting on pericytes (Hall et al., 2014; Mapelli et al., 2017), which are contractile cells that enwrap capillary walls (Dalkara and Alarcon-Martinez, 2015b; Attwell et al., 2016). Here, we focused on capillaries in vermis lobule V and hemisphere lobule VI of the cerebellum.

8.4.1 Structural organization of neurovascular unit elements in the granular layer of cerebellar vermis and hemispheres.

In the granular layer, microvessel walls consisted of tightly connected endothelial cells surrounded by granule cells (asterisks in Fig. 2Ba and 2Bb) but not by smooth muscle cells. The mean internal diameter of capillaries was 2.75±0.15μm (n=50) in the vermis and 2.47±0.11μm (n=49) in the hemisphere, not statistically different (p=0.13). In both vermis and hemisphere, pericytes were in close contact with capillary walls (arrowheads in Fig. 2Ba and 2Bb). Immunostained cerebellar slices showed isolectin B4- and proteoglycan NG2antobody-labeled granular layer capillaries. These primary antibodies stained respectively vessel and pericyte membranes, as reported previously (Mishra et al., 2014; Mapelli et al., 2017) (Fig. 2A and 2B). Capillaries, pericytes and granule cells were observed exploiting the confocal system with a 63X objective.

Cerebellar slices examination with lower magnifications (20X and 40X) (Fig. 2A) allowed to identify the differences between molecular and granular layer vascular network organization in both vermis lobule V and hemisphere lobule VI. Both in vermis and hemisphere, molecular layer showed a regular vascular architecture with superficial arterioles originating from the top of the

lamella, penetrating deep into the layer and giving off the thick net of capillaries in the granular layer (Fig. 2Aa and 2Ab). Therefore, cerebellar vermis and hemisphere had the same neurovascular component which are capillaries, pericytes and granule cells.

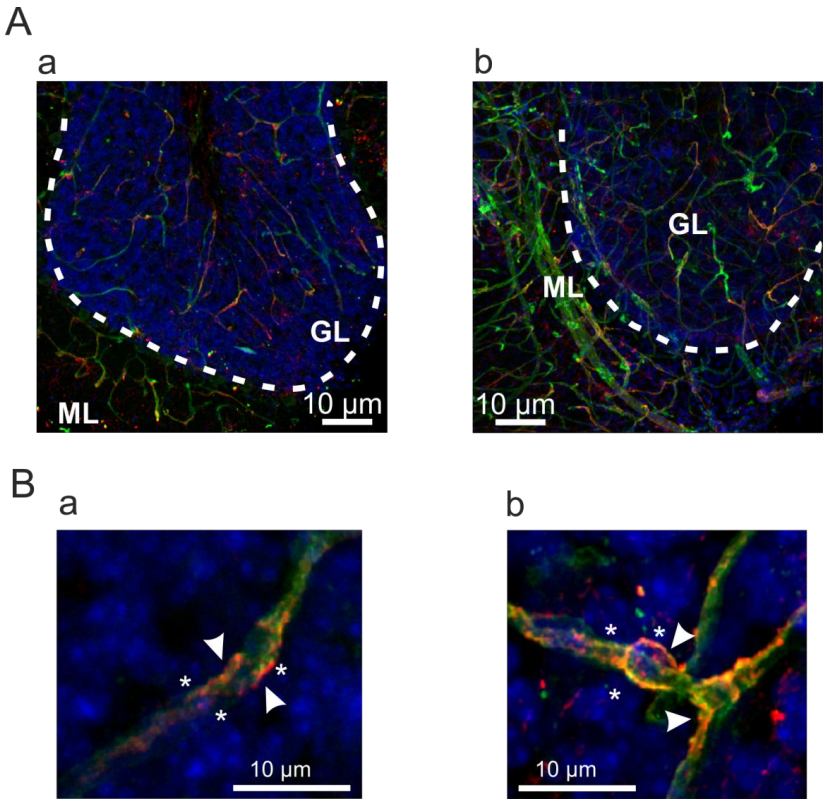

Figure 2 | Immunofluorescence study of cerebellar cortex in mice. Cerebellar slices were stained with IB4 and NG2 in order to stain respectively blood vessel walls (green) and pericytes (red). Granule cells nuclei were stained with DAPI (blue). ***A***, Immunofluorescence in the cortex of cerebellar vermis and hemisphere. ***Aa***, Fluorescent image of cerebellar cortex in vermis lobule V of a cerebellar slice. ML= molecular layer; GL= granular layer. ***Ab***, Immunostained slice showing the cerebellar hemisphere lobule VI. ML= molecular layer; GL= granular layer. ***B***, Immunofluorescence in the granular layer of cerebellar vermis and hemisphere. ***Ba***, High magnification (40x objective) confocal image showing granule cells (asterisks) surrounding capillaries (green) and pericytes (arrowheads) in the granular layer of the vermis. ***Bc***, In the granular layer of the hemisphere, confocal microscopy analysis showed the presence of granule cells (asterisks) located near capillary walls (green) and in close contact with pericytes (arrowheads).

8.4.2 Capillaries responses to mossy fibers stimulation in the granular layer of the cerebellar vermis

Cerebellar vermis slices were pre-incubated with U46619 (75nM), thromboxane A2 agonist, routinely used in neurovascular coupling investigations, in order to re-establish the vascular tone disrupted in *ex-vivo* conditions, where blood vessel perfusion and pressure are absent (Rancillac et al., 2006; Fernandez-Klett et al., 2010; Mishra et al., 2014; Mapelli et al., 2017).

Mossy fibers stimulation in U46619-treated slices of the vermis induced a significant vasodilation at each frequency tested: 6Hz, 20Hz, 50Hz, 100Hz and 300Hz (maximal dilation of, respectively,2.99±0.61%, n=9; p=0.00013; 7.19±1.85%, n=10; p=0.0008; 3.66±0.82%, n=10; p=0.0001; 7.24±1.26%, n=10; p=0.00002; 6.42±1.10%, n=11; p=0.0002) as showed in the time course of capillary diameter percent changes at different frequencies of stimulation (Fig. 3Aa, 3Ba, 3Ca, 3Da, 3Ea).

In order to compare the different vasodilation kinetics at different frequencies, the time course of vessels responses was described at specific time-points during the stimulation (2s, 20s, 35s). The activation of mossy fibers at 6Hz caused granular layer capillaries vasodilation in vermis lobule V during the stimulation period as follows: 0.31±0.31% at 2s, n=9;2.75±0.74% at 20s, n=9; 2.60±0.88% at 35s, n=9 (Fig. 3Ab). The maximal value of capillaries response was observed at 30s (2.99±0.61%, n=9) after the beginning of the stimulation protocol (Fig. 3Aa).

The stimulation at 20Hz induced a rapid vasodilation during the first 20s of stimulation (2s: 1.48±0.56%; n=10; 20s: 5.88±1.63%; n=10) followed by a slow increase in capillary diameters that reach the maximum after 35s (7.19±1.85%; n=10) (Fig. 3Ba and 3Bb). At the end of the stimulus (35s) capillary responses at 20Hz was different to that at 6Hz (6Hz vs 20Hz at 35s: p=0.015). During 50Hz stimulation, the vasodilation observed was smaller than the previous one (Fig. 3Ca). In this case, capillaries increase slowly their lumen diameter with a peak of maximal dilation at the end of the stimulus (2s: 0.20±0.11%; 20s: 2.40±0.58%; 35s 3.66±0.82%; n=10) (Fig. 3Cb). Capillary responses at 20Hz and 50Hz were different during the first part of the stimulation (20Hz vs 50Hz at 2s: p=0.039 and at 20s: p=0.0358) (Fig. 3F) but not at the end of the stimulus (20Hz vs 50Hz at 35s: p=0.995) (Fig. 3F). Mossy fibers stimulation at 100Hz caused an increase in capillary dilation (2s: 0.89±0.49%; n=10; 20s: 4.67±1.50%; n=10; 35s: 7.24±1.26%; n=10) (Fig. 3Da and 3Db) which was similar to that observed at 20Hz (20Hz vs 100Hz at 2s: p=0.443, at 20s: p=0.594 and at 35s: p=0.981) but different to that at 50Hz and 6Hz at 35s (6Hz vs 100Hz at 35s: p=0.014 and 50Hz vs 100Hz, at 35s: p=0.049) (Fig. 3F). Mossy fibers stimulation at 300Hz caused a biphasic vessel response (Fig. 3Ea). During the first part, capillary responses linearly increase (2s:

1.18±0.68%; n=11) until 7s after the start of the stimulus where the time course showed (Fig. 3Ea and 3Eb). From 10s to the end of the stimulation protocol, diameter percent changes of capillaries showed another increase that reach the maximum value at 35s (20s: 3.45±0.82%; n=11 and 35s: 6.42±1.10%; n=11) (Fig. 3Ea and 3Eb). The latter response was similar to that observed at 20Hz and 100Hz (20Hz vs 300Hz at 2s: p=0.742, at 20s: p=0.189 and at 35s: p=0.720; 100Hz vs 300Hz at 2s: p=0.741, at 20s: p=0.474 and at 35s: p=0.629) but significantly different to the stimulation at 6Hz at 35s (6Hz vs 300Hz at 35s: p=0.036) (Fig. 3F). In the vermis, capillary responses to different stimulation patterns are showed in a final figure summarizing our first results (Fig. 3F).

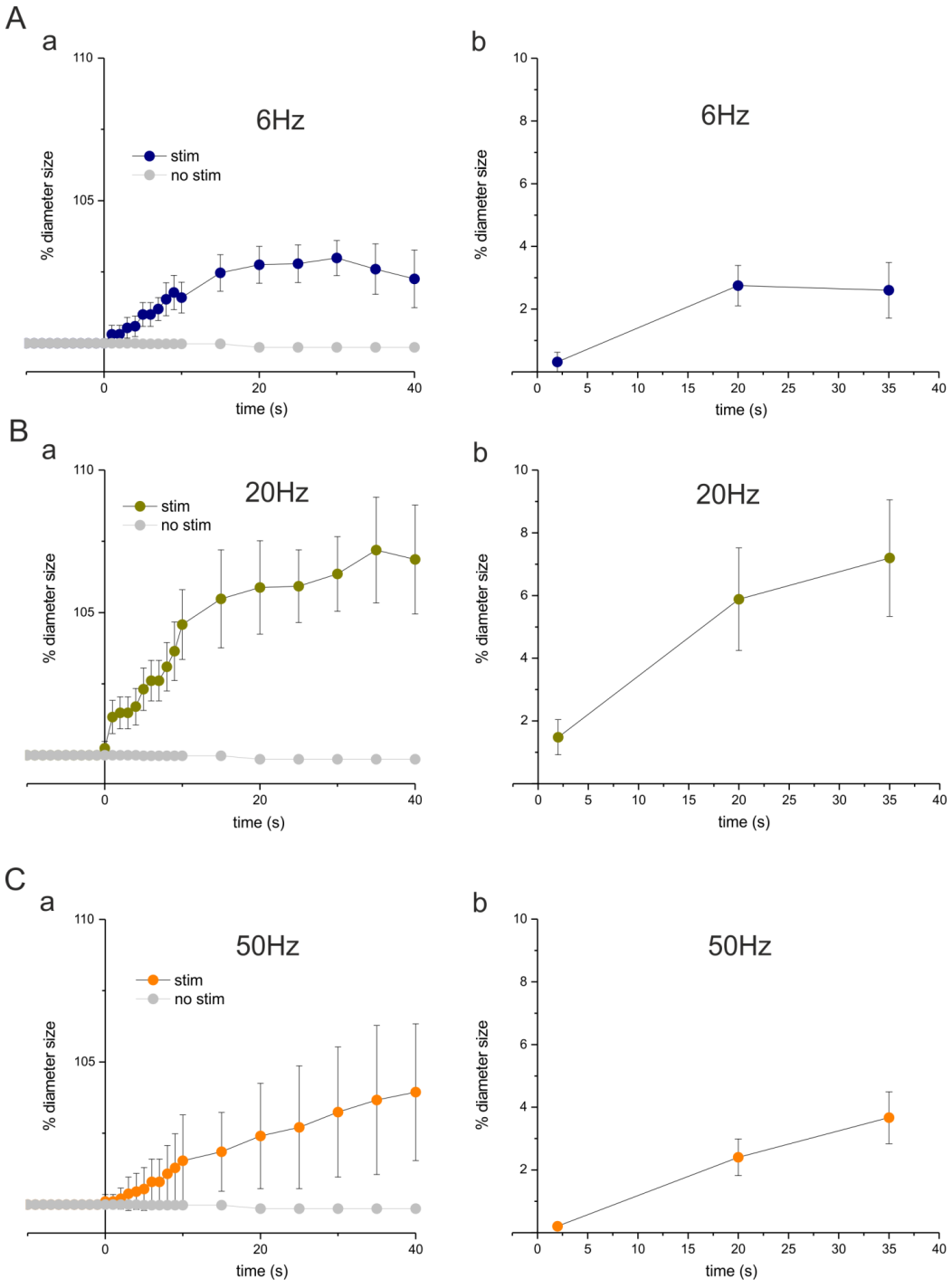
A
a
6Hz
stim
no stim
% diameter size
time (s)
b
6Hz
% diameter size
time (s)
B
a
20Hz
stim
no stim
% diameter size
time (s)
b
20Hz
% diameter size
time (s)
C
a
50Hz
stim
no stim
% diameter size
time (s)
b
50Hz
% diameter size
time (s)

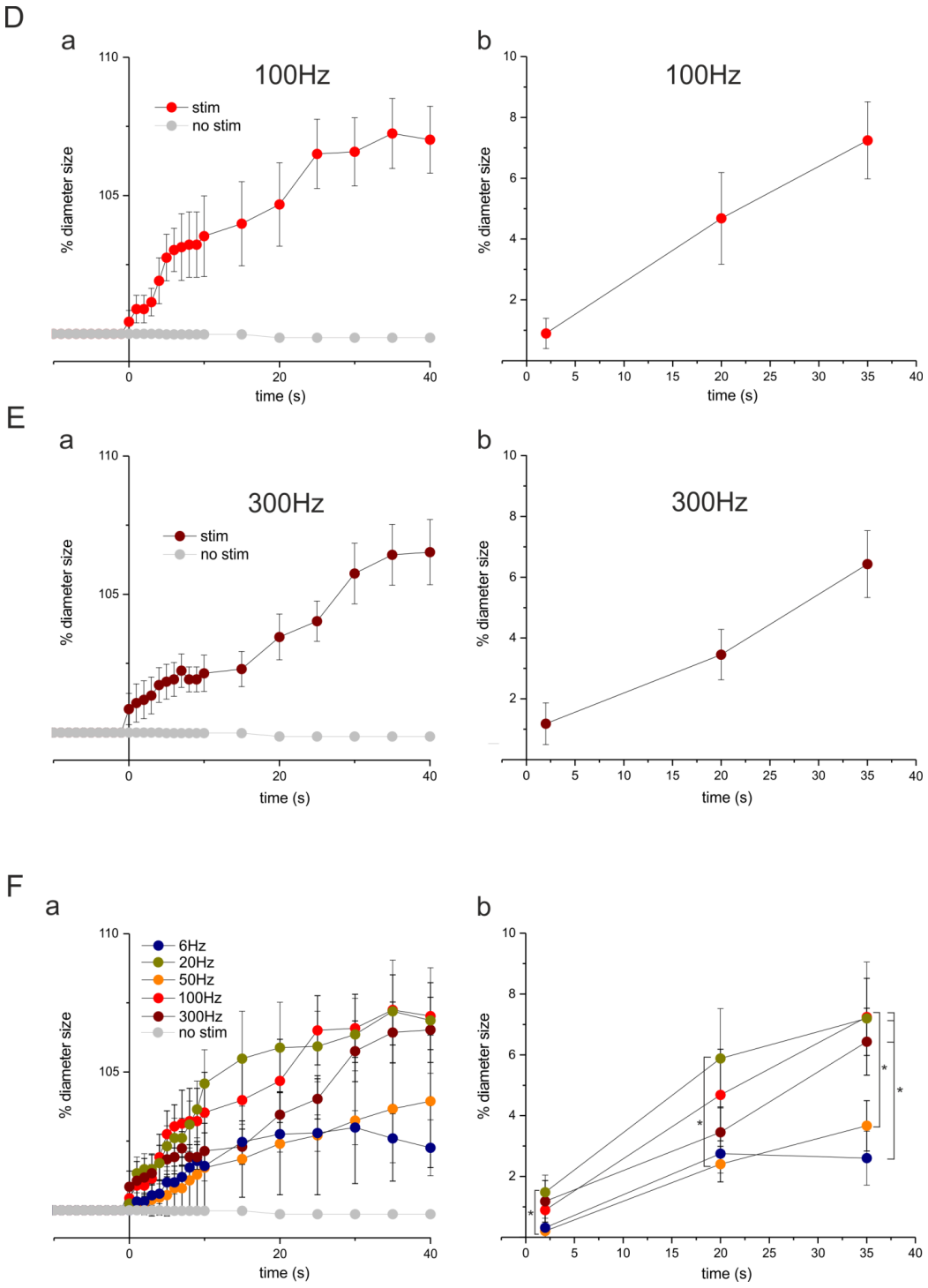
D
a
100Hz
stim
no stim
% diameter size
time (s)
b
100Hz
% diameter size
time (s)
E
a
300Hz
stim
no stim
% diameter size
time (s)
b
300Hz
% diameter size
time (s)
F
a
6Hz
20Hz
50Hz
100Hz
300Hz
no stim
% diameter size
time (s)
b
% diameter size
time (s)

Figure 3 | Vascular responses in the granular layer of cerebellar vermis lobule V during electrical stimulation (15V) at different frequencies. Slices were pre-treated with U46619 (75nM for 1h). The gray traces showed capillary lumen changes (n=8) in absence of stimulation (control experiments). ***A***, Capillary responses in the granular layer during low frequency (6Hz) mossy fibers stimulation for 35s.***Aa***, Time course of averaged percent changes of capillary diameters (n=9; p=0.00013) during 6Hz stimulation frequency. ***Ab***, Capillary diameter sizes at 2s, 20, and 35s. ***B***, Capillary responses in the granular layer during 20Hz mossy fiber stimulation for 35s. ***Ba***, Time course of averaged percent changes of capillary diameters (n=10; p=0.0008) during 20Hz stimulation frequency. ***Bb***, Capillary diameter sizes at 2s, 20, and 35s. ***C***, Capillary responses in the granular layer during 50Hz mossy fibers stimulation for 35s. ***Ca***, Time course of averaged percent changes of capillary diameters (n=10; p=0.0001) during 50Hz stimulation frequency. ***Cb***, Capillary diameter sizes at 2s, 20, and 35s. ***D***, Capillary responses in the granular layer during 100Hz mossy fiber stimulation for 35s. ***Da***, Time course of averaged percent changes of capillary diameters (n=10; p=0.00002) during 100Hz stimulation frequency. ***Db***, Capillary diameter sizes at 2s, 20, and 35s. ***E***, Capillary responses in the granular layer during high frequency (300Hz) mossy fiber stimulation for 35s. ***Ea***, Time course of averaged percent changes of capillary diameters (n=11; p=0.0002) during 300Hz stimulation frequency. ***Eb***, Capillary diameter sizes at 2s, 20, and 35s.***F***, Graphic of capillary responses to different stimulation frequencies in the granular layer of cerebellar vermis lobule V. ***Fa***, Time course of averaged capillary percent diameter changes in response to mossy fibers stimulation. ***Fb***, Modifications of capillary lumen at 2s, 20s and 35s during different frequencies of stimulation.

8.4.3 Capillaries responses to mossy fibers stimulation in the granular layer of the cerebellar hemisphere

In the granular layer of the hemisphere, mossy fibers stimulation induced significant capillary dilation at 6Hz, 20Hz, 50Hz, 100Hz and 300Hz (respectively 4.93±1.06%, n=9; p=0.003; 6.96±1.45%, n=10; p=0.0006; 5.79±0.91%, n=10; p=0.00001; 4.28±1.00%, n=10; p=0.0001; 4.07±1.28%, n=10; p=0.0001), in slices pre-treated with U46619. Time course of vasodilation during all the stimulation frequencies is showed in Fig. 4Aa, 4Ba, 4Ca, 4Da, 4Ea.

Capillary responses induced by mossy fibers stimulation at 6Hz are shown in Fig. 4Aa and 4Ab (2s: 1.49±0.60%, n=9; 20s: 3.55±0.84%, n=9; 35s: 4.93±1.06%, n=9).

Mossy fibers stimulation at 20Hz increased capillary inner diameters (2s: 1.05±0.56%, n=10; 20s: 6.61±1.44%, n=10) (Fig.4Ba and 4Bb). These results were not different to that observed during stimulation at 6Hz (6Hz vs 20Hz, at 2s: p=0.598; at 20s: p=0.092; at 35s: p=0.285). Vascular responses at 50Hz showed an increase in capillary diameters during the stimulation (2s: 0.53±0.28%; n=10; 20s: 4.84±0.91%; n=10; 35s: 5.79±0.91%; n=10) (Fig. 4Ca and 4Cb) which is

similar to that observed at 6Hz and 20Hz (6Hz vs 50Hz, at 2s: p=0.152; at 20s: p=0.317; at 35s: p=0.739 and 20Hz vs 50Hz, at 2s: p=0.425; at 20s: p= 0.312; at 35s: p=0.507). Application of 100Hz stimulation pattern caused vasodilation, as reported for previous frequencies (2s: 1.28±0.54%; n=10; 20s: 4.28±1.00%; n=10) (Fig. 4Da and 4Db). Nevertheless, at the end of the stimulation, capillaries vasodilation was smaller than at 20s (35s: 2.91±1.36%; n=10) (Fig. 4Da and 4Db). These vasodilations were statistically different to that observed during 20Hz stimulation, at 35s (20Hz vs 100Hz, at 35s: p=0.024). Mossy fibers electrical stimulation also induced a substantial rapid vasodilation when frequency was set at 300Hz. In this case, capillaries diameter increased of 2.64±0.84% (n=10) during the first 2s of stimulation (Fig. 4Ea and 4Eb) and reached a peak of 4.45±0.66% (n=10) 20s after the start of the stimulus (Fig. 4Ea and 4Eb). This behavior was similar to that observed at 6Hz and 20Hz (6Hz vs 300Hz, at 2s: p=0.292; at 20s: p=0.409, at 35s: p=0.131 and 20Hz vs 300Hz, at 2s: p=0.134; at 20s: p=0.190; at 35s: p=0.739), but different to that at 50Hz, at 2s and to 100Hz at 35s (50Hz vs 300Hz, at 2s: p= 0.029; 100Hz vs 300Hz, at 35s: p= 0.0.009) (Fig. 4F). Capillary diameters reached the maximal vasodilation in all experiments at 35s with a value of 7.61±1.28% (n=10) (Fig. 4Ea and 4Eb).

The time course of capillary diameter percent changes at different frequencies is summarized in figure 4F, for the cerebellar hemisphere. Capillary responses during mossy fibers stimulation at 100Hz were different compared to stimulation frequencies at 20Hz and 300Hz (100Hz vs 20Hz: p= 0.058 and 100Hz vs 300Hz: p=0.022, at 35s) (Fig. 4F).

Moreover, in the granular layer of hemisphere capillary responses at 50Hz and 100Hz were significantly different from that observed in the granular layer of the vermis at the same frequencies, but at different times (vermis vs hemisphere: p=0.037, at 20s at 50Hz; p= 0.032, at 35s at 100Hz) (Fig. 5B and 5C). There was no difference between capillary responses in vermis and hemisphere during the first 2s of mossy fibers stimulation (Fig. 5A).Some general observation can be already anticipated here, concerning the plots in Fig. 5. First of all, no difference is evident in vermis and hemisphere capillary reactions to the different frequencies tested for brief stimulation (at 2s). Secondly, protracting the stimulation to 20s is able to unravel a significant difference in capillary vasodilation at 50Hz between vermis and hemisphere. Thirdly, further maintenance of the stimulation unravel a difference also at 100Hz.

The plot in Fig. 6 shows a naif representation of the possible trend of vasodilation frequency-dependence for vermis and hemisphere, at 35s (i.e. when the difference is maximal). These results hint to what could be the polynomial trend of different orders for vermis (third order) and hemisphere (negative second order).

.

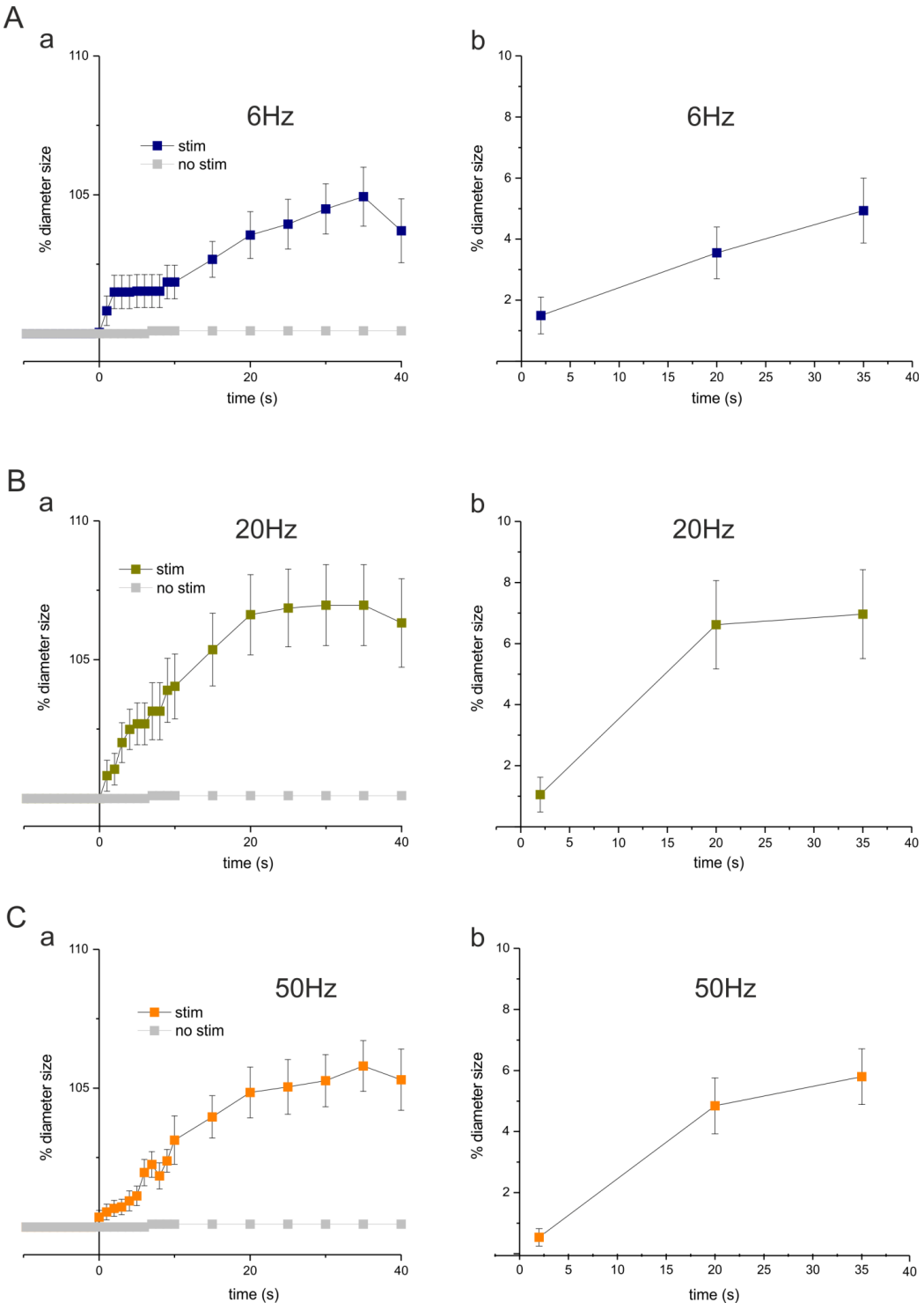
A
a
6Hz
stim
no stim
% diameter size
time (s)
b
6Hz
% diameter size
time (s)
B
a
20Hz
stim
no stim
% diameter size
time (s)
b
20Hz
% diameter size
time (s)
C
a
50Hz
stim
no stim
% diameter size
time (s)
b
50Hz
% diameter size
time (s)

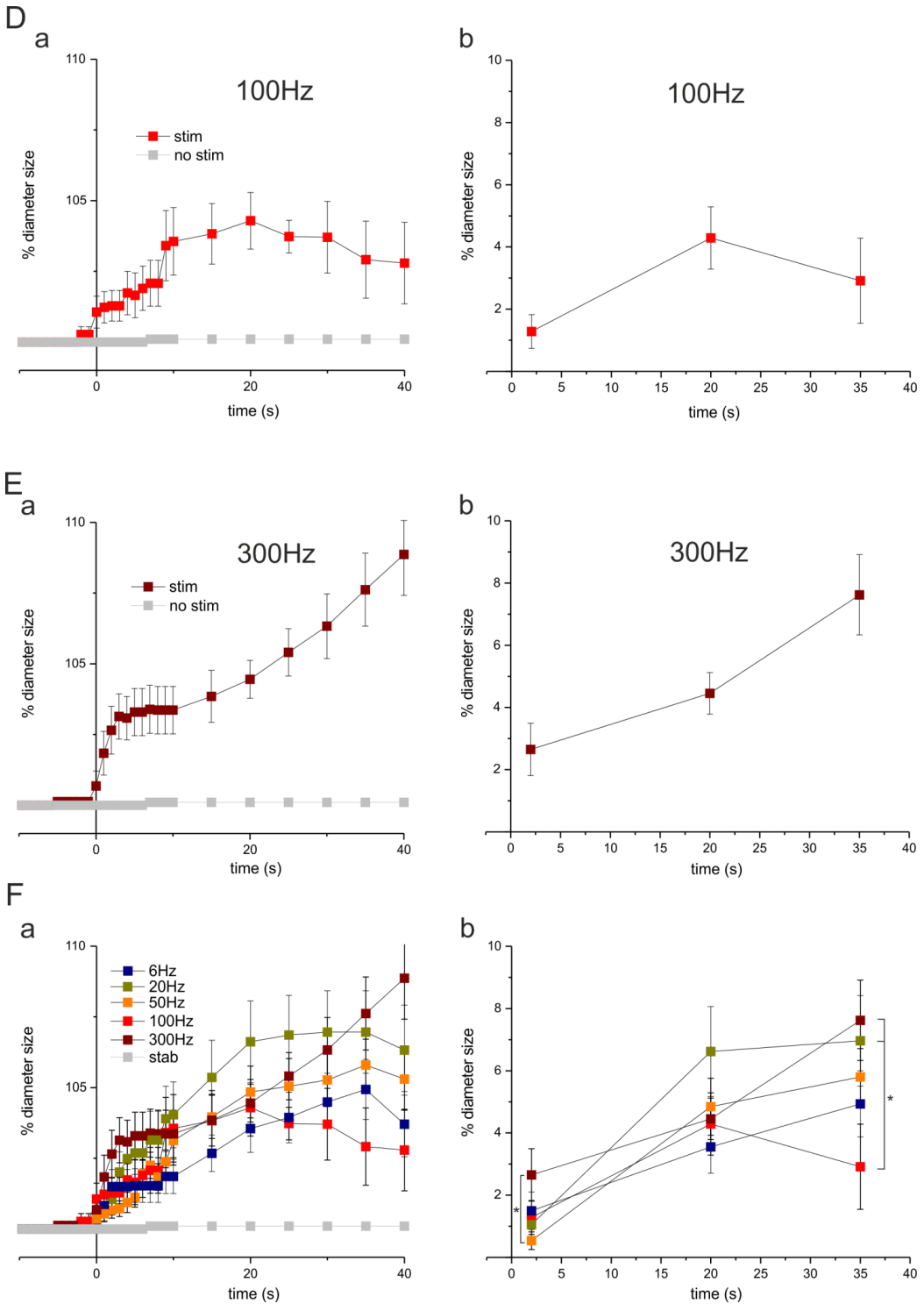
D
a
100Hz
stim
no stim
% diameter size
time (s)
b
100Hz
% diameter size
time (s)
E
a
300Hz
stim
no stim
% diameter size
time (s)
b
300Hz
% diameter size
time (s)
F
a
6Hz
20Hz
50Hz
100Hz
300Hz
stab
% diameter size
time (s)
b
% diameter size
time (s)
*
*

Figure 4 | Vascular responses in the granular layer of cerebellar hemisphere lobule VI during electrical stimulation (15V) at different frequencies. Slices were treated with U46619 (75nM, for 1h). The gray traces showed capillary lumen changes (n=8) in absence of stimulation (control experiments). ***A***, Capillary responses in the granular layer during low frequency (6Hz) mossy fibers stimulation for 35s. ***Aa***, Time course of averaged percent changes of capillary diameters (n=9; p=0.003) during 6Hz stimulation frequency. ***Ab***, Capillary diameter sizes at 2s, 20, and 35s. ***B***, Capillary responses in the granular layer during 20Hz mossy fiber stimulation for 35s. ***Ba***, Time course of averaged percent changes of capillary diameters (n=10; p=0.0006) during 20Hz stimulation frequency. ***Bb***, Capillary diameter sizes at 2s, 20, and 35s. ***C***, Capillary responses in the granular layer during 50Hz mossy fibers stimulation for 35s. ***Ca***, Time course of averaged percent changes of capillary diameters (n=10; p=0.00001) during 50Hz stimulation frequency. ***Cb***, Capillary diameter sizes at 2s, 20, and 35s. ***D***, Capillary responses in the granular layer during 100Hz mossy fiber stimulation for 35s. ***Da***, Time course of averaged percent changes of capillary diameters (n=10; p=0.0001) during 100Hz stimulation frequency. ***Db***, Capillary diameter sizes at 2s, 20, and 35s. ***E***, Capillary responses in the granular layer during high frequency (300Hz) mossy fiber stimulation for 35s. ***Ea***, Time course of averaged percent changes of capillary diameters (n=10; p=0.0001) during 300Hz stimulation frequency. ***Eb***, Capillary diameter sizes at 2s, 20, and 35s. ***F***, Graphic of capillary responses to different stimulation frequencies in the granular layer of cerebellar hemisphere lobule VI. ***Fa***, Time course of averaged capillary percent diameter changes in response to mossy fibers stimulation. ***Fb***, Modifications of capillary lumen at 2s, 20s and 35s during different frequencies of stimulation.

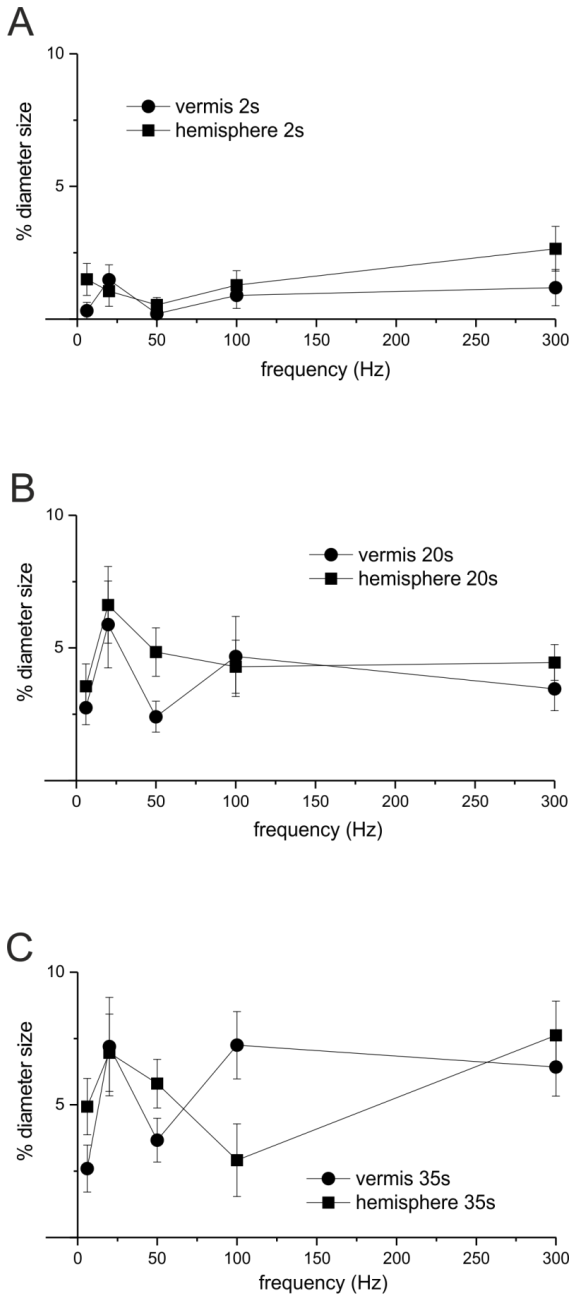

Figure 5 | Capillary diameter modifications in response to different stimulation frequencies (6Hz, 20Hz, 50Hz, 100Hz, 300Hz) for 35s in the granular layer of cerebellar vermis lobule V and hemisphere lobule VI. ***A***, Time course of percent diameter changes at different frequencies during 2s of stimulation in vermis and hemisphere. ***B***, Time course of percent diameter changes at different frequencies during 20s of

stimulation in vermis and hemisphere (vermis vs hemisphere, at 50Hz: p=0.037). ***C***, Time course of percent diameter changes at different frequencies during 35s of stimulation in vermis and hemisphere (vermis vs hemisphere, at 100Hz: p=0.032).

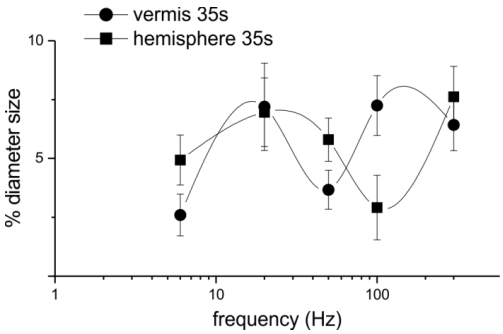

Figure 6 | Plotted percent diameter changes of vermis and hemisphere when the trend of vasodilation showed the maximal difference between these two regions (at 35 s).

8.4.4 LFP responses in the granular layer of cerebellar vermis and hemisphere

In order to correlate granular layer NVC responses with the genesis of different BOLD signals to the same input in the cerebellum as observed by Alahmadi and colleagues (Alahmadi et al., 2017), we are currently investigating granular layer activity during mossy fibers stimulation at the same frequencies used for vascular motility study (i.e. 6 Hz, 20 Hz, 50 Hz, 100 Hz and 300 Hz). As a first test, we characterize granular layer responses to mossy fiber single pulse stimulation in vermis and hemisphere. In the vermis, LFP signals peaked at 1.73±0.04 ms (N2a, n=30) and at 4.05±0.1 ms (N2b, n=30) with a value of respectively -165.48±6.62 µV (n=30) and -60.24±4.68 µV (n=30) (Fig. 7a). In the hemisphere, neuronal responses showed a first peak of -132.02±8.42 µV (N2a, n=32) at 1.97±0.08 ms (n=32) and a second one of -72.34±2.20 µV (N2b, n=32) at 3.95±0.1 ms (n=32) (Fig. 7b). The latency of the first peak was significantly shorter (p=0.012) in the vermis compared to the hemisphere, while the latency of the second peak was similar (p=0.622) in both regions. The amplitude of the first peak was larger in the vermis compared to the hemisphere (p=0.003), while the second peak was smaller in the vermis compared to the hemisphere (p=0.035). As showed in figure 7, the shapes of granular layer LFP were similar between vermis and hemisphere. The LFP waveform observed here (both in vermis and hemisphere granular layers) following mossy fiber stimulation are in line with that observed by Mapelli and D'Angelo in the vermis granular layer of

juvenile rats (Mapelli and D'Angelo, 2007). Since LFP shapes represents the activation of the circuit in the granular layer, we are confident that the circuitry is intact in both vermis and hemispheres slices.

Finally, the average distance from the site of stimulation (on mossy fibers) and the microelectrodes recording the LFP signals in vermis and hemisphere was 126±6.25 μm (n=62). This value is not statistically different (p=0,269) to the distance between the stimulation and the capillaries used for the analysis of vasodilation, in the first part of this work. Taken together, these preliminary observations suggest that granular layer response to mossy fiber stimulation might differ in vermis and hemisphere.

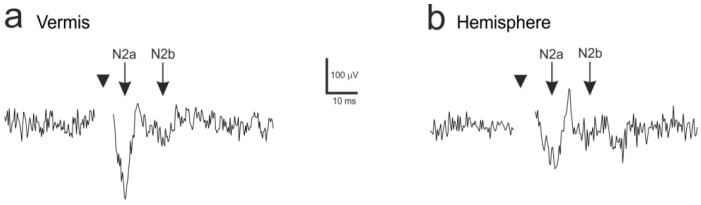

Figure 7 | Granular layer responses to stimulation in vermis and hemisphere. Local field potential in the granular layer of vermis lobule V (a) and hemisphere lobule VI (b) during mossy fibers stimulation with a single impulse. The start of the stimulation is showed by the arrowheads.

8.5 DISCUSSION

Here, we demonstrated that the activation of the input stage of the cerebellar cortex circuit, i.e. mossy fibers-granule cells synapse, caused dilation of capillaries in the granular layer of vermis and hemisphere in mouse cerebellar slices. The different stimulation frequencies used in order to activate the neuronal circuit mimic different states of CNS activation, namely: theta (6Hz), beta (20Hz), gamma (50Hz), fast (100Hz), and ultra-fast (300Hz) bands (according to Buzsaki 2006). These stimulation frequencies were able to induce different degrees of vasodilation. The mechanisms underlying neurovascular responses in the granular layer involves neuronal cells, in particular granule cells as observed by Mapelli and Gagliano in 2017 (Mapelli et al., 2017), capillaries and pericytes, as reported also in several papers (Peppiatt et al., 2006; Hamilton et al., 2010; Hall et al., 2014; Mishra et al., 2016; Mapelli et al., 2017; Winkler et al., 2018). Cerebellar slices immunostaining showed that the granular layer of vermis and hemisphere might have a similar structural organization of neurovascular unit components, since capillaries were in close

contact with pericytes, as described for different brain regions (Hall et al., 2014; Mishra et al., 2014; Attwell et al., 2016). Capillary dilation by pericytes activation is thought to be the main contributor to blood flow increase during neuronal-evoked neurovascular responses and thus substantially contributing to the activity-dependent BOLD genesis (Hall et al., 2014). Therefore, capillary-dependent CBF changes in response to neuronal activity in the granular layer of vermis and hemisphere is likely to contribute to cerebellar BOLD signal genesis.

8.5.1 Vascular responses to different pattern of stimulation in the granular layer of cerebellar vermis.

Mossy fibers stimulation induced a significant dilation in granular layer capillaries of vermis lobule V. Here, three different time points during the stimulation were considered to describe the effect: 2, 20 and 35s. Since the effects were maximal at 35s, this time point was taken into account for further considerations. fMRI observations of Alahmadi and colleagues about human cerebellar vermis lobule V activity during different motor task performance demonstrated that BOLD signals showed a linear proportional increase compared to five grip force levels (Alahmadi et al., 2017). Our findings suggest that vermis is indeed able to generate non-linear neurovascular responses to different patterns of activation.

8.5.2 Vascular responses to different activation pattern in the granular layer of cerebellar hemisphere.

In the granular layer of hemisphere lobule VI, capillaries showed statistically significant dilations when mossy fibers were electrical stimulated with different frequencies. Here, capillaries showed different responses from that observed in vermis. According to Alahmadi's results on human fMRI, hemisphere lobule VI might show different vascular responses during different inputs at different frequencies, as a possible physiological basis of the non-linear imaging signals observed during force-related BOLD measurements (Alahmadi et al., 2017). This has been confirmed by our data, supporting the interpretation that complex motor tasks are associated to the non-linearity of cerebellar BOLD signals. Thus, NVC responses in the hemisphere may explain the non-linear BOLD signals observed in cerebellar fMRI.

Cerebellar vermis and hemisphere showed different neurovascular responses to neuronal activity pattern in the granular layer. In particular, 50Hz and 100Hz frequencies of stimulation induced significantly different capillaries dilation at different times in these two areas. These observations strongly stay for a possible frequency- and time-dependent NVC process of vermis

and hemisphere in the cerebellum. Our results suggest that in cerebellum NVC might be region-dependent, given the same input pattern. These findings lead to hypothesize that the genesis of BOLD signal in the cerebellum could be region-dependent.

In conclusion, this work might provide new clues for the correct interpretation of imaging BOLD signals. Investigating the NVC could also help in the study of neurodegenerative disorders, like Alzheimer's disease, in which neurovascular phenomenon is altered.

8.5.3 Granular layer activity during mossy fibers stimulation in cerebellar vermis and hemisphere

In the granular layer of vermis lobule V and hemisphere lobule VI neuronal activation showed different responses to the same input stimulation. In particular, LFP recordings showed significant discrepancies in terms of delay and peak amplitude of the signals between vermis and hemisphere, during single-pulse stimulation of mossy fibers. Currently, we are investigating granular layer response to different stimulation patterns in both cerebellar regions. However, our preliminary results suggest that granule cells in vermis and hemisphere could generate different responses to the frequencies used for vascular activity investigation. Future experiments will help clarifying these preliminary observations.

8.5.4 Conclusions

These results suggest that capillary responses to mossy fibers input might be frequency- and time-dependent both in cerebellar vermis lobule V and hemisphere lobule VI. Notably, these dependencies showed significant differences in the two regions. Although further characterization of neuronal responses to the same stimulation patterns will be needed to explain the phenomenon, these data provide a substrate to the different BOLD responses observed in human fMRI during grip tasks in cerebellar vermis and hemisphere (Alahmadi et al., 2017). Indeed, our data show that these cerebellar regions respond differently in terms of vascular motility to the same incoming stimuli. This difference is evident with specific time- and frequency-dependencies (20s at 50Hz and 35s at 100Hz). Therefore, vessel responses at the same inputs in these regions were able to generate different vascular events in response to the same input, thus opening the door for a possible region-dependence of BOLD signals genesis in the cerebellum. Moreover, single impulse stimulation showed differencies in neuronal activation of granular layer between vermis and hemisphere. For these reasons, we are hopeful that further investigations on granular layer activity will improve our understanding of the different NVC during different stimulation ranges observed in cerebellar

vermis and hemisphere, by providing the possibility to compare neuronal activity as LFP to vascular responses.

In conclusion, while different cerebellar areas might receive different inputs from other brain regions (as the cerebral cortex), they might be also able to differentiate their BOLD signal independently on a difference in incoming stimuli. This difference might be related to input frequency and could depend on a different entrainment in long-range connections for cerebellar vermis and hemispheres.

These data prompt further investigations aiming at unravelling a possible different frequency-dependence of granule cells responses in vermis and hemisphere, that might be consequent of a different inhibitory activity of Golgi cells in these two cerebellar regions.

Further considerations and speculative data interpretation

The comparison of vasodilation frequency dependence for vermis and hemisphere shown in Fig.5 highlights some considerations.

i) For both vermis and hemisphere, capillary vasodilation is larger at 20Hz than it is for 6 and 50Hz. While the difference 6 vs 20Hz might be easily explained by an increase in the number of stimuli and therefore the number of neuronal responses generated in the same time, the drop in vasodilation observed comparing 20 vs 50Hz cannot be accounted by that. It is possible that, at 50Hz, neuronal responses might adapt or undergo short-term depression, decreasing overall neuronal activity. Again, this would not explain the further increase in vasodilation observed at 100 and 300Hz. Electrophysiological experiments are needed in order to assess the granule cell responses to these patterns of stimulation, in order to be compared to vessels behavior. In particular, extracellular recording of local field potentials in the granular layer might help solve this issue.

ii) For brief stimulations, no difference is revealed for vermis and hemisphere. Since vessel reaction depends on neuronal activity through NVC mechanisms, it is likely that this reflects an overall similarity in neuronal activity (and/or in neuronal metabolic consumption) in these two cerebellar areas during mossy fiber activation, at least at 2s (Fig.5A). When mossy fibers activation is further protracted, a significant difference is unraveled at 50 Hz (Fig.5B) and at 100 Hz (Fig.5C). In particular, capillary vasodilation is larger at 50Hz and smaller at 100Hz in the hemisphere, compared to the vermis at the same frequencies. One can speculate that these differences might depend on different vermis and hemisphere frequency-dependence of neuronal responses.

iii) since oscillation bandwidths in the brain hints for specific interpretation in the matter of local or distant connectivity (i.e. higher frequencies are likely to favor low range connections, while lower frequencies allow the entrainment in long range loops, see for extensive discussion Buzsaki 2016), it is tempting to hypothesize that cerebellar hemisphere, more than the vermis, might be entrained in long-range connections with other brain areas, contributing to low frequency oscillations bandwidths that are related to cognitive performance. This would also be in accordance with the view of cerebellar vermis motor function in the simple transduction of the incoming information from cortex and pontine nuclei to cerebellar nuclei and to output motor neuron (Nagao, 2004). Moreover, the complex NVC responses observed in the hemisphere encouraged the hypothesis of the involvement of these areas in complex information processing and of cerebellar contribution to high brain functions such as cognition.

Importantly, it has to be considered that the NVC mechanisms so far characterized in the granular layer involve, among others, NO release by granule cells and its action on pericytes. Therefore, the considerations reported above are very naive, and not meant to give an exhaustive explanation but just some hints to guide further functional characterizations. Indeed, these speculations need to be addressed by the electrophysiological assessment of granular layer neuronal activity during the stimulation patterns used to characterize vessels responses.

Chapter 9

General discussion

9. General discussion

The phenomenon of NVC is able to modify vessel diameter in response to neuronal activity in order to finely regulate the blood flow to the brain. Tuning vascular responses to neuronal input is the process that allows the brain to adequate the CBF to temporary state of increased or decreased activation in order to satisfy the energy demand of brain cells (Drake and Iadecola, 2007; Iadecola, 2017). NVC provides the physiological basis of the BOLD signals that characterize fMRI acquisitions. This imaging technique is used in diagnostic and research fields to infer brain activity. BOLD signals are generated by HbO_2 and Hbr ratio changes in CBF but the neuronal basis of this imaging response is still far from being understood (Attwell and Iadecola, 2002; Logothetis, 2008; Hillman, 2014).

Although NVC has been deeply investigated in several brain areas including the ML of the cerebellar cortex, biochemical pathways underlying the relationship between neurons and vessels are not completely dissected. In the cerebellar cortex, it has been shown that NVC is driven by MLIs but not by PCs activity (Thomsen et al., 2004; Rancillac et al., 2006). Surprisingly enough, the investigation of the role of cerebellar GL in NVC seems to has been forgotten during the years. Indeed, GL is very suitable for the study of the processes that calibrate vessel diameter in response to neuronal activation. This is mostly due to the great amount of GrCs (they are the most abundant brain neurons) and thus to their elevated energy demand, the presence of enzymes for the synthesis of vasoactive factors such as nNOS, and the already demonstrated ability to release the vasodilator NO during mossy fiber stimulation (Mapelli et al., 2017).

Recently, neurovascular responses were identified at capillary level in different areas of brain and cerebellum. Vasodilation or vasoconstriction events were controlled by vasoactive molecules, synthesized by neurons, that act on pericytes, small contractile cells in contact with the capillaries of the neurovascular unit (Fisher, 2009; Hamilton et al., 2010; Attwell et al., 2016). Capillaries ability to increase their lumen diameter before the arterioles and the propagation of the vasodilating signal to the upstream vessels lead to hypothesize that these tiny vessels are the first elements that contribute to the regulation of local blood flow. Moreover, capillaries were thought to be the main responsible for BOLD signals generation (Hall et al., 2014; Hall et al., 2016).

As the first step in a comprehensive study of NVC and the possible correlation with BOLD signal, we investigated vascular responses to neuronal activity in the more suitable brain area (i.e. the cerebellar GL) and tested how vessels diameters changed following neuronal activation resembling physiological conditions.

At first, we investigated the role of cerebellar GL in NVC in order to unveil the biochemical pathway underlying this phenomenon using a pharmacological approach. In the GL, the dense network of tiny capillaries wrapped by pericytes, showed by immunofluorescent staining, participate in neurovascular events in response to neuronal activation. The vasoactive molecules were released following GrCs excitation, after NMDARs and mGluRs activation, as demonstrated by capillary responses during MFs stimulation in presence of APV+7ClKyn and MCPG+CPPG (respectively NMDARs and mGluRs receptors inhibitors). Moreover, our experimental investigation on the nature of molecules involved in the vasodilating pathway (i.e. mossy fibers stimulation in presence of NO synthesis and sGC activation inhibitors) revealed that NO contribute to the majority of the vasodilation observed in GL. Thus, NO is most likely to contribute to CBF increases. NO is a well-known vasodilator and contribute to vasodilation in several brain areas. Here we showed that NO is also the main responsible of NVC in both molecular and granular layers of the cerebellum (Rancillac et al., 2006; Mapelli et al., 2017). One of NO effects on vascular motility is the ability to inhibit the production of the main vasoconstrictor synthesized by glial cells (Attwell et al., 2010). Our data showed that during NO synthesis inhibition capillary constriction is mediated by mGluRs activation. In these conditions, MFs stimulation in the presence of mGluRs antagonists showed a significant reduction of vasoconstriction in GL. Therefore, in the cerebellar GL, the vasoconstriction is controlled by the vasodilator agent. Thus, GrCs activity controls the balance between these opposite NVC responses. Since GrCs are the most abundant brain neurons, which generate the highest cerebellar energy demands, as mentioned before, NVC mechanisms must originate adequate vascular responses and blood flow changes to supply the metabolic requirements of these neurons during GL information processing. Contrarily, when GrCs are inhibited or simply not activated, the absence of NO production allows the synthesis of vasoconstrictors. In this case, neurovascular balance is shifted towards vasoconstriction. Therefore, these findings suggest that GrCs are the center of NVC in the cerebellar GL and encourage to speculate that their pivotal role might widely contribute to cerebellar BOLD signal genesis. Moreover, NVC mechanisms unraveling may help in the study of neurodegenerative disorders in which neurovascular functions are compromised.

In humans, fMRI investigations showed that the cerebellum responds to the motor task performance in a region-dependent manner. In particular, cerebellar vermis showed linear force-related BOLD signals while hemisphere generated non-linear imaging responses (Alahmadi et al., 2017). Since in the same investigation the cerebral cortex showed non-linear responses, the question arises about whether cerebellar non-linearity depended on non-linear input coming from the cortex,

or on an intrinsic cerebellar ability to generate non-linear responses to increasing input frequencies. We investigated this issue in mouse cerebellar slices, in order to isolate cerebellar responses in different regions (namely the vermis and the hemispheres) and to have complete control over the input patterns used to stimulate incoming fibers. Our results demonstrated that GL capillaries responded with significant vasodilations to different patterns of mossy fibers stimulation, that mimic different states of cerebellum activity. In vermis and hemisphere, vasodilations changes during 35s and depending on the frequencies of stimulation. Moreover, these two regions responded to the same frequency patterns (at 50Hz and 100Hz) with significantly different vasodilations. Moreover, neuronal responses to single input stimulation showed differences between the GL of vermis and hemisphere. Histological inspection of the tissue did not reveal differences in the vascular organization in both cerebellar vermis and hemisphere, showing capillaries surrounded by pericytes in close proximity to granule cells. Taken together, these observations stay for the existence of a region-dependent phenomenon of NVC in vermis and hemisphere and thus the involvement of these processes in the mechanisms that participate in the genesis of different BOLD signals in the cerebellum. These results show that the cerebellum is indeed able to generate non-linear neurovascular responses to increasing frequencies of the input. Interestingly, supposing that the frequency-dependence of vasodilations hints for a frequency-dependence of GrCs responses, it can be hypothesized that the cerebellar vermis and hemisphere neuronal activity differently contribute to the genesis of BOLD signals. Future investigations will address GrCs responses to these same input patterns in cerebellar vermis and hemispheres, together with GoCs - mediated inhibition, in order to unravel the neuronal origin of the differences in the NVC in these two regions.

Future investigations and speculations

The findings described in this work of thesis might bear a high impact on the scientific community, given the important implications on region-specific cerebellar computation and BOLD signals interpretation. First of all, we demonstrated the possible pivotal role of GrCs in cerebellar NVC. Secondly, neurovascular responses of the vermis and hemisphere prompt to hypothesize the involvement of these regions in different information processing, thus fostering the functional role of the cerebellum in high cognitive task as yet proposed by several studies (Leiner et al., 1989; Schmahmann, 2010). During evolution, cerebellum enlargement might have given to humans a functional strategy for adaptation. The different evolution history and size of cerebellum among species could reflect the different contribution of this area to the ability in adaptation through cleverness (Leiner et al., 1993; Glickstein and Doron, 2008).

Overall, our results provide new clues for cerebellar BOLD signals interpretation and for future investigations of cerebellar contribution to cognition, memory, language, and other functions in which only recently the cerebellum has been found involved.

Bibliography

Akgoren N, Fabricius M, Lauritzen M (1994) Importance of nitric oxide for local increases of blood flow in rat cerebellar cortex during electrical stimulation. Proc Natl Acad Sci U S A 91:5903-5907.

Akgoren N, Mathiesen C, Rubin I, Lauritzen M (1997) Laminar analysis of activity-dependent increases of CBF in rat cerebellar cortex: dependence on synaptic strength. Am J Physiol 273:H1166-1176.

Akgören N, Fabricius M, Lauritzen M (1994) Importance of nitric oxide for local increases of blood flow in rat cerebellar cortex during electrical stimulation. Proc Natl Acad Sci U S A 91:5903-5907.

Alahmadi AA, Pardini M, Samson RS, D'Angelo E, Friston KJ, Toosy AT, Gandini Wheeler-Kingshott CA (2015) Differential involvement of cortical and cerebellar areas using dominant and nondominant hands: An FMRI study. Hum Brain Mapp 36:5079-5100.

Alahmadi AA, Pardini M, Samson RS, Friston KJ, Toosy AT, D'Angelo E, Gandini Wheeler-Kingshott CA (2017) Cerebellar lobules and dentate nuclei mirror cortical force-related-BOLD responses: Beyond all (linear) expectations. Hum Brain Mapp 38:2566-2579.

Alahmadi AA, Samson RS, Gasston D, Pardini M, Friston KJ, D'Angelo E, Toosy AT, Wheeler-Kingshott CA (2016) Complex motor task associated with non-linear BOLD responses in cerebro-cortical areas and cerebellum. Brain Struct Funct 221:2443-2458.

Albus JS (1971) A theory of cerebellar function. Mathematical Biosciences 10:25-61.

Ambrosi G, Flace P, Lorusso L, Girolamo F, Rizzi A, Bosco L, Errede M, Virgintino D, Roncali L, Benagiano V (2007) Non-traditional large neurons in the granular layer of the cerebellar cortex. Eur J Histochem 51 Suppl 1:59-64.

Armano S, Rossi P, Taglietti V, D'Angelo E (2000) Long-term potentiation of intrinsic excitability at the mossy fiber-granule cell synapse of rat cerebellum. J Neurosci 20:5208-5216.

Arthurs OJ, Boniface S (2002) How well do we understand the neural origins of the fMRI BOLD signal? Trends Neurosci 25:27-31.

Attwell D, Iadecola C (2002) The neural basis of functional brain imaging signals. Trends Neurosci 25:621-625.

Attwell D, Mishra A, Hall CN, O'Farrell FM, Dalkara T (2016) What is a pericyte? J Cereb Blood Flow Metab 36:451-455.

Attwell D, Buchan AM, Charpak S, Lauritzen M, Macvicar BA, Newman EA (2010) Glial and neuronal control of brain blood flow. Nature 468:232-243.

Balcerczyk A, Soszynski M, Bartosz G (2005) On the specificity of 4-amino-5-methylamino-2',7'-difluorofluorescein as a probe for nitric oxide. Free Radic Biol Med 39:327-335.

Batchelor AM, Bartus K, Reynell C, Constantinou S, Halvey EJ, Held KF, Dostmann WR, Vernon J, Garthwaite J (2010) Exquisite sensitivity to subsecond, picomolar nitric oxide transients conferred on cells by guanylyl cyclase-coupled receptors. Proc Natl Acad Sci U S A 107:22060-22065.

Bjaalie JG, Leergaard TB (2000) Functions of the pontine nuclei in cerebro-cerebellar communication. In: Trends Neurosci, pp 152-153. England.

Bosman LW, Koekkoek SK, Shapiro J, Rijken BF, Zandstra F, van der Ende B, Owens CB, Potters JW, de Gruijl JR, Ruigrok TJ, De Zeeuw CI (2010) Encoding of whisker input by cerebellar Purkinje cells. J Physiol 588:3757-3783.

Bouvier G, Higgins D, Spolidoro M, Carrel D, Mathieu B, Léna C, Dieudonné S, Barbour B, Brunel N, Casado M (2016a) Burst-Dependent Bidirectional Plasticity in the Cerebellum Is Driven by Presynaptic NMDA Receptors. Cell Rep 15:104-116.

Bouvier G, Higgins D, Spolidoro M, Carrel D, Mathieu B, Lena C, Dieudonne S, Barbour B, Brunel N, Casado M (2016b) Burst-Dependent Bidirectional Plasticity in the Cerebellum Is Driven by Presynaptic NMDA Receptors. Cell Rep 15:104-116.

Busija DW, Bari F, Domoki F, Louis T (2007) Mechanisms involved in the cerebrovascular dilator effects of N-methyl-d-aspartate in cerebral cortex. Brain Res Rev 56:89-100.

Buzsaki G (2006) Rhythms of the brain. US, New York: Oxford University Press.

Caesar K, Thomsen K, Lauritzen M (2003) Dissociation of spikes, synaptic activity, and activity-dependent increments in rat cerebellar blood flow by tonic synaptic inhibition. Proc Natl Acad Sci U S A 100:16000-16005.

Cauli B, Hamel E (2010) Revisiting the role of neurons in neurovascular coupling. Front Neuroenergetics 2:9.

Cauli B, Tong XK, Rancillac A, Serluca N, Lambolez B, Rossier J, Hamel E (2004) Cortical GABA interneurons in neurovascular coupling: relays for subcortical vasoactive pathways. J Neurosci 24:8940-8949.

Cesana E, Pietrajtis K, Bidoret C, Isope P, D'Angelo E, Dieudonne S, Forti L (2013) Granule cell ascending axon excitatory synapses onto Golgi cells implement a potent feedback circuit in the cerebellar granular layer. J Neurosci 33:12430-12446.

Chadderton P, Margrie TW, Häusser M (2004) Integration of quanta in cerebellar granule cells during sensory processing. Nature 428:856-860.

Cheron G, Marquez-Ruiz J, Dan B (2016) Oscillations, Timing, Plasticity, and Learning in the Cerebellum. Cerebellum 15:122-138.

Christie JM, Jahr CE (2008) Dendritic NMDA receptors activate axonal calcium channels. Neuron 60:298-307.

Courtemanche R, Lamarre Y (2005) Local field potential oscillations in primate cerebellar cortex: synchronization with cerebral cortex during active and passive expectancy. J Neurophysiol 93:2039-2052.

Courtemanche R, Pellerin JP, Lamarre Y (2002) Local field potential oscillations in primate cerebellar cortex: modulation during active and passive expectancy. J Neurophysiol 88:771-782.

Cryan JF, Holmes A (2005) The ascent of mouse: advances in modelling human depression and anxiety. Nat Rev Drug Discov 4:775-790.

D'Angelo E (2014) The organization of plasticity in the cerebellar cortex: from synapses to control. Prog Brain Res 210:31-58.

D'Angelo E, De Zeeuw CI (2009) Timing and plasticity in the cerebellum: focus on the granular layer. Trends Neurosci 32:30-40.

D'Angelo E, De Filippi G, Rossi P, Taglietti V (1995) Synaptic excitation of individual rat cerebellar granule cells in situ: evidence for the role of NMDA receptors. J Physiol 484 (Pt 2):397-413.

D'Angelo E, Rossi P, Armano S, Taglietti V (1999) Evidence for NMDA and mGlu receptor-dependent long-term potentiation of mossy fiber-granule cell transmission in rat cerebellum. J Neurophysiol 81:277-287.

D'Angelo E, Solinas S, Mapelli J, Gandolfi D, Mapelli L, Prestori F (2013) The cerebellar Golgi cell and spatiotemporal organization of granular layer activity. Front Neural Circuits 7:93.

D'Angelo E, Antonietti A, Casali S, Casellato C, Garrido JA, Luque NR, Mapelli L, Masoli S, Pedrocchi A, Prestori F, Rizza MF, Ros E (2016) Modeling the Cerebellar Microcircuit: New Strategies for a Long-Standing Issue. Front Cell Neurosci 10:176.

D'Errico A, Prestori F, D'Angelo E (2009) Differential induction of bidirectional long-term changes in neurotransmitter release by frequency-coded patterns at the cerebellar input. J Physiol 587:5843-5857.

Dalkara T, Alarcon-Martinez L (2015a) Cerebral microvascular pericytes and neurogliovascular signaling in health and disease. Brain Res 1623:3-17.

Dalkara T, Alarcon-Martinez L (2015b) Cerebral microvascular pericytes and neurogliovascular signaling in health and disease. Brain Res.

De Smet HJ, Paquier P, Verhoeven J, Marien P (2013) The cerebellum: its role in language and related cognitive and affective functions. Brain Lang 127:334-342.

De Zeeuw CI, Hoebeek FE, Schonewille M (2008) Causes and Consequences of Oscillations in the Cerebellar Cortex. Neuron 58:655-658.

Delvendahl I, Hallermann S (2016) The Cerebellar Mossy Fiber Synapse as a Model for High-Frequency Transmission in the Mammalian CNS. Trends Neurosci 39:722-737.

Diedrichsen J, Verstynen T, Schlerf J, Wiestler T (2010) Advances in functional imaging of the human cerebellum. Curr Opin Neurol 23:382-387.

Dillon-Carter O, Chuang DM (1989) Homologous desensitization of muscarinic cholinergic, histaminergic, adrenergic, and serotonergic receptors coupled to phospholipase C in cerebellar granule cells. J Neurochem 52:598-603.

Diwakar S, Lombardo P, Solinas S, Naldi G, D'Angelo E (2011) Local field potential modeling predicts dense activation in cerebellar granule cells clusters under LTP and LTD control. PLoS One 6:e21928.

Domoki F, Perciaccante JV, Shimizu K, Puskar M, Busija DW, Bari F (2002) N-methyl-D-aspartate-induced vasodilation is mediated by endothelium-independent nitric oxide release in piglets. Am J Physiol Heart Circ Physiol 282:H1404-1409.

Donoghue JP, Sanes JN, Hatsopoulos NG, Gaal G (1998) Neural discharge and local field potential oscillations in primate motor cortex during voluntary movements. J Neurophysiol 79:159-173.

Drake CT, Iadecola C (2007) The role of neuronal signaling in controlling cerebral blood flow. Brain Lang 102:141-152.

Duchemin S, Boily M, Sadekova N, Girouard H (2012) The complex contribution of NOS interneurons in the physiology of cerebrovascular regulation. Front Neural Circuits 6:51.

Dzamba D, Honsa P, Anderova M (2013) NMDA Receptors in Glial Cells: Pending Questions. In: Curr Neuropharmacol, pp 250-262.

Fernandez-Klett F, Offenhauser N, Dirnagl U, Priller J, Lindauer U (2010) Pericytes in capillaries are contractile in vivo, but arterioles mediate functional hyperemia in the mouse brain. Proc Natl Acad Sci U S A 107:22290-22295.

Filosa JA, Blanco VM (2007) Neurovascular coupling in the mammalian brain. Exp Physiol 92:641-646.

Filosa JA, Iddings JA (2013) Astrocyte regulation of cerebral vascular tone. Am J Physiol Heart Circ Physiol 305:H609-619.

Filosa JA, Morrison HW, Iddings JA, Du W, Kim KJ (2016) Beyond neurovascular coupling, role of astrocytes in the regulation of vascular tone. Neuroscience 323:96-109.

Fisher M (2009) Pericyte signaling in the neurovascular unit. Stroke 40:S13-15.

Gall D, Prestori F, Sola E, D'Errico A, Roussel C, Forti L, Rossi P, D'Angelo E (2005) Intracellular calcium regulation by burst discharge determines bidirectional long-term synaptic plasticity at the cerebellum input stage. J Neurosci 25:4813-4822.

Galliano E, De Zeeuw CI (2014) Questioning the cerebellar doctrine. Prog Brain Res 210:59-77.

Gao Z, van Beugen BJ, De Zeeuw CI (2012) Distributed synergistic plasticity and cerebellar learning. Nat Rev Neurosci 13:619-635.

Garreffa G, Colonnese C, Macri MA, Modugno N, Rocca R, Calistri V, De Cesare E, Venditti E, Maraviglia B (2003) BOLD signal sign and transient vessels volume variation. Magn Reson Imaging 21:1207-1212.

Garthwaite J (2016) From synaptically localized to volume transmission by nitric oxide. J Physiol 594:9-18.

Garthwaite J, Garthwaite G (1987) Cellular origins of cyclic GMP responses to excitatory amino acid receptor agonists in rat cerebellum in vitro. J Neurochem 48:29-39.

Garthwaite J, Garthwaite G, Palmer RM, Moncada S (1989) NMDA receptor activation induces nitric oxide synthesis from arginine in rat brain slices. Eur J Pharmacol 172:413-416.

Girouard H, Iadecola C (2006) Neurovascular coupling in the normal brain and in hypertension, stroke, and Alzheimer disease. J Appl Physiol (1985) 100:328-335.

Glickstein M, Doron K (2008) Cerebellum: connections and functions. Cerebellum 7:589-594.

Grant RI, Hartmann DA, Underly RG, Berthiaume AA, Bhat NR, Shih AY (2017) Organizational hierarchy and structural diversity of microvascular pericytes in adult mouse cortex. J Cereb Blood Flow Metab:271678x17732229.

Guerra G, Lucariello A, Perna A, Botta L, De Luca A, Moccia F (2018) The Role of Endothelial Ca(2+) Signaling in Neurovascular Coupling: A View from the Lumen. Int J Mol Sci 19.

Hall CN, Howarth C, Kurth-Nelson Z, Mishra A (2016) Interpreting BOLD: towards a dialogue between cognitive and cellular neuroscience. Philos Trans R Soc Lond B Biol Sci 371.

Hall CN, Reynell C, Gesslein B, Hamilton NB, Mishra A, Sutherland BA, O'Farrell FM, Buchan AM, Lauritzen M, Attwell D (2014) Capillary pericytes regulate cerebral blood flow in health and disease. Nature 508:55-60.

Hamilton NB, Attwell D, Hall CN (2010) Pericyte-mediated regulation of capillary diameter: a component of neurovascular coupling in health and disease. Front Neuroenergetics 2.

Herculano-Houzel S (2009) The human brain in numbers: a linearly scaled-up primate brain. Front Hum Neurosci 3:31.

Herculano-Houzel S (2010) Coordinated Scaling of Cortical and Cerebellar Numbers of Neurons. Front Neuroanat 4.

Herzfeld DJ, Kojima Y, Soetedjo R, Shadmehr R (2015) Encoding of action by the Purkinje cells of the cerebellum. Nature 526:439-442.

Hill RA, Tong L, Yuan P, Murikinati S, Gupta S, Grutzendler J (2015) Regional Blood Flow in the Normal and Ischemic Brain Is Controlled by Arteriolar Smooth Muscle Cell Contractility and Not by Capillary Pericytes. Neuron 87:95-110.

Hillman EM (2014) Coupling mechanism and significance of the BOLD signal: a status report. Annu Rev Neurosci 37:161-181.

Hopper RA, Garthwaite J (2006) Tonic and phasic nitric oxide signals in hippocampal long-term potentiation. J Neurosci 26:11513-11521.

Howarth C, Peppiatt-Wildman CM, Attwell D (2010) The energy use associated with neural computation in the cerebellum. J Cereb Blood Flow Metab 30:403-414.

Howarth C, Gleeson P, Attwell D (2012) Updated energy budgets for neural computation in the neocortex and cerebellum. J Cereb Blood Flow Metab 32:1222-1232.

Iadecola C (2002) Intrinsic signals and functional brain mapping: caution, blood vessels at work. Cereb Cortex 12:223-224.

Iadecola C (2004) Neurovascular regulation in the normal brain and in Alzheimer's disease. Nat Rev Neurosci 5:347-360.

Iadecola C (2017) The Neurovascular Unit Coming of Age: A Journey through Neurovascular Coupling in Health and Disease. Neuron 96:17-42.

Iadecola C, Nedergaard M (2007) Glial regulation of the cerebral microvasculature. Nat Neurosci 10:1369-1376.

Iadecola C, Li J, Ebner TJ, Xu X (1995) Nitric oxide contributes to functional hyperemia in cerebellar cortex. https://doiorg/101152/ajpregu19952685R1153.

Iadecola C, Li J, Xu S, Yang G (1996) Neural mechanisms of blood flow regulation during synaptic activity in cerebellar cortex. J Neurophysiol 75:940-950.

Iadecola C, Yang G, Ebner TJ, Chen G (1997) Local and propagated vascular responses evoked by focal synaptic activity in cerebellar cortex. J Neurophysiol 78:651-659.

Ito M (2006) Cerebellar circuitry as a neuronal machine. Prog Neurobiol 78:272-303.

Kansal K, Yang Z, Fishman AM, Sair HI, Ying SH, Jedynak BM, Prince JL, Onyike CU (2017) Structural cerebellar correlates of cognitive and motor dysfunctions in cerebellar degeneration. Brain 140:707-720.

Kisler K, Nelson AR, Montagne A, Zlokovic BV (2017) Cerebral blood flow regulation and neurovascular dysfunction in Alzheimer disease. Nat Rev Neurosci 18:419-434.

Kolinko Y, Cendelin J, Kralickova M, Tonar Z (2016) Smaller Absolute Quantities but Greater Relative Densities of Microvessels Are Associated with Cerebellar Degeneration in Lurcher Mice. Front Neuroanat 10:35.

Korbo L, Andersen BB, Ladefoged O, Moller A (1993) Total numbers of various cell types in rat cerebellar cortex estimated using an unbiased stereological method. Brain Res 609:262-268.

Krogh A (1929) The exchange of substances through the capillary wall, The Anatomy and Physiology of the Capillary. In, pp 193-216. *New Haven: Yale University Press*.

Krueger M, Bechmann I (2010) CNS pericytes: concepts, misconceptions, and a way out. Glia 58:1-10.

Kuper M, Kaschani P, Thurling M, Stefanescu MR, Burciu RG, Goricke S, Maderwald S, Ladd ME, Hautzel H, Timmann D (2016) Cerebellar fMRI Activation Increases with Increasing Working Memory Demands. Cerebellum 15:322-335.

Lauritzen M (2001) Relationship of spikes, synaptic activity, and local changes of cerebral blood flow. J Cereb Blood Flow Metab 21:1367-1383.

Lauritzen M, Mathiesen C, Schaefer K, Thomsen KJ (2012) Neuronal inhibition and excitation, and the dichotomic control of brain hemodynamic and oxygen responses. Neuroimage 62:1040-1050.

Lee RM (1995) Morphology of cerebral arteries. Pharmacol Ther 66:149-173.

Leiner HC, Leiner AL, Dow RS (1989) Reappraising the cerebellum: what does the hindbrain contribute to the forebrain? Behav Neurosci 103:998-1008.

Leiner HC, Leiner AL, Dow RS (1993) Cognitive and language functions of the human cerebellum. Trends Neurosci 16:444-447.

Lindauer U, Leithner C, Kaasch H, Rohrer B, Foddis M, Fuchtemeier M, Offenhauser N, Steinbrink J, Royl G, Kohl-Bareis M, Dirnagl U (2010) Neurovascular coupling in rat brain operates independent of hemoglobin deoxygenation. J Cereb Blood Flow Metab 30:757-768.

Liu X, Li C, Falck JR, Roman RJ, Harder DR, Koehler RC (2008) Interaction of nitric oxide, 20-HETE, and EETs during functional hyperemia in whisker barrel cortex. Am J Physiol Heart Circ Physiol 295:H619-631.

Logothetis NK (2008) What we can do and what we cannot do with fMRI. Nature 453:869-878.

Logothetis NK, Wandell BA (2004) Interpreting the BOLD signal. Annu Rev Physiol 66:735-769.

Logothetis NK, Pauls J, Augath M, Trinath T, Oeltermann A (2001) Neurophysiological investigation of the basis of the fMRI signal. Nature 412:150-157.

Lok J, Gupta P, Guo S, Kim WJ, Whalen MJ, van Leyen K, Lo EH (2007) Cell-cell signaling in the neurovascular unit. Neurochem Res 32:2032-2045.

Lu K, Clark JW, Jr., Ghorbel FH, Robertson CS, Ware DL, Zwischenberger JB, Bidani A (2004) Cerebral autoregulation and gas exchange studied using a human cardiopulmonary model. Am J Physiol Heart Circ Physiol 286:H584-601.

Maffei A, Prestori F, Shibuki K, Rossi P, Taglietti V, D'Angelo E (2003) NO enhances presynaptic currents during cerebellar mossy fiber-granule cell LTP. J Neurophysiol 90:2478-2483.

Mapelli J, D'Angelo E (2007) The spatial organization of long-term synaptic plasticity at the input stage of cerebellum. J Neurosci 27:1285-1296.

Mapelli L, Solinas S, D'Angelo E (2014) Integration and regulation of glomerular inhibition in the cerebellar granular layer circuit. Front Cell Neurosci 8:55.

Mapelli L, Rossi P, Nieus T, D'Angelo E (2009) Tonic activation of GABAB receptors reduces release probability at inhibitory connections in the cerebellar glomerulus. J Neurophysiol 101:3089-3099.

Mapelli L, Pagani M, Garrido JA, D'Angelo E (2015) Integrated plasticity at inhibitory and excitatory synapses in the cerebellar circuit. *Front Cell Neurosci* 9.

Mapelli L, Gagliano G, Soda T, Laforenza U, Moccia F, D'Angelo EU (2017) Granular Layer Neurons Control Cerebellar Neurovascular Coupling Through an NMDA Receptor/NO-Dependent System. J Neurosci 37:1340-1351.

Marr D (1969) A theory of cerebellar cortex. J Physiol 202:437-470.

Mathiesen C, Caesar K, Akgoren N, Lauritzen M (1998) Modification of activity-dependent increases of cerebral blood flow by excitatory synaptic activity and spikes in rat cerebellar cortex. J Physiol 512 (Pt 2):555-566.

McConnell HL, Kersch CN, Woltjer RL, Neuwelt EA (2017) The Translational Significance of the Neurovascular Unit. J Biol Chem 292:762-770.

Mehta B, Begum G, Joshi NB, Joshi PG (2008) Nitric oxide-mediated modulation of synaptic activity by astrocytic P2Y receptors. J Gen Physiol 132:339-349.

Metea MR, Newman EA (2006) Glial cells dilate and constrict blood vessels: a mechanism of neurovascular coupling. J Neurosci 26:2862-2870.

Middleton FA, Strick PL (2001) Cerebellar projections to the prefrontal cortex of the primate. J Neurosci 21:700-712.

Miller NR, Burton Walsh F, Fletcher Hoy W (2005) Anatomy and Physiology of the Cerebrovascular System, Walsh and Hoyt's Clinical Neuro-ophthalmology. In, VI Edition, pp 1901-1966. Lippincott Williams & Wilkins.

Mishra A (2017) Binaural blood flow control by astrocytes: listening to synapses and the vasculature. J Physiol 595:1885-1902.

Mishra A, O'Farrell FM, Reynell C, Hamilton NB, Hall CN, Attwell D (2014) Imaging pericytes and capillary diameter in brain slices and isolated retinae. Nat Protoc 9:323-336.

Mishra A, Reynolds JP, Chen Y, Gourine AV, Rusakov DA, Attwell D (2016) Astrocytes mediate neurovascular signaling to capillary pericytes but not to arterioles. Nat Neurosci 19:1619-1627.

Mock M, Schwarz C, Thier P (1997) Electrophysiological properties of rat pontine nuclei neurons In vitro II. Postsynaptic potentials. J Neurophysiol 78:3338-3350.

Monaghan A, Anderson K (1991) Heterogeneity and organizaton of excitatory amino acid receptors and transporters. In: Excitatory amino acids and synaptic function (H W, A T, eds), pp 33-54. London: Academic.

Morishita W, Sastry BR (1996) Postsynaptic mechanisms underlying long-term depression of GABAergic transmission in neurons of the deep cerebellar nuclei. J Neurophysiol 76:59-68.

Mulligan SJ, MacVicar BA (2004) Calcium transients in astrocyte endfeet cause cerebrovascular constrictions. Nature 431:195-199.

Muoio V, Persson PB, Sendeski MM (2014) The neurovascular unit - concept review. Acta Physiol (Oxf) 210:790-798.

Muñoz MF, Puebla M, Figueroa XF (2015) Control of the neurovascular coupling by nitric oxide-dependent regulation of astrocytic Ca2+ signaling. Front Cell Neurosci 9.

Nagao S (2004) Pontine nuclei-mediated cerebello-cerebral interactions and its functional role. Cerebellum 3:11-15.

Namin SM, Nofallah S, Joshi MS, Kavallieratos K, Tsoukias NM (2013) Kinetic analysis of DAF-FM activation by NO: toward calibration of a NO-sensitive fluorescent dye. Nitric Oxide 28:39-46.

Nippert AR, Biesecker KR, Newman EA (2018) Mechanisms Mediating Functional Hyperemia in the Brain. Neuroscientist 24:73-83.

O'Hearn E, Molliver ME (2009) Organizational principles and microcircuitry of the cerebellum. http://dxdoiorg/101080/09540260120082083.

Otsu Y, Couchman K, Lyons DG, Collot M, Agarwal A, Mallet J-M, Pfrieger FW, Bergles DE, Charpak S (2014) Calcium dynamics in astrocyte processes during neurovascular coupling. Nature Neuroscience 18:210.

Ouardouz M, Sastry BR (2000) Mechanisms underlying LTP of inhibitory synaptic transmission in the deep cerebellar nuclei. J Neurophysiol 84:1414-1421.

Pellerin JP, Lamarre Y (1997) Local field potential oscillations in primate cerebellar cortex during voluntary movement. J Neurophysiol 78:3502-3507.

Peppiatt CM, Howarth C, Mobbs P, Attwell D (2006) Bidirectional control of CNS capillary diameter by pericytes. Nature 443:700-704.

Petersen SE, Fox PT, Posner MI, Mintun M, Raichle ME (1988) Positron emission tomographic studies of the cortical anatomy of single-word processing. Nature 331:585.

Petzold G, German Center for Neurodegenerative Diseases (DZNE) L-E-A, 53175 Bonn, Germany, Department of Neurology UHB, Sigmund-Freud-Str. 25, 53127 Bonn, Germany, Department of Molecular and Cellular Biology and Center for Brain Science HU, 16 Divinity Avenue, Cambridge, MA 02138, USA (2011) Role of Astrocytes in Neurovascular Coupling. Neuron 71:782-797.

Powell K, Mathy A, Duguid I, Häusser M (2015) Synaptic representation of locomotion in single cerebellar granule cells. Elife 4.

Prestori F, Bonardi C, Mapelli L, Lombardo P, Goselink R, De Stefano ME, Gandolfi D, Mapelli J, Bertrand D, Schonewille M, De Zeeuw C, D'Angelo E (2013) Gating of long-term potentiation by nicotinic acetylcholine receptors at the cerebellum input stage. PLoS One 8:e64828.

Purves D, Augustine GJ, Fitzpatrick D, Katz LC, LaMantia A-S, McNamara JO, Williams SM (2001) Neuroscience.

Raichle ME, Fiez JA, Videen TO, MacLeod AM, Pardo JV, Fox PT, Petersen SE (1994) Practice-related changes in human brain functional anatomy during nonmotor learning. Cereb Cortex 4:8-26.

Ramakrishnan KB, Voges K, De Propris L, De Zeeuw CI, D'Angelo E (2016) Tactile Stimulation Evokes Long-Lasting Potentiation of Purkinje Cell Discharge In Vivo. Front Cell Neurosci 10:36.

Rancillac A, Rossier J, Guille M, Tong XK, Geoffroy H, Amatore C, Arbault S, Hamel E, Cauli B (2006) Glutamatergic Control of Microvascular Tone by Distinct GABA Neurons in the Cerebellum. J Neurosci 26:6997-7006.

Rancz EA, Ishikawa T, Duguid I, Chadderton P, Mahon S, Hausser M (2007a) High-fidelity transmission of sensory information by single cerebellar mossy fibre boutons. Nature 450:1245-1248.

Rancz EA, Ishikawa T, Duguid I, Chadderton P, Mahon S, Häusser M (2007b) High-fidelity transmission of sensory information by single cerebellar mossy fibre boutons. Nature 450:1245-1248.

Rand S, Swenson M (2006) Review of clinical and functional neuroscience. In.

Ribatti D (2009) William Harvey and the discovery of the circulation of the blood. J Angiogenes Res 1:3.

Robberechts Q, Wijnants M, Giugliano M, De Schutter E (2010) Long-term depression at parallel fiber to Golgi cell synapses. J Neurophysiol 104:3413-3423.

Rodrigo J, Springall DR, Uttenthal O, Bentura ML, Abadia-Molina F, Riveros-Moreno V, Martinez-Murillo R, Polak JM, Moncada S (1994) Localization of nitric oxide synthase in the adult rat brain. Philos Trans R Soc Lond B Biol Sci 345:175-221.

Roggeri L, Rivieccio B, Rossi P, D'Angelo E (2008) Tactile stimulation evokes long-term synaptic plasticity in the granular layer of cerebellum. J Neurosci 28:6354-6359.

Romero RR (2011) Marcello Malpighi (1628-1694), founder of microanatomy. In, 29 Edition, pp 399-402. *Int. J. Morphol.*

Rosenegger DG, Gordon GR (2015) A slow or modulatory role of astrocytes in neurovascular coupling. Microcirculation 22:197-203.

Sakagami K, Kawamura H, Wu DM, Puro DG (2001) Nitric oxide/cGMP-induced inhibition of calcium and chloride currents in retinal pericytes. Microvasc Res 62:196-203.

Salerno JC (2008) Neuronal nitric oxide synthase: prototype for pulsed enzymology. FEBS Lett 582:1395-1399.

Salerno JC, Ghosh DK (2009) Space, time and nitric oxide--neuronal nitric oxide synthase generates signal pulses. FEBS J 276:6677-6688.

Schmahmann JD (1991) An emerging concept. The cerebellar contribution to higher function. Arch Neurol 48:1178-1187.

Schmahmann JD (2010) The role of the cerebellum in cognition and emotion: personal reflections since 1982 on the dysmetria of thought hypothesis, and its historical evolution from theory to therapy. Neuropsychol Rev 20:236-260.

Schmahmann JD, Sherman JC (1998) The cerebellar cognitive affective syndrome. Brain 121 (Pt 4):561-579.

Schwarz C, Mock M, Thier P (1997) Electrophysiological properties of rat pontine nuclei neurons In vitro. I. Membrane potentials and firing patterns. J Neurophysiol 78:3323-3337.

Siero JC, Petridou N, Hoogduin H, Luijten PR, Ramsey NF (2011) Cortical depth-dependent temporal dynamics of the BOLD response in the human brain. J Cereb Blood Flow Metab 31:1999-2008.

Siero JC, Ramsey NF, Hoogduin H, Klomp DW, Luijten PR, Petridou N (2013) BOLD specificity and dynamics evaluated in humans at 7 T: comparing gradient-echo and spin-echo hemodynamic responses. PLoS One 8:e54560.

Snyder SH (1992) Nitric oxide: first in a new class of neurotransmitters. Science 257:494-496.

Southam E, Morris R, Garthwaite J (1992) Sources and targets of nitric oxide in rat cerebellum. Neurosci Lett 137:241-244.

Sweeney MD, Ayyadurai S, Zlokovic BV (2016) Pericytes of the neurovascular unit: key functions and signaling pathways. Nat Neurosci 19:771-783.

Sweeney MD, Sagare AP, Zlokovic BV (2018) Blood-brain barrier breakdown in Alzheimer disease and other neurodegenerative disorders. Nat Rev Neurol.

Swenson RS, Kosinski RJ, Castro AJ (1984) Topography of spinal, dorsal column nuclear, and spinal trigeminal projections to the pontine gray in rats. J Comp Neurol 222:301-311.

Sá-Pereira I, Brites D, Brito MA (2012) Neurovascular unit: a focus on pericytes. Mol Neurobiol 45:327-347.

Thomsen K, Offenhauser N, Lauritzen M (2004) Principal neuron spiking: neither necessary nor sufficient for cerebral blood flow in rat cerebellum. J Physiol 560:181-189.

Thomsen K, Piilgaard H, Gjedde A, Bonvento G, Lauritzen M (2009) Principal cell spiking, postsynaptic excitation, and oxygen consumption in the rat cerebellar cortex. J Neurophysiol 102:1503-1512.

Timmann D, Drepper J, Frings M, Maschke M, Richter S, Gerwig M, Kolb FP (2010) The human cerebellum contributes to motor, emotional and cognitive associative learning. A review. Cortex 46:845-857.

Uhlirova H et al. (2016) Cell type specificity of neurovascular coupling in cerebral cortex. Elife 5.

Usowicz MM, Gallo V, Cull-Candy SG (1989) Multiple conductance channels in type-2 cerebellar astrocytes activated by excitatory amino acids. Nature 339:380-383.

van Beugen BJ, Gao Z, Boele HJ, Hoebeek F, De Zeeuw CI (2013) High frequency burst firing of granule cells ensures transmission at the parallel fiber to purkinje cell synapse at the cost of temporal coding. Front Neural Circuits 7:95.

Wiestler T, McGonigle DJ, Diedrichsen J (2011) Integration of sensory and motor representations of single fingers in the human cerebellum. J Neurophysiol 105:3042-3053.

Winkler EA, Department of Neurological Surgery University of California San Francisco San Francisco C, Rutledge WC, Department of Neurological Surgery University of California San Francisco San Francisco C, Kalani MYS, Department of Neurosurgery Clinical Neurosciences Center University of Utah Salt Lake City U, Rolston JD, Department of Neurosurgery Clinical Neurosciences Center University of Utah Salt Lake City U (2018) Pericytes Regulate Cerebral Blood Flow and Neuronal Health at a Capillary Level. Neurosurgery 81.

Witter L, Rudolph S, Pressler RT, Lahlaf SI, Regehr WG (2016) Purkinje Cell Collaterals Enable Output Signals from the Cerebellar Cortex to Feed Back to Purkinje Cells and Interneurons. Neuron 91:312-319.

Wolf T, Lindauer U, Villringer A, Dirnagl U (1997) Excessive oxygen or glucose supply does not alter the blood flow response to somatosensory stimulation or spreading depression in rats. Brain Res 761:290-299.

Xu J, Chuang DM (1987) Serotonergic, adrenergic and histaminergic receptors coupled to phospholipase C in cultured cerebellar granule cells of rats. Biochem Pharmacol 36:2353-2358.

Yang G, Iadecola C (1996) Glutamate microinjections in cerebellar cortex reproduce cerebrovascular effects of parallel fiber stimulation. Am J Physiol 271:R1568-1575.

Yang G, Iadecola C (1997) Obligatory role of NO in glutamate-dependent hyperemia evoked from cerebellar parallel fibers. Am J Physiol 272:R1155-1161.

Yang G, Iadecola C (1998) Activation of cerebellar climbing fibers increases cerebellar blood flow: role of glutamate receptors, nitric oxide, and cGMP. Stroke 29:499-507; discussion 507-498.

Yang G, Chen G, Ebner TJ, Iadecola C (1999) Nitric oxide is the predominant mediator of cerebellar hyperemia during somatosensory activation in rats. Am J Physiol 277:R1760-1770.

Yang G, Huard JM, Beitz AJ, Ross ME, Iadecola C (2000) Stellate neurons mediate functional hyperemia in the cerebellar molecular layer. J Neurosci 20:6968-6973.

Yang G, Feddersen RM, Zhang F, Clark HB, Beitz AJ, Iadecola C (1998) Cerebellar vascular and synaptic responses in normal mice and in transgenics with Purkinje cell dysfunction. Am J Physiol 274:R529-540.

Zimmermann K (1923) Der feinere Bau der Blutkapillaren. Z Anat Entwicklungsgesch 69:29-109.

Zlokovic BV (2005) Neurovascular mechanisms of Alzheimer's neurodegeneration. Trends Neurosci 28:202-208.

Zlokovic BV (2011) Neurovascular pathways to neurodegeneration in Alzheimer's disease and other disorders. Nat Rev Neurosci 12:723-738.

Appendix

curriculum vitae

publications

other publication

Curriculum vitae

Personal Information

Name	Giuseppe Gagliano
Date of birth	2 April 1990
Place of birth	Palermo, Italy

Education

2015 – 2018	PhD student in Biomedical Sciences, University of Pavia, Italy Supervisor: Prof. Egidio D'Angelo
2013 – 2015	Master degree in Biomedical Sciences, University of Pavia, Italy Final mark: 110/110 cum laude
2010 – 2011	Erasmus student, University of A Coruña, Spain
2009 – 2013	Bachelor degree in Biological Sciences, University of Palermo, Italy
2004 – 2009	Scientific High-school, Bagheria, Italy

Training and courses

2018	Supervisor of bachelor degree student thesis
2017 March	Training course *e-Learning* Safety and health in workplaces, University of Pavia, Italy
2017 March	Qualification to practice biologist profession Ordine Nazionale dei Biologi (ONB), Rome, Italy
2015	Internship, Laboratory of Neurophysiology, University of Pavia, Italy Supervisor: Dr. Lisa Mapelli
2014	Internship, Laboratory of Physiology, University of Pavia, Italy Supervisor: Dr. Francesco Moccia
2013 April	English course Basil Paterson College of Edinburgh, Edinburgh, Scotland
2012	Internship, Laboratory of Neurophysiology, University of Malta, Malta Supervisor: Prof. Giuseppe Di Giovanni
2012 February	DELE - Diploma of Spanish as a Foreign Language – C2 level Institute Cervantes of Madrid, Madrid, Spain

Others

2018 - 2019	Delegate of PhD student Dept. of Brain and Behavioral Sciences, University of Pavia, Pavia
2017 December	Best poster award 3rd International School of Brain and Circuits "Camillo Golgi", Erice, Italy
2017 December	Poster oral presentation 3rd International School of Brain and Circuits "Camillo Golgi", Erice, Italy
2016 June	Award by Sicilian Regional Institution for academic career

Publications

Gagliano G, Mapelli L, Soda T, Laforenza U, Moccia F, D'Angelo E. Neurovascular responses of the granular layer of cerebellar vermis and hemispheres to different input patterns. *Frontiers Cellular Neuroscience, Conference Abstract: From cell physiology to integrated signals and emerging brain functions* (2018) *(in press)*.

Gagliano G, Mapelli L, Soda T, Laforenza U, Moccia F, D'Angelo E. Neurovascular coupling in the cerebellar granular layer. *Frontiers Cellular Neuroscience*. *Conference Abstract: The Cerebellum inside out: cells, circuits and functions* (2017). DOI:10.3389/conf. fncel.2017.37.000025.

Mapelli L*, **Gagliano G***, Soda T, Laforenza U, Moccia F, D'Angelo E. Granular layer neurons control cerebellar neurovascular coupling through an NDMA receptor/NO-dependent system. *The journal of Neuroscience,37(5):1340-1351*(2017).

Ronco V, Potenza DM, Denti F, Vullo S, **Gagliano G**, Guerra G, Pinton P, Genazzani AA, Mapelli L, Lim D, Moccia F. A novel Ca2+-mediated cross-talk between endoplasmic reticulum and acidic organelles: implicationsfor NAADP-dependent Ca2+ signalling. *Cell Calcium, 57 (2) 89-100* (2015).

Mapelli L, Soda T, **Gagliano G**, Moccia F, D'Angelo E. Neurovascular coupling at the cerebellar granular layer. *Vascular Pharmacology, 2015;75:64* (2015).

DOI:10.1016/j.vph.2015.11.057.

Articles in preparation

Gagliano G, Soda T, Laforenza U, Moccia F, Mapelli L, D'Angelo E. Different neurovascular responses in the granular layer of the cerebbellar vermis and hemisphere. (*in preparation*)

Other publication

Cell Calcium 57 (2015) 89–100

Contents lists available at ScienceDirect

Cell Calcium

journal homepage: www.elsevier.com/locate/ceca

A novel Ca^{2+}-mediated cross-talk between endoplasmic reticulum and acidic organelles: Implications for NAADP-dependent Ca^{2+} signalling

Virginia Ronco[a,1], Duilio Michele Potenza[b,1], Federico Denti[b], Sabrina Vullo[b], Giuseppe Gagliano[b], Marialuisa Tognolina[c], Germano Guerra[d], Paolo Pinton[e], Armando A. Genazzani[a], Lisa Mapelli[c,f], Dmitry Lim[a,*,2], Francesco Moccia[b,**,2]

[a] Department of Pharmaceutical Sciences, Università del Piemonte Orientale "Amedeo Avogadro", 28100 Novara, Italy
[b] Laboratory of General Physiology, Department of Biology and Biotechnology "Lazzaro Spallanzani", University of Pavia, 27100 Pavia, Italy
[c] Laboratory of Neurophysiology, Department of Brain and Behavioural Sciences, University of Pavia, 27100 Pavia, Italy
[d] Department of Medicine and Health Sciences, University of Molise, 86100 Campobasso, Italy
[e] Department of Morphology, Surgery and Experimental Medicine, Section of Pathology, Oncology and Experimental Biology, Laboratory for Technologies of Advanced Therapies (LTTA), University of Ferrara, 44121 Ferrara, ItalyfCentro Fermi, 00184 Roma, Italy
[f] Centro Fermi, 00184 Roma, Italy

ARTICLE INFO

Article history:
Received 4 December 2014
Accepted 1 January 2015
Available online 21 January 2015

Keywords:
Lysosomal calcium
ER calcium
Lysosome-ER crosstalk
NAADP
NAADP-dependent Ca^{2+} signalling

ABSTRACT

Nicotinic acid adenine dinucleotide phosphate (NAADP) serves as the ideal trigger of spatio-temporally complex intracellular Ca^{2+} signals. However, the identity of the intracellular Ca^{2+} store(s) recruited by NAADP, which may include either the endolysosomal (EL) or the endoplasmic reticulum (ER) Ca^{2+} pools, is still elusive. Here, we show that the Ca^{2+} response to NAADP was suppressed by interfering with either EL or ER Ca^{2+} sequestration. The measurement of EL and ER Ca^{2+} levels by using selectively targeted aequorin unveiled that the preventing ER Ca^{2+} storage also affected ER Ca^{2+} loading and vice versa. This indicates that a functional Ca^{2+}-mediated cross-talk exists at the EL–ER interface and exerts profound implications for the study of NAADP-induced Ca^{2+} signals. Extreme caution is warranted when dissecting NAADP targets by pharmacologically inhibiting EL and/or the ER Ca^{2+} pools. Moreover, Ca^{2+} transfer between these compartments might be essential to regulate vital Ca^{2+}-dependent processes in both organelles.

1. Introduction

Nicotinic acid adenine dinucleotide phosphate (NAADP) represents the latest addition to the restricted family of intracellular Ca^{2+}-releasing messengers [1], already including inositol-1,4,5-trisphosphate and cyclic ADP-ribose (cADPr). NAADP may be synthesized upon cellular stimulation or activation of cell surface receptors to regulate a plethora of intracellular processes, including fertilization [2,3], muscle contraction [4], nitric oxide (NO) production [5], and glucose metabolism [6]. Its efficacy in triggering cytosolic Ca^{2+} elevations, as compared to either $InsP_3$ or cADPr, is underscored by the low doses of NAADP required to activate cell signalling, spanning from pM to low nM concentrations [7]. While $InsP_3$ and cADPr have long been known to mobilize Ca^{2+} from endoplasmic reticulum (ER), by activating $InsP_3$ ($InsP_3$Rs) and ryanodine (RyRs) receptors [8], respectively, the molecular target of NAADP has been far more elusive. Pioneering work conducted on sea urchin egg homogenates demonstrated that the NAADP-sensitive Ca^{2+} store is physically and pharmacologically separated from that recruited by $InsP_3$ and cADPr [9,10]. Consistent with this observation, NAADP was later found to discharge Ca^{2+} from acidic lysosome-like organelles in sea urchin eggs [11], where the newly discovered family of two-pore channels (TPCs) serve as the long-sought NAADP receptors [9,12]. However, this mechanism does not underlie NAADP-mediated Ca^{2+} signalling in the closely related starfish oocytes; herein, NAADP does not mobilize Ca^{2+} from acidic Ca^{2+} stores [13], but activates a plasmalemmal inwardly rectifying Ca^{2+} permeable channel [14,15]. Subsequent work has

* Corresponding author at: Department of Pharmaceutical Sciences, University of Eastern Piedmont "Amedeo Avogadro", Via Bovio 6, 28100 Novara, Italy. Tel.: +39 0321 375827; fax: +39 0321 375821.
** Corresponding author at: Laboratory of General Physiology, Department of Biology and Biotechnology "Lazzaro Spallanzani", University of Pavia, Via Forlanini 6, 27100 Pavia, Italy. Tel.: +39 0382 987169; fax: +39 0382 987527.
E-mail addresses: dmitry.lim@pharm.unipmn.it (D. Lim), francesco.moccia@unipv.it (F. Moccia).
[1] These authors equally contributed to the work and share First Authorship.
[2] These authors should be considered as co-last authors and share Senior Authorship.

http://dx.doi.org/10.1016/j.ceca.2015.01.001
0143-4160/

shown that NAADP may release Ca^{2+} from acidic organelles of the endolysosomal (EL) system, which include early, late and recycling endosomes, in mammal cells: TPCs mediate a trigger Ca^{2+} release that is amplified into a regenerative Ca^{2+} wave by the Ca^{2+}-dependent recruitment of RyRs and/or $InsP_3Rs$ [7,9]. Alternatively, NAADP may gate TPCs to shuttle EL Ca^{2+} into ER by stimulating Sarco-Endoplasmic Reticulum Ca^{2+}-ATPase (SERCA) activity, thereby promoting further Ca^{2+} liberation via either $InsP_3Rs$ and/or RyRs [4,16,17]. This model has been challenged by several observations, according to which RyRs type 1 and 2 (RyR1 and RyRs2) may serve as primary target for NAADP both in naïve cells and in planar lipid bilayers [18–20]. The debate around the primary site of action of NAADP remains therefore, highly controversial [18,21–23]. Whereas gene silencing experiments have demonstrated TPC contribution to NAADP-evoked Ca^{2+} signals, the involvement of acidic organelles has been mainly supported by the use of pharmacological tools [7,9,24,25]. A number of drugs have been utilized to either disrupt or interfere with lysosome acidification, thereby disrupting their Ca^{2+} storage ability and preventing the Ca^{2+} response to NAADP. These compounds include: glycyl-L-phenylalanine-2-naphthylamide (GPN), a substrate of lysosomal cathepsin C whose cleavage causes osmotic lysis of lysosomes; bafilomycin A1, a highly selective inhibitor of V-type H^+-ATPase that drives the proton gradient responsible for Ca^{2+} sequestration; and nigericin, a H^+/K^+ ionophore which dissipates the proton gradient across lysosome membrane [9,24–26]. A recent series of studies have disclosed the tight and finely tuned inter-organellar communication that occurs during intracellular Ca^{2+} movement between EL and ER compartments and vice versa [27–31]. In this regard, only a few studies have assessed whether the pharmacological disruption of acidic Ca^{2+} stores affects ER Ca^{2+} loading [27,29,32–34], thereby inadvertently masking its participation to the onset and development of NAADP-evoked Ca^{2+} signals. In turn, there is scant information about the consequences of ER SERCA blockade by thapsigargin, cyclopiazonic acid (CPA) and 2,5-di-(t-butyl)-1,4-hydroquinone (TBHQ) on the Ca^{2+} content of acidic stores [24,25,33].

The present investigation was endeavoured to first dissect the intracellular Ca^{2+} stores responsible for NAADP-induced Ca^{2+} release in HeLa cells, a widely employed cell model to study intracellular Ca^{2+} signalling. This step was essential to then unveil: (1) whether and how the pharmacological manipulation of the EL Ca^{2+} pool impairs ER Ca^{2+} levels and vice versa and (2) to ascertain the implications of the ER–EL Ca^{2+} movements for NAADP-induced Ca^{2+} signals. We took benefit from "whole-cell patch-clamp" recordings to dyalize NAADP into the cytosol and monitor the activation of a Ca^{2+}-dependent membrane current as surrogate of the concomitant intracellular Ca^{2+} response [35–37]. Additionally, we used aequorin-based Ca^{2+} probes to assess the effects of GPN, bafilomycin A1, nigericin, and thapsigargin on both ER and EL Ca^{2+} loading. Our data provide further support to the trigger hypothesis, whereby NAADP engages TPCs to discharge a local bolus of Ca^{2+} which is in turn amplified by adjoining RyRs and $InsP_3Rs$. However, we further demonstrated that a functional Ca^{2+}-mediated cross-talk does occur between EL and ER Ca^{2+} stores to reciprocally control their refilling. It turns out that the pharmacological manipulation of acidic organelles may exert profound consequences on the extent of ER Ca^{2+} storage and vice versa; this feature should be taken in account when investigating the primary target of NAADP in mammal cells.

2. Materials and methods

2.1. Cell cultures

HeLa cells were cultured in DMEM (Sigma) medium supplemented with 10% FBS (Immunological Sciences), 2 mM glutamine and 1% penicillin streptomycin (Sigma) in humidified atmosphere containing 5% CO_2. Cells were grown to 80% confluence and passaged twice a week. For experiments the cells were plated onto glass coverslips at concentrations 5×10^4 per ml (24 mm diameter coverslips in 6 well plates) or 3×10^4 per ml (13 mm diameter coverslips in 24 well plates).

2.2. Electrophysiological recordings

Membrane currents were recorded from isolated HeLa cells (3 days in culture) by using the conventional whole cell patch-clamp configuration and a L/M EPC-7 patch-clamp amplifier (List-Electronic; Darmstadt, Germany) [38]. Whole cell currents were sampled at 1 kHz and acquired by exploiting the Strathclyde electrophysiology software WinWCP (courtesy of Dr. John Dempster, University of Strathclyde, Glasgow UK). Alternatively, they were recorded by using a Multiclamp 700B amplifier (−3 dB; cut-off frequency = 10 kHz) driven by PClamp 10 software (Molecular Devices, Union City, CA, USA). Pipettes were pulled from thin-walled borosilicate glass using a Sutter Instruments P-87 pipette puller and had resistances of 3–5 MΩ when filled with high-K^+ internal solution. Patch pipettes were pulled from borosilicate glass capillaries (Warner Instruments Corp., Hamden, CT, USA) and filled with the following solution: KCl (140 mM), NaCl (8 mM), $MgCl_2$ (1.5 mM), HEPES (10 mM), EGTA (0.05 mM), titrated to pH = 7.2 with KOH. NAADP was added at the final concentration of 10 nM, otherwise stated. In order to assess the Ca^{2+}-sensitivity of NAADP-evoked currents, EGTA was added at a final concentration of 10 mM. Cells were maintained in a standard physiological salt solution [38]: NaCl (150 mM), KCl (6 mM), $MgCl_2$ (1 mM), $CaCl_2$ (1.5 mM), HEPES (10 mM), glucose (10 mM) adjusted to pH = 7.4 with NaOH. Access resistances were <10 MΩ following series resistance compensation. Current-voltage (*I–V*) curves were obtained by applying, every 1 s, 100 ms voltage ramps ranging from −100 mV to +100 mV and delivered from a holding potential of 0 mV [39]. Currents were normalized by dividing the amplitudes (measured from the voltage ramps at −80 mV and +80 mV) by the cell capacitance. Capacitative currents were compensated before each ramp by using the amplifier's built-in compensation section. All leak currents were subtracted by averaging the first two to ten ramp currents, and then subtracting this from all subsequent currents. Pooled data are given as mean ± Se and statistical evaluation was carried out using Student's unpaired *T*-test. Experiments were carried out at room temperature (20–23 °C).

2.3. Generation of CathD-Aeq Ca^{2+} probe and aequorin Ca^{2+} measurements

CathD-Aeq and ER-Aeq aequorin-based Ca^{2+} sensors were used to measure the rate of Ca^{2+} uptake and the steady-state Ca^{2+} levels in the endo-lysosomal organelles (EL) and in the ER, respectively. The ER-Aeq Ca^{2+} probe was described in [40]. For generation of the CathD-Aeq Ca^{2+} probe a fragment of the cathepsin D (CathD) cDNA was first amplified using the following primers: Forward: 5′-ggaagcttgaattcgccaccatgcagcccctccag-3′ Reverse: 5′-ggaagcttgagggtcttcccggcctgcgacacct-3′ which caused the addition of a HindIII site in the 5′ non-coding region and downstream the lysosomal targeting sequence of the CathD cDNA, but not the catalytic region [41]. This HindIII fragment was then inserted, in appropriately prepared pcDNA3 vector, in front of the HA1-tagged Asp119Ala aequorin (Aeq) mutant [42] obtaining the CathD-Aeq chimaera. Both probes were transfected into HeLa cells using Lipofectamine 2000 reagent (Life Technologies, Milano, Italy) the day before the experiment. Transfected apo-aequorins were reconstituted in modified Krebs–Ringer buffer (KRB, 135 mM NaCl, 5 mM KCl, 0.4 mM KH_2PO_4, 1 mM $MgSO_4$, 5.5 mM glucose, 20 mM HEPES

(pH 7.4) supplemented with 600 μM EGTA, 5 μM coelenterazine n and 300 μM ionomycin (all reagents from Sigma) for 1 h at 4 °C. After reconstitution the cells were washed 3 times with KRB containing 600 μM EGTA and 2% BSA, followed by 3 washes with KRB containing 100 μM EGTA after which the coverslips were transferred into perfusion chamber of a custom built aequorinometer (CAIRN research, UK). The cells were perfused with KRB containing 100 μM EGTA at 37 °C. After 3 min of baseline recording the perfusion solution was switched to KRB supplemented with 2 mM Ca^{2+} and recording continued until the [Ca^{2+}] in the EL or ER did reach the steady-state level. At the end of each experiment, for quantification of the intra-organellar Ca^{2+} levels, the cells were perfused with distilled water containing 100 mM Ca^{2+} and 100 μM digitonin to discharge the remaining Aeq pool. The light signals were calibrated off-line into [Ca^{2+}] values using an algorithm developed by Brini and coworkers [43].

2.4. Fura-2 Ca^{2+} measurements

HeLa cells were loaded with 5 μM Fura-2 AM in presence of 0.02% of Pluronic-127 (both from Life Technologies) and 10 μM sulfinpyrazone in KRB containing 2 mM $CaCl_2$ (30 min, room temperature), after which the cells were washed and left for other 30 min to allow de-esterification of Fura-2. After that the coverslips were mounted into acquisition chamber and places on the stage of a Leica DMI6000 epifluorescent microscope equipped with S Fluor ×40/1.3 objective. The probe was excited by alternate 340 and 380 nm using a Polychrome IV monochromator (Till Photonics, Munich, Germany) and the Fura-2 emission light was filtered through 520/20 bandpass filter and collected by a cooled CCD camera (Hamamatsu, Japan). The fluorescence signals were acquired and processed using MetaFluor software (Molecular Device, Sunnyvale, CA, USA). To quantify the differences in the amplitudes of Ca^{2+} transients the ratio values were normalized using the formula $\Delta F/F_0$ (referred to as normalized Fura-2 ratio, "Norm. Fura ratio").

2.5. Immunocytochemistry

1.5×10^4 HeLa cells, grown on 13 mm coverslips in 24 w/plates, were transfected with 0.3 μg CD-Aeq cDNA using Lipofectamine 2000 reagent. After 24 h, cells were fixed with 4% formaldehyde, permeabilized with 0.1% Triton X-100 and probed with anti-hemagglutinin epitope (HA, Roche, Mannheim, Germany), anti-Lamp2b, anti-mannose-6-phosphate receptor (M6PR), anti-early endosome antigen 1 (EEA) (all from Abcam, Cambridge, UK) and anti-endoplasmic reticulum-Golgi intermediate compartment (ERGIC, Sigma) primary antibodies (all 1:50) in phosphate buffered saline (PBS) supplemented with 1% gelatine (1 h 37 °C). The cells were then washed 3 times with PBS and secondary Alexa Fluor conjugated antibody (1:200) were applied in PBS with 1% gelatine for 1 h at RT. The coverslips were then washed and mounted on a glass slides using FluoroShield mounting medium (Sigma). The cells were examined using a Leica DMI6000 epifluorescent microscope equipped with S Fluor ×40/1.3 objective. Fluorescent signals were acquired and processed using Leica-Metamorph software.

2.6. Chemicals

All chemicals, unless otherwise stated, were of analytical grade and obtained from Sigma.

2.7. Statistical analysis

Two-tail unpaired Student's *t*-test was used for statistical analysis. Differences were considered significant at $p < 0.05$.

3. Results

3.1. NAADP induces Ca^{2+}-dependent non-selective cationic currents mediated by TRPM4 in HeLa cells

The whole-cell patch-clamp configuration was utilized to dyalise the cells with an intracellular solution containing 10 nM NAADP and record the subsequent bioelectrical response. This manoeuvre permits to detect NAADP-induced changes in submembranal Ca^{2+} concentration, as shown in earlier studies conducted in mammalian cells [35,36,44,45]. Currents were measured by applying consecutive 400-ms voltage spanning −90 mV to +90 mV starting from a holding potential of 0 mV. The cytosolic infusion of NAADP induced tonic inward (at −80 mV) and outward (at +80 mV) currents with an average latency of 182.9 ± 21.2 s ($n = 51$) in 51 out of 68 cells (Fig. 1A). These currents could either be sustained over time (as shown in Fig. 1A and E) or rapidly decay to the baseline (as shown in Fig. 1G). In the remaining 17 cells, the inclusion of NAADP in the patch-pipette elicited membrane current oscillations at both −80 mV and +80 mV after an average delay of 119.7 ± 31.7 s ($n = 17$) (Fig. 1C). There was no significant difference in the lag time of the bioelectrical response to NAADP between tonic and spiking cells ($p < 0.05$). The *I–V* relationship of NAADP-evoked ionic currents was measured by subtracting the background *I–V* curve to that obtained after full development of the current (Fig. 1B) or at the oscillation peak (Fig. 1D), depending on the pattern of the signal. In both cases, it did not show any detectable rectification and reversed at around 0 mV: as expected, the reversal potential (E_{rev}) of NAADP-induced currents measured in tonic cells (4.5 ± 1.1 mV, $n = 41$) was not significantly different ($p < 0.05$) from that obtained in oscillating ones (6.3 ± 1.9 mV, $n = 14$). Therefore, the biophysical characterization of NAADP-induced currents reveals that the same conductance is activated in both non-spiking and spiking cells, and the data collected from both cell types were computed together in subsequent experiments. The hallmarks of NAADP receptors in mammalian cells are their homologous desensitization at high NAADP doses and their sensitivity to Ned-19, which blocks the binding site for NAADP [9]. Consistent with these features, the amplitude of NAADP-induced currents in HeLa cells was significantly reduced by either of the following treatments: (1) cytosolic dialysis of 50–100 μM NAADP (Fig. 1E and F) or (2) inclusion of Ned-19 (10 μM) in the patch-pipette (Fig. 1G and H).

The fact that NAADP-induced currents invert polarity at potentials close to 0 mV suggests they are carried by a non-selective cation channel [36,37,44]. In agreement with this hypothesis, the replacement of extracellular Na^+ with an equimolar amount of the non-permeable $NMDG^+$ suppressed the inward current, while only slightly affecting the outward component, and caused a shift of E_{rev} towards more negative values (Fig. 2A and B). In the same cells, removal of extracellular Ca^{2+} (0 Ca^{2+}) did not exert any effect both on the amplitude and on the polarity of NAADP-induced currents (Fig. 2A). Conversely, when K^+ in the intracellular solution was substituted with NMDG, the outward current was abrogated and the *I–V* relationship did not reverse even at +90 mV (Fig. 2C and D). Overall, these results indicate that NAADP activates a non-selective cation channel that conducts both Na^+ and K^+, but not Ca^{2+}. Melastatin transient receptor potential channel 4 (TRPM4) is a well known Ca^{2+}-activated non-selective cation conductance that is impermeable to Ca^{2+} [46]. In order to assess whether this is the membrane pathway recruited by NAADP in HeLa cells, we probed the effect of several TRPM4 blockers. Trivalent cations are widely employed to inhibit TRP channels at high micromolar concentrations [47,48], while flufenamic acid (FFA) and 9-phenanthrol (9-Phen) are selective inhibitors of TRPM4 [46]. As depicted in Fig. 2E and F, 30 min pre-treatment with either La^{3+} (50 μM), Gd^{3+} (50 μM), FFA (20 μM) or 9-Phen (30 μM) abolished NAADP-elicited

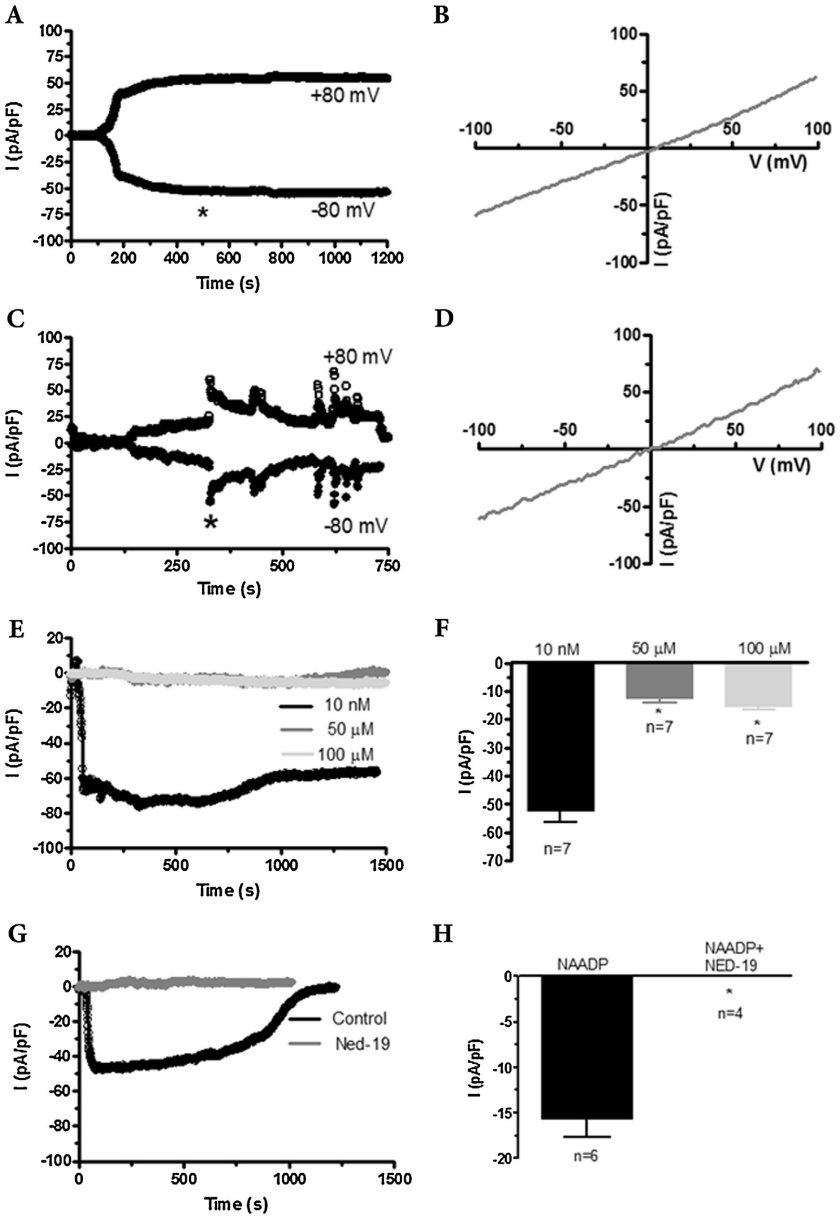

Fig. 1. NAADP-induced membrane currents in HeLa cells. (A) Membrane currents were activated by dialysing HeLa cells with NAADP (10 nM) and monitored by applying conventional voltage ramps (−100 to +100 mV in 50 ms at 0.5 Hz) from a holding potential of 0 mV. Current amplitudes at −80 and +80 mV were measured and plotted against the time to obtain the time course of current development. (B) The *I–V* relationship of NAADP-evoked current was obtained when indicated by the asterisk in panel A. (C) Current oscillations were initiated by NAADP (10 nM) infusion in a fraction of cells and plotted as shown in panel A. (D) *I–V* relationship of NAADP-induced current oscillations measured at the time indicated by the asterisk in panel C. (E) Dialysis of higher NAADP concentrations (50 and 100 µM) failed to induce any membrane current, thereby hinting at the desensitization of NAADP receptors. (F) Mean ± SE of the amplitude of the current peak recorded at different doses of NAADP. (G) The inclusion of NED-19 (10 µM) along with NAADP (10 nM) into the patch pipette prevented the onset of the bioelectrical signal. (H) Mean ± SE of the amplitude of NAADP-evoked currents in the presence and absence of NED-19 (10 µM). NAADP was applied at 10 nM.

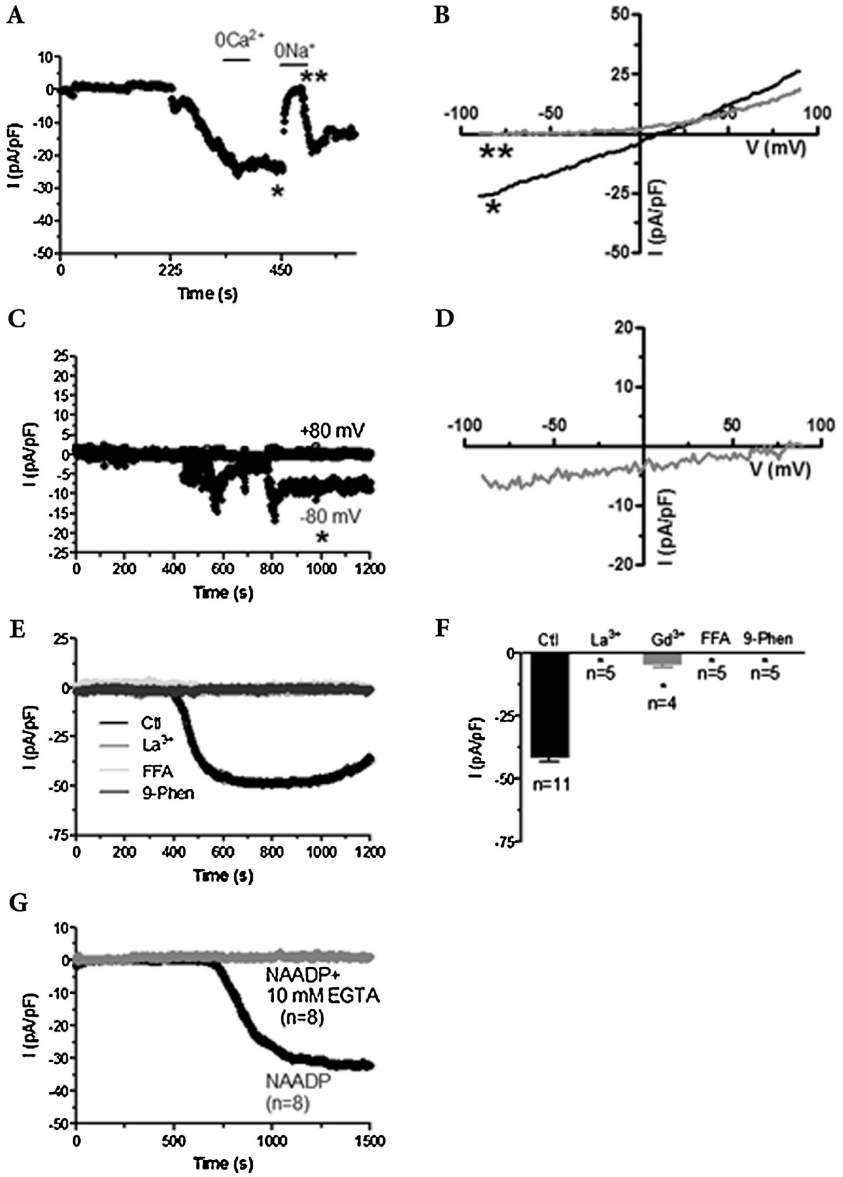

Fig. 2. NAADP-induced membrane currents are mediated by TRPM4. (A) NAADP-induced membrane currents were not inhibited by removal of external Ca^{2+} ($0Ca^{2+}$), but were reversibly abolished by replacing extracellular Na^+ with N-methyl-D-glucamine ($0Na^+$). NAADP was applied at 10 nM. (B) *I–V* relationships of NAADP-induced currents recorded from the cell displayed in panel A in the presence and absence of external Na^+ ($0Na^+$). The *I–V* relationships were taken at the times indicated by the asterisks in panel A. (C) Membrane currents evoked by cytosolic dialysis of NAADP (10 nM) when intracellular K^+ was replaced by NMDG. (D) *I–V* relationship of the NAADP-evoked current recorded in the absence of intracellular K^+ at the time indicated by the asterisk in panel C. (E) NAADP-elicited membrane current under control conditions (Ctl) and in the presence of La^{3+} (50 μM), flufenamic acid (FFA; 20 μM), and 9-Phenanthrol (30 μM). (F) Mean ± SE of the amplitude of NAADP-evoked currents under the designated treatments. (G) NAADP-evoked currents in the absence and presence of 10 mM EGTA in the patch pipette to prevent a global increase in $[Ca^{2+}]_i$.

currents in HeLa cells. This pharmacological profile is compatible with TRPM4 engagement by intracellularly infused NAADP. In agreement with this hypothesis, NAADP did not activate any current when 10 mM EGTA was included in the recording pipette to prevent any increase in $[Ca^{2+}]_i$ (Fig. 2G). Preliminary experiments showed that the cytosolic dialysis of 10 mM EGTA does not trigger any current in the absence of NAADP, which indicates that store-operated Ca^{2+} entry (SOCE) is not activated under these conditions ($n = 8$; data not shown). Taken together, these results demonstrate that NAADP stimulates TRPM4 by causing a cytosolic elevation in $[Ca^{2+}]_i$ upon the mobilization of an intracellular Ca^{2+} pool, as indirectly confirmed by the lack of effect of 0 Ca^{2+} saline (Fig. 2A).

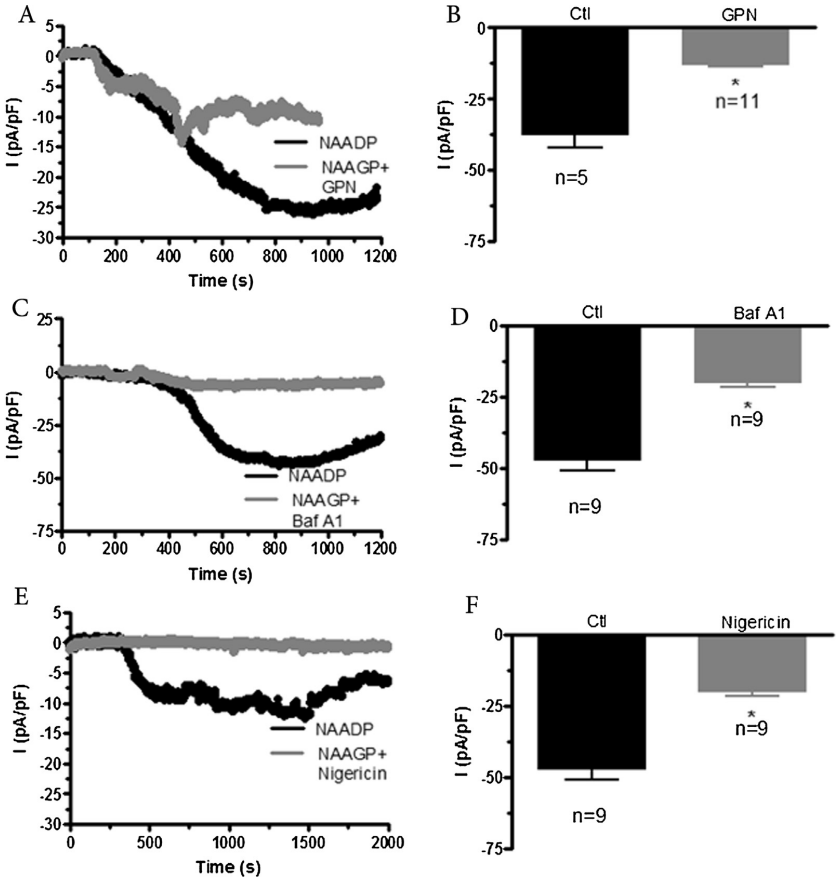

Fig. 3. The disruption of acidic organelles suppresses NAADP-induced membrane currents. NAADP-induced membrane currents were hindered by pre-treating the cells with glycyl-L-phenylalanine-2-naphthylamide (GPN; 200 μM, 1 h) (A and B), bafilomycin A1 (Baf A1; 100 nM, 1 h) (C and D), and nigericin (50 μM, 20 min) (E and F). In each experiment, NAADP was dyalised through the patch pipette at 10 nM. In Panels B, D and F, mean ± SE of the amplitude of NAADP-evoked currents under the designated treatments.

TRPM4-mediated currents may, therefore, be utilized to monitor the intracellular Ca^{2+} response to NAADP in HeLa cells, as shown in other cell types [36,45].

3.2. Acidic store blockers impair NAADP-induced Ca^{2+} signals in HeLa cells

A number of drugs are currently exploited to disrupt Ca^{2+} storage by acidic organelles and prevent NAADP-induced intracellular Ca^{2+} release [7,9,24]. GPN promotes osmotic bursting of lysosomes, bafilomycin A1 prevents EL vesicle acidification and their consequent intralumenal Ca^{2+} sequestration, and nigericin dissipates the proton gradient [32]. Each protocol described in the following experiments has been widely utilized to interfere with EL function and affect NAADP-evoked Ca^{2+} discharge [7,9]. Pre-incubating the cells with GPN (200 μM, 1 h) (Fig. 3A and B) and bafilomycin A1 (100 nM, 1 h) (Fig. 3C and D), significantly ($p < 0.05$) reduced NAADP-elicited currents, while nigericin (50 μM, 20 min) fully suppressed them (Fig. 3E and F). This result indicates that Ca^{2+}-mobilization from acidic organelles contributes to TRPM4 activation by NAADP HeLa cells.

3.3. Thapsigargin-sensitive Ca^{2+} pools contribute to shape NAADP-elicited increase in $[Ca^{2+}]_i$

The contribution of $InsP_3$- and ryanodine-sensitive Ca^{2+} stores to NAADP signalling in HeLa cells was then probed by first pre-treating the cells with thapsigargin (2 μM, 1 h) to deplete Ca^{2+} from ER [49]. This treatment abolished the Ca^{2+} response to NAADP in HeLa cells (Fig. 4A and D). Likewise, direct delivery of heparin (1 mg/ml) along with NAADP through the patch pipette to block $InsP_3Rs$ [3] significantly ($p < 0.05$) decreased both the amplitude and the duration of NAADP-induced Ca^{2+} release (Fig. 4B and D). Finally, the pharmacological inhibition of RyRs with either ryanodine or tetracaine abrogated the onset of NAADP-evoked Ca^{2+} signals [50]. In mode detail, intracellular dialysis from a patch pipette of ryanodine (100 μM) along with NAADP suppressed the ensuing Ca^{2+} mobilization in 2 out of 6 cells (Fig. 4C) and significantly ($p < 0.05$) reduced the magnitude of the Ca^{2+} transient occurring in the remaining 4 (Fig. 4D). Similarly, cytosolic infusion of tetracaine (100 μM) prevented the development of the Ca^{2+} response to NAADP (Fig. 4C and D). Collectively, these results suggest that RyRs directly participate to the generation of

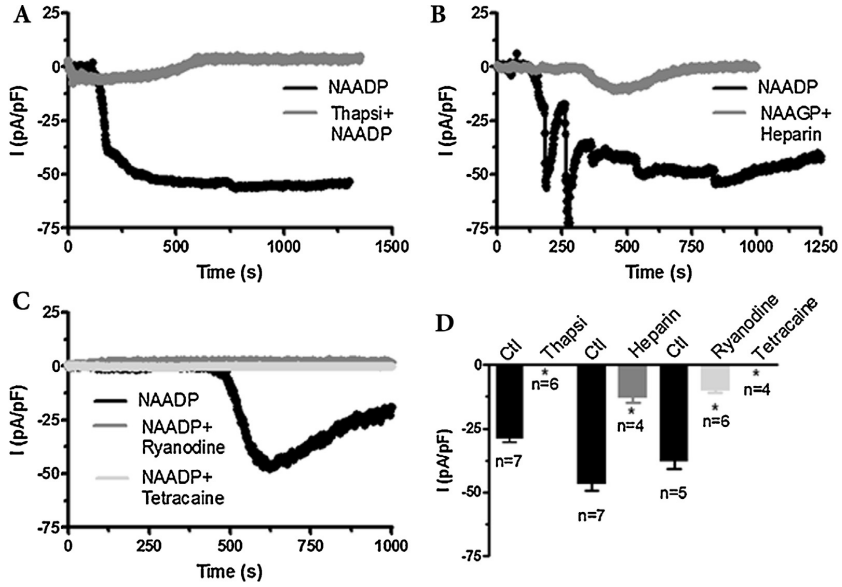

Fig. 4. The inhibition of Ca^{2+} release from the endoplasmic reticulum Ca^{2+} stores affects the bioelectrical response to NAADP. (A) Pre-incubating the cells with thapsigargin (2 μM, 1 h) abrogated NAADP-induced membrane currents. (B) The cytosolic infusion of heparin (1 mg/ml) along with NAADP (10 nM) through the patch pipette reduced and shortened NAADP-elicited current. (C) The cytosolic dialysis of ryanodine (100 μM) or tetracaine (100 μM) abated the bioelectrical response to NAADP (10 nM). (D) Mean ± SE of the amplitude of NAADP-evoked currents under the designated treatments.

NAADP-evoked Ca^{2+} signals, while $InsP_3R$ are required to sustain them over time. It turns out that both EL and ER Ca^{2+} stores shape the Ca^{2+} response to NAADP in HeLa cells.

3.4. GPN, bafilomycin 1 and nigericin inhibit Ca^{2+} sequestration by both endo-lysosomes and endoplasmic reticulum

Once established that both acidic organelles and the ER are recruited by NAADP to induce intracellular Ca^{2+} signals in HeLa cells, we harnessed aequorin-based Ca^{2+} fluorophores to assess the effects of GPN, bafilomycin A1, nigericin, and thapsigargin on both ER and EL Ca^{2+} filling. To assess the extent of Ca^{2+} filling of lysosomal lumen, we have generated a new lysosome-targeted Aeq probe by fusing full-length cathepsin D cDNA to the N-terminus of HA1-Aeq(mut) cassette under control of CMV promoter, designated as CathD-Aeq (Supplementary Fig. 1A). Immunocytochemical analysis of CathD-AEQ, expressed in HeLa cells, revealed co-localisation of the probe with the lysosomal marker Lamp2b (Supplementary Fig. 1B-a) and with the late endosomal marker M6PR (Supplementary Fig. 1B-b), but not with markers of early endosomes (EEA; Supplementary Fig. 1B-c) or with the ER marker (Ergic; Supplementary Fig. 1B-d), thus indicating correct sorting of CathD-Aeq probe to EL compartments [51]. Both ER and EL Aeq probes bear a single amino acid (Asp119→Ala) substitution to decrease the affinity of Aeq to Ca^{2+} [52]. First, we assured that Aeq(mut) functions properly at the acidic pH (4.5–5.5) of the endo-lysosomal lumen and the results may be compared with those of the ER-Aeq. We quantified the light emitted by Aeq(mut) in lysates prepared from transfected HeLa cells with pH ranging form 3.85 to 7.5 upon addition of 100 mM Ca^{2+}, and we found that at the extreme acidic pH 3.85 there was nonsignificant increase of the emitted light by about 10% as compared with that emitted at pH 7 (Supplementary Fig. 1C), demonstrating that Aeq(mut) is functional in acidic conditions and may be used for Ca^{2+} measurements in EL organelles. Next, we checked whether CathD-Aeq correctly reports Ca^{2+} concentrations in acidic conditions. Supplementary Fig. 1D shows that addition 50 μM Ca^{2+} results in robust detection of [Ca^{2+}] in the entire pH range from pH 3.85 to pH 7. Next, we compared the steady state Ca^{2+} levels in ER and EL lumens. Direct measurement of the EL Ca^{2+} content revealed that rate of refilling and steady state level of Ca^{2+} in the EL compartment were not different from those of the ER (Fig. 5A and B), thereby confirming previous indirect estimations of high EL Ca^{2+} content [53,54].

Next, we investigated whether pharmacological disruption of acidic stores specifically affects EL Ca^{2+} dynamics. Unexpectedly, GPN exerted a dose-dependent inhibition of Ca^{2+} uptake not only by EL organelles (Fig. 5A), but also by the ER Ca^{2+} pool (Fig. 5B). In particular, at 200 μM (20 min pre-treatment), the effect of GPN was even more pronounced for ER loading (36.3 ± 15.9% vs. control samples, $p = 0.009$) (Fig. 5B), as compared to EL Ca^{2+} uptake (65.3 ± 15.4% vs. control samples, $p = 0.012$) (Fig. 5A). Similarly, overnight pre-incubation with 100 nM bafilomycin A1 hindered Ca^{2+} sequestration by both EL (Fig. 6A) and ER (Fig. 6B) compartments, although the inhibition of EL Ca^{2+} loading was slightly larger (49.2 ± 4.5% vs. control, $p = 1.7e{-}6$) than ER Ca^{2+} refilling (65.9 ± 9.03% vs. control, $p = 2.5e{-}5$) (Fig. 6). Likewise, nigericin (50 μM, 20 min) dose-dependently decreased Ca^{2+} uptake in both EL and ER compartments (Fig. 7). 20 μM nigericin inhibited to the same extent both EL (31.8 ± 12% vs. control, $p = 0.00036$) and ER (33.3 ± 9.9% vs. control, $p = 8.2e{-}5$) Ca^{2+} uptake (Fig. 7). Overall, these results clearly indicate that the pharmacological disruption of lysosomal Ca^{2+} content leads to a dramatic reduction in ER Ca^{2+} levels as well.

3.5. Inhibitors of SERCA pump block Ca^{2+} sequestration by both endoplasmic reticulum and endo-lysosomes

Next, we investigated whether specific SERCA blockers, such as thapsigargin and tBHQ, impact on EL Ca^{2+} sequestration. Fig. 8

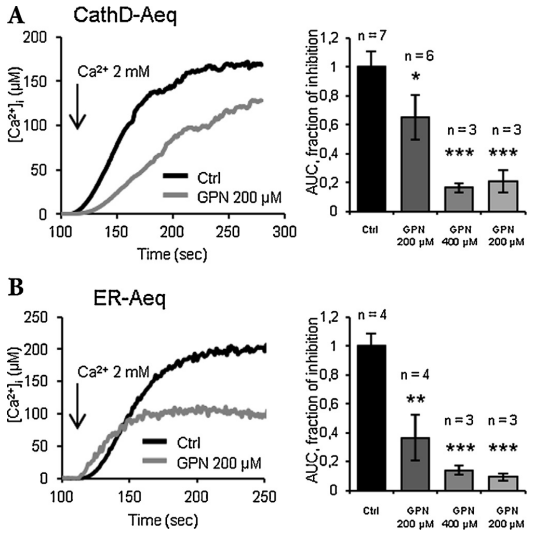

Fig. 5. Effect of GPN on EL and ER luminal Ca^{2+}. HeLa cells, were transfected with CathD-Aeq (A) or ER-Aeq (B), and 24 h later were reconstituted with coelenterazine n in KRB solution supplied with 600 µM EGTA and 3 µM ionomycin at 4 °C for 1 h. GPN, at indicated concentration, was added to the reconstitution solution for 20 min. After reconstitution, the cells were perfused with 2 mM Ca^{2+} (arrow) and the steady state Ca^{2+} levels in the EL (A) and ER (B) were measured. GPN was present in perfusion medium for the duration of the recording. The data are summarized in histograms and expressed as mean ± SD of areas under the curves (AUC) normalized to control. *, $p < 0.05$; ***, $p < 0.001$.

shows that thapsigargin (20 nM, 10 min) prevented Ca^{2+} uptake into both EL (Fig. 8A) and ER (Fig. 8B) compartments. However, 5 nM thapsigargin was ineffective on EL (Fig. 8A), but not ER Ca^{2+} sequestration (69.8 ± 17.7% vs. control, $p = 4e{-}6$) (Fig. 8B). In the same way, 100 µM tBHQ, a SERCA antagonist that binds to a different site with respect to thapsigargin, suppressed Ca^{2+} uptake in both endo-lysosomes and ER (Fig. 8). A recent study suggested that tBHQ and high concentrations of thapsigargin may also target lysosomal SERCA3 [55], but this finding is likely to be confined to human platelets [24]. In addition, EL Ca^{2+} uptake is abrogated by low nM doses of thapsigargin, which is ineffective on this SERCA isoform [55]. Therefore, it is conceivable that both thapsigargin and tBHQ inhibit SERCA-mediated Ca^{2+} sequestration into ER under our conditions. It turns out that EL Ca^{2+} refilling depends on the proper Ca^{2+} uptake by ER in HeLa cells.

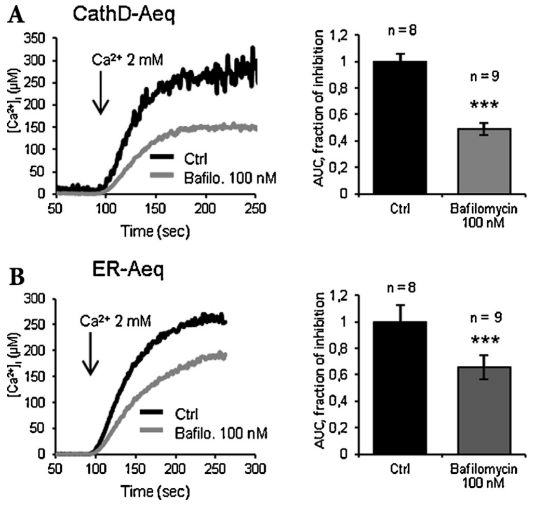

Fig. 6. Effect of bafilomycin A1 on EL and ER luminal Ca^{2+}. HeLa cells, transfected with CathD-Aeq (A) or ER-Aeq (B) and pre-treated with bafilomycin A1 (100 nM, 24 h) were reconstituted with 3 µM coelenterazine n in KRB supplied with 600 µM EGTA and 3 µM ionomycin at 4 °C for 1 h. After reconstitution, the cells were perfused with 2 mM Ca^{2+} (arrow) and the steady state Ca^{2+} levels in the EL (A) and ER (B) lumen were measured. The data, summarized in histograms, expressed as mean ± SD of areas under the curves (AUC) reported to control. ***, $p < 0.001$.

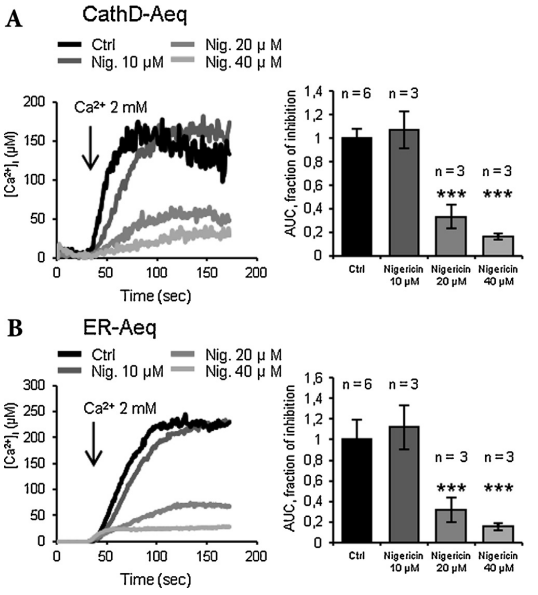

Fig. 7. Effect of nigericin on EL and ER luminal Ca^{2+}. HeLa cells, expressing CathD-Aeq (A) or ER-Aeq (B) were reconstituted with 3 µM coelenterazine n in KRB supplied with 600 µM EGTA and 3 µM ionomycin at 4 °C for 1 h. After reconstitution, the cells were perfused with 2 mM Ca^{2+} (arrow) and the steady state Ca^{2+} levels in the EL (A) and ER (B) lumen were measured. Indicated concentrations of nigericin were added to reconstitution solution 15–20 min prior to Ca^{2+} addition. The data, summarized in histograms, are expressed as mean ± SD of areas under the curves (AUC) reported to control. *n* indicates number of independent measurements per condition. ***, $p < 0.001$.

3.6. GPN, bafilomycin A1, and nigericin affect intracellular Ca^{2+} release by tBHQ

The results hitherto obtained provided the evidence that lysosomotropic agents, such as GPN, bafilomycin A1, and nigericin, interfere with ER Ca^{2+} filling. On the other hand, well established inhibitors of SERCA activity prevent EL Ca^{2+} sequestration as well. To consolidate these findings and further analyze the interaction between EL and ER Ca^{2+} stores, we took advantage from single cell imaging of fura-2/AM-loaded cells to assess whether the pharmacological blockade of EL Ca^{2+} uptake affects ER Ca^{2+} levels. As expected [27,56], the induction of osmotic bursting with GPN (200 µM) in the absence of extracellular Ca^{2+} (0 Ca^{2+}) elicited a Ca^{2+} transient which lasted for about 5 min (Fig. 9A, grey tracing). Perfusion of vehicle (DMSO) to control cells did not change cytosolic Ca^{2+} levels (Fig. 9A, black tracing). After GPN-induced $[Ca^{2+}]_i$ rise, tBHQ (20 µM) was added to the perfusion medium to examine ER Ca^{2+} content. In control experiments, tBHQ produced

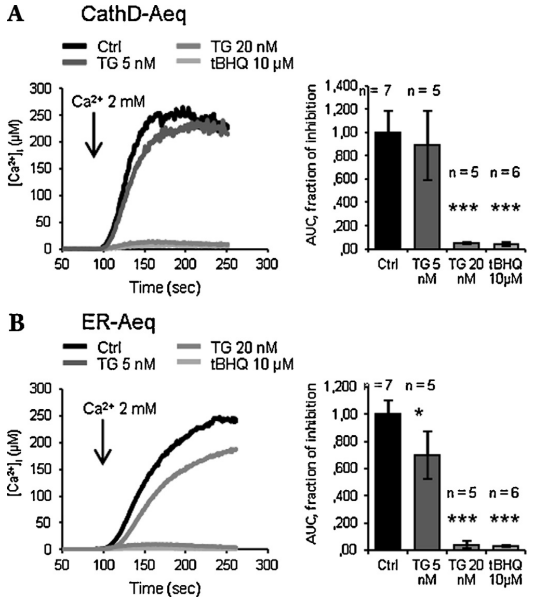

Fig. 8. Effect of thapsigargin and tBHQ on EL and ER luminal Ca^{2+}. HeLa cells, transfected with CathD-Aeq (A) or ER-Aeq (B), and 24 h later were reconstituted with coelenterazine n in KRB solution supplied with 600 µM EGTA and 3 µM ionomycin at 4 °C for 1 h. After reconstitution, the cells were perfused with 2 mM Ca^{2+} (arrow) and the steady state Ca^{2+} levels in the EL (A) and ER (B) were measured. Thapsigargin (TG, 5 or 20 µM) or tBHQ (10 µM) were added to the cells 5 minutes before addition of Ca^{2+}. tBHQ was present in perfusate throughout all the experiment. The data are summarized in histograms and expressed as mean ± SD of areas under the curves (AUC) normalized to control. *, $p < 0.05$; ***, $p < 0.001$.

an elevation in $[Ca^{2+}]_i$ due to passive emptying of the ER Ca^{2+} pool (black tracing and column in Fig. 9A). However, GPN pre-treatment significantly reduced the amplitude of the following Ca^{2+} response to tBHQ (12.8 ± 4.4% vs. control, $p = 2e{-}19$) (grey tracing and column in Fig. 9A). In an inverted experimental setting, when the ER Ca^{2+} stores were first emptied by tBHQ (20 µM, 10 min) and $[Ca^{2+}]_i$ returned to the near-baseline level, application of GPN (200 µM) essentially failed to elevate Ca^{2+} in the cytosol (33.17 ± 22.56% vs. control, $p = 2e{-}37$) (Fig. 9B). Unlike GPN, acute addition of bafilomycin A1 (1 µM) did not alter resting Ca^{2+} levels in HeLa cells (not shown), while over-night pre-incubation with 100 nM bafilomycin A1 significantly reduced the magnitude of tBHQ-induced intracellular Ca^{2+} mobilization (53.3 ± 22.3% vs. control, $p = 4e{-}34$) (Fig. 9C). Finally, nigericin (50 µM) evoked a biphasic increase in $[Ca^{2+}]_i$ which returned to the baseline within 5 min and dampened the subsequent tBHQ-induced Ca^{2+} signal (36.8 ± 23% vs. control, $p = 5e{-}18$) (Fig. 9D). Overall, these data confirm that the disruption of the EL Ca^{2+} pool interferes with ER Ca^{2+} loading and vice versa. As a consequence of the functional cross-talk between these two Ca^{2+} storage compartments, extreme caution is warranted when drawing any conclusion on the intracellular target(s) recruited by NAADP exclusively on the basis of pharmacological manipulation.

4. Discussion

NAADP is the most suitable intracellular messenger to either discharge intraluminally stored Ca^{2+} [7,9,16] or to gate Ca^{2+} inflow in response to extracellular stimulation [2,12,14,57], thereby regulating a host of cellular functions. While TPCs have been clearly

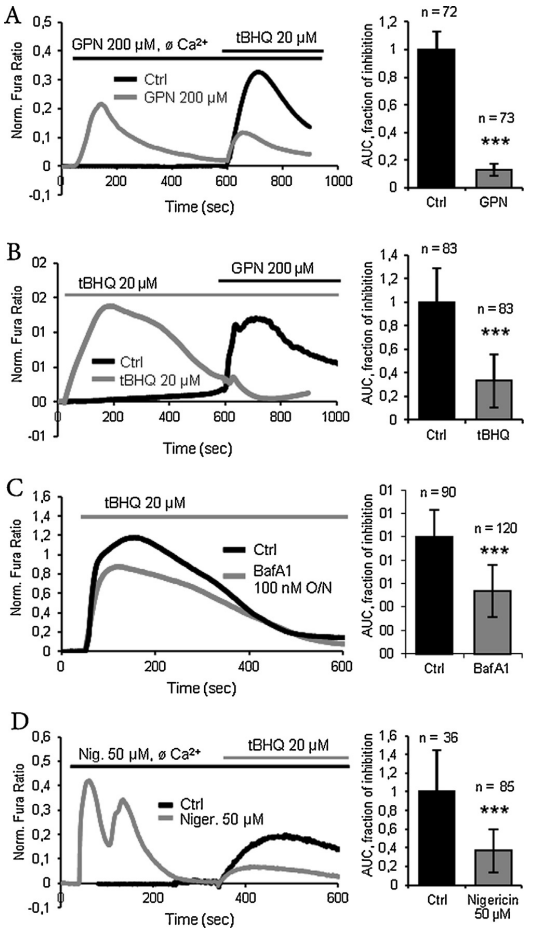

Fig. 9. Effect of bafilomycin, GPN and nigericin on tBHQ-sensitive Ca^{2+} compartments. HeLe cells were loaded with Fura-2/AM and transferred onto the stage of an epifluorescent microscope. (A) The cells were perfused first with GPN (200 µM, 10 min, grey line and column) or with vehicle (DMSO)-containing (black line and column) Ca^{2+}-free KRB, after that perfusion was switched to the tBHQ-containing (20 µM) solution. (B) The cells were first perfused with tBHQ (20 µM, 10 min), after which 200 µM GPN was added to the perfusion solution. (C) HeLa cells were incubated overnight (O/N) with 100 nM bafilomycin A1 (BafA1, grey line and column). At the day of experiment, the cells were loaded with Fura-2/AM and perfused with Ca^{2+}-free KRB supplemented with 20 µM tBHQ. 100 nM BafA1 was present in all solutions. (D) The cells were first perfused with nigericin (50 µM, 5 min, grey line and column) or with vehicle containing KRB (black line and column). After which, 20 µM tBHQ was added to perfusate. The data are summarized in histograms and expressed as mean ± SD of areas under the curves (AUC) normalized to control. ***, $p < 0.001$.

established to mobilize Ca^{2+} from acidic lysosome-like vesicles in sea urchin eggs [58], the target organelle(s) and cognate receptor(s) of NAADP in mammalian cells are far from being clearly elucidated [7,9,18–20]. The controversial issue as to whether NAADP serves as a triggering signal to initiate intracellular Ca^{2+} waves by recruiting either $InsP_3Rs$ and/or RyRs upon lysosomal Ca^{2+} release or it directly activates ER-located RyRs has been fuelled by our poor knowledge of the ER–EL Ca^{2+} cross-talk [28,59,60]. This deficit in our knowledge of the basic mechanisms of organellar interaction might have biased the interpretation of many data produced by the pharmacological manipulation of the multiple Ca^{2+} pools endowed

to mammalian cells [61]. Accordingly, convincing evidence has been provided to demonstrate that, apart from the anterograde Ca^{2+} signal delivered from the acidic stores to ER, ER itself can signal in a retrograde fashion to acidic vesicles [27–31]. This bidirectional Ca^{2+} chatter controls intraluminal Ca^{2+} levels in both compartments, a feature that should be taken into account both when disrupting EL Ca^{2+} accumulation and when depleting ER Ca^{2+} stores. Therefore, we accomplished the present investigation to understand: (1) whether and how classic inhibitors of ER- and EL-dependent Ca^{2+} release affect NAADP-induced Ca^{2+} signals in HeLa cells; (2) whether interfering with ER Ca^{2+} sequestration impairs EL Ca^{2+} uptake and vice versa; and (3) to assess the functional implications of this Ca^{2+}-mediated cross-talk for NAADP-evoked Ca^{2+} signals.

The "whole-cell" patch-clamp technique has been widely employed to investigate the Ca^{2+} response to NAADP by monitoring the activation of Ca^{2+}-dependent non-selective cation channels [35,36,44,45]. This sophisticated tool enables to detect sub-membranal Ca^{2+} elevations that may be missed by utilizing epifluorescence or confocal Ca^{2+} imaging [37]. The following pieces of evidence suggest that the ion currents recorded in HeLa cells dyalized with NAADP truly reflect a concomitant increase in cytosolic Ca^{2+} concentration. First, NAADP triggers either single, long lasting or oscillatory membrane currents which disappear if NAADP is omitted from the patch pipette or if EGTA is supplemented to the intracellular solution to buffer cytosolic Ca^{2+}. EGTA is a slow Ca^{2+} buffer which is normally effective at preventing global changes in $[Ca^{2+}]_i$ [44,62]. Therefore, we speculate that the Ca^{2+} response to NAADP takes place in the bulk cytosol rather than being confined to the sub-membranal domain. Second, the magnitude of NAADP-induced Ca^{2+} currents is significantly reduced when NAADP is infused at 50–100 μM, which is fully consistent with the well known desensitization of mammalian NAADP receptors in the high micromolar range [9]. Third, the Ca^{2+} response to NAADP is abrogated by Ned-19, which selectively antagonizes NAADP binding to its receptor site [9,63]. Thus, NAADP triggers the activation of Ca^{2+}-dependent currents in HeLa cells, thereby rendering these cells a suitable model to investigate the underlying Ca^{2+} stores. The Ca^{2+}-sensitive membrane conductance recruited by NAADP under our conditions is likely to be mediated by TRPM4. First, NAADP-induced currents display the same biophysical features, i.e. linear *I–V* relationship, E_{rev} close to 0 mV, permeability to the monovalent cations Na^+ and Cs^+, but not to Ca^{2+}, as TRPM4-mediated currents both in naïve cells [64–66] and in heterologous expression systems [67]. Second, the pharmacological profile of NAADP-elicited currents is fully compatible with that of TRPM4 [46,47]. Third, a functional TRPM4 protein is expressed in HeLa cells, albeit its endogenous biophysical and pharmacological properties are yet to be evaluated [68]. In this view, NAADP has long been known to activate Ca^{2+}-dependent non-selective cation currents in mouse pancreatic β-cells [36,45], which are abrogated following pharmacological inhibition of TRPM4 [32]. Conversely, NAADP-evoked membrane depolarization in neurons of the rat medulla oblongata has been ascribed to TRPM2 stimulation, as the underlying current is conducted by extracellular Ca^{2+} and requires intracellular Ca^{2+} release to develop [44].

The pharmacological manipulation of the intracellular Ca^{2+} pools carried out by utilizing a number of drugs affecting either ER (i.e. thapsigargin, CPA and tBHQ) or endolysosomal (i.e. GPN, bafilomycin A1, and nigericin) Ca^{2+} content led to the proposal of the trigger hypothesis, according to which NAADP induces a local Ca^{2+} discharge from acidic stores thereby eliciting a secondary larger discharge from the ER [7,9]. Alternatively, NAADP may directly stimulate RyRs to give raise to a regenerative Ca^{2+} wave which is independent on the activation of the EL Ca^{2+} store [19,20]. In order to dissect the signalling pathways downstream NAADP infusion in HeLa cells, we sought to selectively abrogate either ER- or EL-dependent Ca^{2+} mobilization. We found that the disruption of the acidic Ca^{2+} reservoir with three different drugs (i.e. GPN by inducing osmotic lysis of organelles containing the lysosomal hydrolase cathepsin C; bafilomycin A1 preventing vesicle acidification; nigericin by dissipating the proton gradient across the organelle membrane, thereby preventing pH-dependent accumulation of Ca^{2+} in the acidic compartment) hindered NAADP-induced currents. Similarly, the bioelectrical response to NAADP was abated by previous depletion of the ER Ca^{2+} pool with thapsigargin and by RyR inhibition with ryanodine and tetracaine. The blockade of $InsP_3Rs$ with heparin did not suppress the current, but it significantly reduced both its amplitude and duration. Taken together, these results suggest that both ER and EL Ca^{2+} stores are recruited to shape the Ca^{2+} response to NAADP in HeLa cells. One could argue that the Ca^{2+} trigger model would nicely fit these results, thereby suggesting that NAADP stimulates TPCs to release Ca^{2+} from acidic stores and engage the neighbouring RyRs and $InsP_3Rs$ through the mechanism of CICR. Consistently, over-expression of TPC2 has been shown to enhance NAADP-elicited Ca^{2+} signalling in HeLa cells [69]. A recent series of elegant studies conducted by three separate groups have, however, unveiled the bidirectional nature of Ca^{2+} movements occurring at the ER–EL interface [29,31,60]. In addition of being directly loaded into ER lumen following NAADP-dependent TPC activation [4,16,17], Ca^{2+} can be sequestered back into EL Ca^{2+} stores upon ER-induced Ca^{2+} mobilization [29,31,60]. This Ca^{2+}-mediated cross-talk between two physically distinct Ca^{2+} pools might bias any conclusion drawn based on the selective inhibition of Ca^{2+} uptake by each of them. Therefore, we exploited optical reporters specifically generated to monitor Ca^{2+} uptake into EL and ER lumen, respectively, to assess whether the pharmacological manipulation of the ER Ca^{2+} pool interferes with ER Ca^{2+} storage and vice versa. As expected, GPN, bafilomycin A1 and nigericin inhibited Ca^{2+} accumulation within EL vesicles, as well as thapsigargin and tBHQ prevented SERCA-mediated Ca^{2+} sequestration into the ER. Nevertheless, disrupting EL ability to store Ca^{2+} significantly reduced ER Ca^{2+} content and, vice versa, the inhibition of SERCA activity prevented Ca^{2+} loading into acidic organelles. These results might be explained by the reciprocal sensing and control of Ca^{2+} levels in one store by another. According to the protocol applied in experiments described in Figs. 5–8, at point zero all intracellular Ca^{2+} stores are nominally depleted by the incubation in presence of EGTA and ionomycin. When Ca^{2+} is re-added to the cells, it is assumed to simultaneously reach the Ca^{2+} transporters of both EL and ER membranes. If the Ca^{2+} content of two organelles were independently regulated, the inhibition of Ca^{2+} uptake by one store would not affect the uptake by the other one. It appears, however, that the transport of Ca^{2+} into EL compartment is blocked when Ca^{2+} uptake into ER is inhibited and vice versa. In other words, to have functional Ca^{2+} uptake by either EL or ER, its counterpart must have a certain level of Ca^{2+} in its lumen or the Ca^{2+} transporting system active. Thus, it might be speculated that in HeLa cells, EL and ER reciprocally sense and control the Ca^{2+} filling of the adjacent organelle. This might be realized through an agonist-induced Ca^{2+} elevation but might also be via Ca^{2+} leakage mechanism, perhaps through constitutively open TPCs, RyRs or $InsP_3Rs$. These data suggests that Ca^{2+} accumulation within both compartments requires a tight and finely tuned Ca^{2+} exchange at the ER–EL interface and builds a new level of complexity to our understanding of control of cellular Ca^{2+} homeostasis [60]. Consequently, the blockade of Ca^{2+} refilling into either of the two Ca^{2+} pools leads to an appreciable decrease in the intraluminal Ca^{2+} levels of the other. Consistently, Fura-2 imaging experiments revealed that: (1) pre-treating HeLa cells with GPN, bafilomycin A1, and nigericin abrogated the subsequent Ca^{2+} response to tBHQ, which supports the notion that the ER Ca^{2+} reservoir is depleted

by emptying the EL Ca^{2+} pool; and (2) pre-incubating the cells with tBHQ prevented the elevation in $[Ca^{2+}]_i$ induced by directly liberating EL Ca^{2+}. These findings support the aequorin experiment on bi-directional control of Ca^{2+} load, and are corroborated by the observations that all the studies addressing ER–EL interactions reported a close (about 20 nm) apposition between acidic organelles and ER tubules [27–29,31]. It turns out that establishing the sub-cellular location of the first Ca^{2+} deposit activated by NAADP exclusively based on the sensitivity of NAADP-evoked Ca^{2+} signals to SERCA blockers, GPN, bafilomycin A1 and nigericin may lead to unreliable conclusions. The observation that TPC2 is indispensable for triggering NAADP-induced Ca^{2+} signals in HeLa cells concurs in favour of EL involvement in the onset of their Ca^{2+} response [69]. However, our data strongly suggest that the effect of lysosome manipulation on ER Ca^{2+} handling and vice versa should be carefully evaluated to prevent any misleading interpretation of data engendered by the selective disruption of intracellular Ca^{2+} stores, as recently illustrated in mouse hippocampal neurons and astrocytes [34], HEK293 cells [29], human skin fibroblasts [27], and mouse primary pancreatic β-cells [32,33].

In conclusion, the present manuscript provides the evidence that a functional coupling does exist at the ER–EL interface and maintains the proper Ca^{2+} levels within both compartments. This feature might be relevant to the regulation of Ca^{2+}-dependent EL functions, such as control of lysosomal pH and enzyme activity, vesicle trafficking and TPC gating [28,31,60], under both physiological and pathological (i.e. Niemann–Pick type C disease, amyotrophic lateral sclerosis and Alzheimer's disease) conditions. Likewise, it will be intriguing to investigate whether any imbalance in steady state ER Ca^{2+} concentration, that may dictate either pro-survival or pro-apoptotic programmes depending on how intraluminal Ca^{2+} levels vary [70], is underpinned by parallel changes in ER Ca^{2+} content. As a consequence, extreme caution is warranted when drawing straightforward conclusions about the sub-cellular location of NAADP-sensitive stores by exclusively relying on pharmacological tools.

Conflict of interest

The authors declare no conflict of interests.

Acknowledgements

We would like to thank C. Agnoletto for performing certain preliminary experiments. PP was supported by the Italian Association for Cancer Research (AIRC, IG 14442); Telethon (GGP11139B); local funds from the University of Ferrara; and the Italian Ministry of Education, University and Research (COFIN, 20129JLHSY_002; FIRB, RBAP11FXBC_002; and Futuro in Ricerca, RBFR10EGVP_001). We also acknowledge Prof. Franco Tanzi, University of Pavia, for continuous support and collaboration.

Appendix A. Supplementary data

Supplementary data associated with this article can be found, in the online version, at http://dx.doi.org/10.1016/j.ceca.2015.01.001.

References

[1] A. Galione, A.J. Morgan, A. Arredouani, L.C. Davis, K. Rietdorf, M. Ruas, J. Parrington, NAADP as an intracellular messenger regulating lysosomal calcium-release channels, Biochem. Soc. Trans. 38 (2010) 1424–1431.
[2] D. Lim, K. Kyozuka, G. Gragnaniello, E. Carafoli, L. Santella, NAADP+ initiates the Ca^{2+} response during fertilization of starfish oocytes, FASEB J. 15 (2001) 2257–2267.
[3] F. Moccia, G.A. Nusco, D. Lim, K. Kyozuka, L. Santella, NAADP and InsP3 play distinct roles at fertilization in starfish oocytes, Dev. Biol. 294 (2006) 24–38.
[4] T.P. Collins, R. Bayliss, G.C. Churchill, A. Galione, D.A. Terrar, NAADP influences excitation–contraction coupling by releasing calcium from lysosomes in atrial myocytes, Cell Calcium 50 (2011) 449–458.
[5] G.C. Brailoiu, B. Gurzu, X. Gao, R. Parkesh, P.K. Aley, D.I. Trifa, A. Galione, N.J. Dun, M. Madesh, S. Patel, G.C. Churchill, E. Brailoiu, Acidic NAADP-sensitive calcium stores in the endothelium: agonist-specific recruitment and role in regulating blood pressure, J. Biol. Chem. 285 (2010) 37133–37137.
[6] R. Masgrau, G.C. Churchill, A.J. Morgan, S.J. Ashcroft, A. Galione, NAADP: a new second messenger for glucose-induced Ca^{2+} responses in clonal pancreatic beta cells, Curr. Biol. 13 (2003) 247–251.
[7] A. Galione, J. Parrington, T. Funnell, Physiological roles of NAADP-mediated Ca^{2+} signaling, Sci. China Life Sci. 54 (2011) 725–732.
[8] F. Moccia, R. Berra-Romani, F. Tanzi, Update on vascular endothelial Ca^{2+} signalling: a tale of ion channels, pumps and transporters, World J. Biol. Chem. 3 (2012) 127–158.
[9] A. Galione, NAADP receptors, Cold Spring Harb. Perspect. Biol. 3 (2011) a004036.
[10] A. Galione, G.C. Churchill, Interactions between calcium release pathways: multiple messengers and multiple stores, Cell Calcium 32 (2002) 343–354.
[11] G.C. Churchill, J.S. O'Neill, R. Masgrau, S. Patel, J.M. Thomas, A.A. Genazzani, A. Galione, Sperm deliver a new second messenger: NAADP, Curr. Biol. 13 (2003) 125–128.
[12] A.J. Morgan, Sea urchin eggs in the acid reign, Cell Calcium 50 (2011) 147–156.
[13] F. Moccia, R.A. Billington, L. Santella, Pharmacological characterization of NAADP-induced Ca^{2+} signals in starfish oocytes, Biochem. Biophys. Res. Commun. 348 (2006) 329–336.
[14] F. Moccia, D. Lim, G.A. Nusco, E. Ercolano, L. Santella, NAADP activates a Ca^{2+} current that is dependent on F-actin cytoskeleton, FASEB J. 17 (2003) 1907–1909.
[15] F. Moccia, D. Lim, K. Kyozuka, L. Santella, NAADP triggers the fertilization potential in starfish oocytes, Cell Calcium 36 (2004) 515–524.
[16] G.C. Churchill, A. Galione, NAADP induces Ca^{2+} oscillations via a two-pool mechanism by priming IP3- and cADPR-sensitive Ca^{2+} stores, EMBO J. 20 (2001) 2666–2671.
[17] A. Macgregor, M. Yamasaki, S. Rakovic, L. Sanders, R. Parkesh, G.C. Churchill, A. Galione, D.A. Terrar, NAADP controls cross-talk between distinct Ca^{2+} stores in the heart, J. Biol. Chem. 282 (2007) 15302–15311.
[18] A.H. Guse, Linking NAADP to ion channel activity: a unifying hypothesis, Sci. Signal. 5 (2012) e18.
[19] W. Dammermann, B. Zhang, M. Nebel, C. Cordiglieri, F. Odoardi, T. Kirchberger, N. Kawakami, J. Dowden, F. Schmid, K. Dornmair, M. Hohenegger, A. Flügel, A.H. Guse, B.V. Potter, NAADP-mediated Ca^{2+} signaling via type 1 ryanodine receptor in T cells revealed by a synthetic NAADP antagonist, Proc. Natl. Acad. Sci. U. S. A. 106 (2009) 10678–10683.
[20] M. Hohenegger, J. Suko, R. Gscheidlinger, H. Drobny, A. Zidar, Nicotinic acid-adenine dinucleotide phosphate activates the skeletal muscle ryanodine receptor, Biochem. J. 367 (2002) 423–431.
[21] A. Jha, E. Brailoiu, S. Muallem, How does NAADP release lysosomal Ca (2+)? Channels (Austin) 8 (2014) 174–175.
[22] A.J. Morgan, A. Galione, Two-pore channels (TPCs): current controversies, Bioessays 36 (2014) 173–183.
[23] J.S. Marchant, S. Patel, Questioning regulation of two-pore channels by NAADP, Messenger (Los Angel) 2 (2013) 113–119.
[24] A.J. Morgan, F.M. Platt, E. Lloyd-Evans, A. Galione, Molecular mechanisms of endolysosomal Ca^{2+} signalling in health and disease, Biochem. J. 439 (2011) 349–374.
[25] S. Patel, R. Docampo, Acidic calcium stores open for business: expanding the potential for intracellular Ca^{2+} signaling, Trends Cell Biol. 20 (2010) 277–286.
[26] B. Esposito, G. Gambara, A.M. Lewis, F. Palombi, A. D'Alessio, L.X. Taylor, A.A. Genazzani, E. Ziparo, A. Galione, G.C. Churchill, A. Filippini, NAADP links histamine H1 receptors to secretion of von Willebrand factor in human endothelial cells, Blood 117 (2011) 4968–4977.
[27] B.S. Kilpatrick, E.R. Eden, A.H. Schapira, C.E. Futter, S. Patel, Direct mobilisation of lysosomal Ca^{2+} triggers complex Ca^{2+} signals, J. Cell Sci. 126 (2013) 60–66.
[28] A.K. Lam, A. Galione, The endoplasmic reticulum and junctional membrane communication during calcium signaling, Biochim. Biophys. Acta 1833 (2013) 2542–2559.
[29] C.I. López-Sanjurjo, S.C. Tovey, D.L. Prole, C.W. Taylor, Lysosomes shape Ins(1,4,5)P3-evoked Ca^{2+} signals by selectively sequestering Ca^{2+} released from the endoplasmic reticulum, J. Cell Sci. 126 (2013) 289–300.
[30] L. McGuinness, S.J. Bardo, N.J. Emptage, The lysosome or lysosome-related organelle may serve as a Ca^{2+} store in the boutons of hippocampal pyramidal cells, Neuropharmacology 52 (2007) 126–135.
[31] A.J. Morgan, L.C. Davis, S.K. Wagner, A.M. Lewis, J. Parrington, G.C. Churchill, A. Galione, Bidirectional Ca^{2+} signaling occurs between the endoplasmic reticulum and acidic organelles, J. Cell Biol. 200 (2013) 789–805.
[32] A. Arredouani, A.M. Evans, J. Ma, J. Parrington, M.X. Zhu, A. Galione, An emerging role for NAADP-mediated Ca^{2+} signaling in the pancreatic β-cell, Islets 2 (2010) 323–330.
[33] J.G. Duman, L. Chen, A.E. Palmer, B. Hille, Contributions of intracellular compartments to calcium dynamics: implicating an acidic store, Traffic 7 (2006) 859–872.
[34] V. Pandey, C.C. Chuang, A.M. Lewis, P.K. Aley, E. Brailoiu, N.J. Dun, G.C. Churchill, S. Patel, Recruitment of NAADP-sensitive acidic Ca^{2+} stores by glutamate, Biochem. J. 422 (2009) 503–512.
[35] P.J. Calcraft, M. Ruas, Z. Pan, X. Cheng, A. Arredouani, X. Hao, J. Tang, K. Rietdorf, L. Teboul, K.T. Chuang, P. Lin, R. Xiao, C. Wang, Y. Zhu, Y. Lin, C.N. Wyatt, J.

Parrington, J. Ma, A.M. Evans, A. Galione, M.X. Zhu, NAADP mobilizes calcium from acidic organelles through two-pore channels, Nature 459 (2009) 596–600.
[36] J.M. Cancela, G.C. Churchill, A. Galione, Coordination of agonist-induced Ca^{2+}-signalling patterns by NAADP in pancreatic acinar cells, Nature 398 (1999) 74–76.
[37] F. Moccia, G.A. Nusco, D. Lim, E. Ercolano, G. Gragnaniello, E.R. Brown, L. Santella, Ca^{2+} signalling and membrane current activated by cADPr in starfish oocytes, Pflugers Arch. 446 (2003) 541–552.
[38] F. Moccia, C. Frost, R. Berra-Romani, F. Tanzi, D.J. Adams, Expression and function of neuronal nicotinic ACh receptors in rat microvascular endothelial cells, Am. J. Physiol. Heart Circ. Physiol. 286 (2004) H486–H491.
[39] R. Takezawa, H. Cheng, A. Beck, J. Ishikawa, P. Launay, H. Kubota, J.P. Kinet, A. Fleig, T. Yamada, R. Penner, A pyrazole derivative potently inhibits lymphocyte Ca^{2+} influx and cytokine production by facilitating transient receptor potential melastatin 4 channel activity, Mol. Pharmacol. 69 (2006) 1413–1420.
[40] C. Lazzari, C. Peggion, R. Stella, M.L. Massimino, D. Lim, A. Bertoli, M.C. Sorgato, Cellular prion protein is implicated in the regulation of local Ca^{2+} movements in cerebellar granule neurons, J. Neurochem. 116 (2011) 881–890.
[41] P. Metcalf, M. Fusek, Two crystal structures for cathepsin D: the lysosomal targeting signal and active site, EMBO J. 12 (1993) 1293–1302.
[42] M. Bonora, C. Giorgi, A. Bononi, S. Marchi, S. Patergnani, A. Rimessi, R. Rizzuto, P. Pinton, Subcellular calcium measurements in mammalian cells using jellyfish photoprotein aequorin-based probes, Nat. Protocols 8 (2013) 2105–2118.
[43] M. Brini, R. Marsault, C. Bastianutto, J. Alvarez, T. Pozzan, R. Rizzuto, Transfected aequorin in the measurement of cytosolic Ca^{2+} concentration ($[Ca^{2+}]c$). A critical evaluation, J. Biol. Chem. 270 (1995) 9896–9903.
[44] G.C. Brailoiu, E. Brailoiu, R. Parkesh, A. Galione, G.C. Churchill, S. Patel, N.J. Dun, NAADP-mediated channel 'chatter' in neurons of the rat medulla oblongata, Biochem. J. 419 (2009) 91–97.
[45] J.M. Cancela, O.V. Gerasimenko, J.V. Gerasimenko, A.V. Tepikin, O.H. Petersen, Two different but converging messenger pathways to intracellular Ca(2+) release: the roles of nicotinic acid adenine dinucleotide phosphate, cyclic ADP-ribose and inositol trisphosphate, EMBO J. 19 (2000) 2549–2557.
[46] H. Abriel, N. Syam, V. Sottas, M.Y. Amarouch, J.S. Rougier, TRPM4 channels in the cardiovascular system: physiology, pathophysiology, and pharmacology, Biochem. Pharmacol. 84 (2012) 873–881.
[47] L. Dwyer, P.L. Rhee, V. Lowe, H. Zheng, L. Peri, S. Ro, K.M. Sanders, S.D. Koh, Basally activated nonselective cation currents regulate the resting membrane potential in human and monkey colonic smooth muscle, Am. J. Physiol. Gastrointest. Liver Physiol. 301 (2011) G287–G296.
[48] F. Moccia, S. Dragoni, F. Lodola, E. Bonetti, C. Bottino, G. Guerra, U. Laforenza, V. Rosti, F. Tanzi, Store-dependent Ca(2+) entry in endothelial progenitor cells as a perspective tool to enhance cell-based therapy and adverse tumour vascularization, Curr. Med. Chem. 19 (2012) 5802–5818.
[49] R. Berra-Romani, A. Raqeeb, J. Torres-Jácome, A. Guzman-Silva, G. Guerra, F. Tanzi, F. Moccia, The mechanism of injury-induced intracellular calcium concentration oscillations in the endothelium of excised rat aorta, J. Vasc. Res. 49 (2012) 65–76.
[50] D.J. West, A.J. Williams, Pharmacological regulators of intracellular calcium release channels, Curr. Pharm. Des. 13 (2007) 2428–2442.
[51] J. Huotari, A. Helenius, Endosome maturation, EMBO J. 30 (2011) 3481–3500.
[52] M. Montero, M. Brini, R. Marsault, J. Alvarez, R. Sitia, T. Pozzan, R. Rizzuto, Monitoring dynamic changes in free Ca2+ concentration in the endoplasmic reticulum of intact cells, EMBO J. 14 (1995) 5467–5475.
[53] K.A. Christensen, J.T. Myers, J.A. Swanson, pH-dependent regulation of lysosomal calcium in macrophages, J. Cell Sci. 115 (2002) 599–607.
[54] C.C. Scott, J. Gruenberg, Ion flux and the function of endosomes and lysosomes: pH is just the start: the flux of ions across endosomal membranes influences endosome function not only through regulation of the luminal pH, Bioessays 33 (2011) 103–110.
[55] J.A. Rosado, Acidic Ca^{2+} stores in platelets, Cell Calcium 50 (2011) 168–174.
[56] T. Haller, P. Dietl, P. Deetjen, H. Völkl, The lysosomal compartment as intracellular calcium store in MDCK cells: a possible involvement in InsP3-mediated Ca^{2+} release, Cell Calcium 19 (1996) 157–165.
[57] I. Berg, B.V. Potter, G.W. Mayr, A.H. Guse, Nicotinic acid adenine dinucleotide phosphate (NAADP$^+$) is an essential regulator of T-lymphocyte Ca^{2+}-signaling, J. Cell Biol. 150 (2000) 581–588.
[58] G.C. Churchill, Y. Okada, J.M. Thomas, A.A. Genazzani, S. Patel, A. Galione, NAADP mobilizes Ca^{2+} from reserve granules, lysosome-related organelles, in sea urchin eggs, Cell 111 (2002) 703–708.
[59] S. Patel, E. Brailoiu, Triggering of Ca^{2+} signals by NAADP-gated two-pore channels: a role for membrane contact sites? Biochem. Soc. Trans. 40 (2012) 153–157.
[60] R. van der Kant, J. Neefjes, Small regulators, major consequences – Ca^{2+} and cholesterol at the endosome–ER interface, J. Cell Sci. 127 (2014) 929–938.
[61] M.J. Berridge, M.D. Bootman, H.L. Roderick, Calcium signalling: dynamics, homeostasis and remodelling, Nat. Rev. Mol. Cell Biol. 4 (2003) 517–529.
[62] S. Patel, J.S. Marchant, E. Brailoiu, Two-pore channels: regulation by NAADP and customized roles in triggering calcium signals, Cell Calcium 47 (2010) 480–490.
[63] J.S. Marchant, Y. Lin-Moshier, T.F. Walseth, S. Patel, The molecular basis for Ca^{2+} signalling by NAADP: Two-pore channels in a complex? Messenger (Los Angel) 1 (2012) 63–76.
[64] M.Y. Amarouch, N. Syam, H. Abriel, Biochemical, single-channel, whole-cell patch clamp, and pharmacological analyses of endogenous TRPM4 channels in HEK293 cells, Neurosci. Lett. 541 (2013) 105–110.
[65] V. Marigo, K. Courville, W.H. Hsu, J.M. Feng, H. Cheng, TRPM4 impacts on Ca^{2+} signals during agonist-induced insulin secretion in pancreatic beta-cells, Mol. Cell. Endocrinol. 299 (2009) 194–203.
[66] H. Morita, A. Honda, R. Inoue, Y. Ito, K. Abe, M.T. Nelson, J.E. Brayden, Membrane stretch-induced activation of a TRPM4-like nonselective cation channel in cerebral artery myocytes, J. Pharmacol. Sci. 103 (2007) 417–426.
[67] N.D. Ullrich, T. Voets, J. Prenen, R. Vennekens, K. Talavera, G. Droogmans, B. Nilius, Comparison of functional properties of the Ca^{2+}-activated cation channels TRPM4 and TRPM5 from mice, Cell Calcium 37 (2005) 267–278.
[68] R. Armisén, K. Marcelain, F. Simon, J.C. Tapia, J. Toro, A.F. Quest, A. Stutzin, TRPM4 enhances cell proliferation through up-regulation of the β-catenin signaling pathway, J. Cell. Physiol. 226 (2011) 103–109.
[69] Y. Lu, B.X. Hao, R. Graeff, C.W. Wong, W.T. Wu, J. Yue, Two pore channel 2 (TPC2) inhibits autophagosomal-lysosomal fusion by alkalinizing lysosomal pH, J. Biol. Chem. 288 (2013) 24247–24263.
[70] H. Ivanova, T. Vervliet, L. Missiaen, J.B. Parys, H. De Smedt, G. Bultynck, Inositol 1 4,5-trisphosphate receptor-isoform diversity in cell death and survival, Biochim. Biophys. Acta (2014).

Ringrazio il Professor D'Angelo per questi tre anni di dottorato.

Grazie Lisa, per avermi guidato durante il mio percorso e per tutto ciò che mi ha insegnato.

Grazie a Voi, per tutto ciò che avete fatto per me, per il vostro aiuto, per i consigli dati e per avermi fatto sentire parte di una grande famiglia.

Grazie mille ai miei genitori e ai miei fratelli, grazie a via Olevano e via Orsi e grazie a Te che sei riuscita a tirare fuori tutto il meglio che c'è in me.